

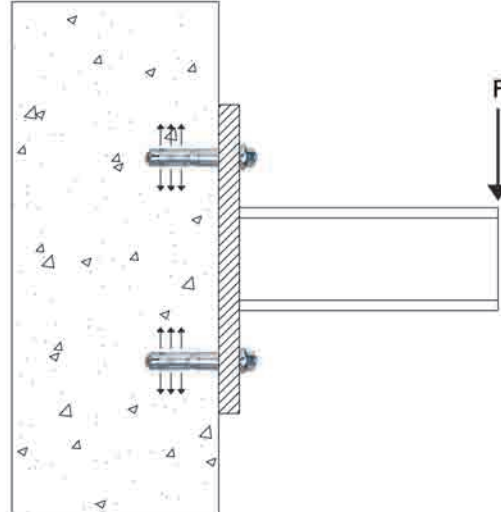
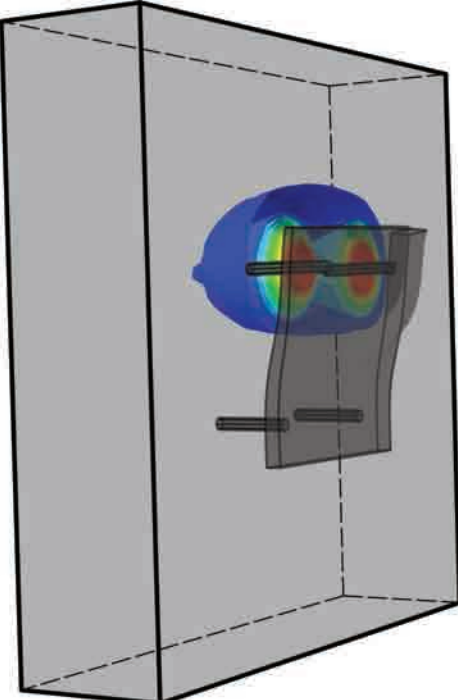
Load capacity of anchorage to concrete at nuclear facilities

Numerical studies of headed studs and expansion anchors

DANIEL ERIKSSON & TOBIAS GASCH



KTH Architecture and
the Built Environment



Master of Science Thesis
Stockholm, Sweden 2011

@Seismicisolation

@Seismicisolation



Load capacity of anchorage to concrete at nuclear facilities

Numerical studies of headed studs and expansion anchors

Daniel Eriksson and Tobias Gasch

June 2011

©Daniel Eriksson and Tobias Gasch 2011
Royal Institute of Technology (KTH)
Department of Civil and Architectural Engineering
Division of Concrete Structures
Stockholm, Sweden, 2011

Abstract

The aim of this thesis was to study the load bearing capacity of anchor plates, used for anchorage to concrete located at nuclear facilities. Two different type of anchor plates were examined, which together constitute the majority of the anchor plates used at Forsmark nuclear facility in Sweden. The first is a cast-in-place anchor plate with headed studs and the second is a post-installed anchor plate which uses sleeve-type expansion anchors. Hence, anchors with both a mechanical or a frictional interlock to the concrete were examined. The main analysis tool was the finite element method, through the use of the two commercially available software packages ABAQUS and ADINA and their non-linear material models for concrete and steel. As a first step, the numerical methods were verified against experimental results from the literature. However, these only concern single anchors. The results from the verifications were then used to build the finite element models of the anchor plates. These were then subjected to different load combinations with the purpose to find the ultimate load capacity. Failure loads from the finite element analyses were then compared to the corresponding loads calculated according to the new European technical specification SIS-CEN/TS 1992-4 (2009).

Most of the failure loads from the numerical analyses were higher than the loads obtained from the technical specification, although in some cases the numerical results were lower than the technical specification value. However, many conservative assumptions regarding the finite element models were made, hence there might still be an overcapacity present. All analyses that underestimate the failure load were limited to large and slender anchor plates, which exhibit an extensive bending of the steel plate. The bending of the steel plate induce shear forces on the anchors, which leads to a lower tensile capacity. In design codes, which assume rigid steel plates, this phenomenon is neglected. The failure loads from all different load combinations analysed were then used to develop failure envelopes as a demonstration of a useful technique, which can be utilised in the design process of complex load cases.

Keywords: anchor plates, headed studs, expansion anchors, concrete, finite element analysis, non-linear material models, failure envelopes

@Seismicisolation

Sammanfattning

Syftet med denna uppsats var att utvärdera bärformågan hos förankringsplattor, monterade i kärnkraftverk där de används för infästningar till betong. Två typer av förankringsplattor har studerats, vilka tillsammans representerar en majoritet av förankringsplattorna som används vid kärnkraftverket i Forsmark. Den första är en ingjuten förankringsplatta som använder infästningar med huvud, medan den andra är en eftermonterad förankringsplatta som använder expansionsankare. Detta innebär att både ankare med hak- eller friktionsverkan har studerats. De numeriska analyserna genomfödes med finita element metoden genom de två kommersiella programmen ABAQUS och ADINA och deras respektive icke-linjära materialmodeller för att beskriva betong respektive stål. Som ett första steg verifierades dessa numeriska metoder mot experimentell data från litteraturen. Dessa försök behövde endast enskilda ankare, försök på ankargrupper saknas. Resultaten från verifikationerna användes sedan för att bygga de finita element modellerna av förankringsplattorna, som sedan belastades med olika lastkombinationer. Brottlasterna erhållna från de numeriska analyserna jämfördes sedan med deras motsvarande laster beräknade enligt den nya Europeiska tekniska specifikationen SIS-CEN/TS 1992-4 (2009).

De flesta brottlasterna från de numeriska analyserna påvisade en högre brottlast i jämförelse med lasterna erhållna från den tekniska specifikationen, även om vissa av de numeriska resultaten var lägre än de handberäknade värdena. Dock bör det noteras att många konservativa antaganden gjordes då de finita element modellerna skapades och därfor kan ändå en överkapacitet finnas. All de analyser som påvisade en för låg brottlast var begränsade till stora och slanka stålplattor som därfor utsattes för en kraftig böjning. Plattböjningen inducerar skjukvrafter på ankarna vilket leder till en lägre dragkapacitet. I den tekniska specifikationen, som antar en stel stålplatta, försummas detta fenomen. Brottlasterna från de olika lastkombinationerna användes sedan för att utveckla interaktionssamband mellan olika lastkombinationer för att påvisa och demonstrera en teknik som kan vara användbar i dimensioneringsprocessen då komplexa lastfall föreligger.

Nyckelord: förankringsplattor, infästningar med huvud, expansionsankare, betong, finit element analys, icke-linjära materialmodeller, interaktionssamband

@Seismicisolation

Preface

The research presented in this thesis has been carried out from February to June 2011 at Vattenfall Power Consultant AB in collaboration with the Division of Concrete Structures, Department of Civil and Architectural Engineering at the Royal Institute of Technology (KTH). The project was initiated by Dr. *Richard Malm*, who also supervised the project.

We wish to express our sincere gratitude and thankfulness to Dr. *Richard Malm* for his advise, encouragement and guidance during the project. We would also like to thank him for all the opportunities he has given us during the project and for the future.

Secondly, we would like to thank M.Sc. *Magnus Lundin* and M.Sc. *Patrik Gatter* at Vattenfall for giving us the opportunity to carry out this project and for their support. We would also like to thank all our other co-workers at our division at Vattenfall. A special thank to M.Sc. *Fredrik Wennstam* for his advise and help.

A thank goes M.Sc. *Anders Bergkvist* and his colleagues at Forsmark FTFB for their input to the project.

At last, we would like to show our gratitude to Associate Prof. Dr. *Gunnar Tibert* at the Department of Mechanics at the Royal Institute of Technology for introducing us to the research area.

Stockholm, June 2011

Daniel Eriksson and Tobias Gasch

@Seismicisolation

Contents

Abstract	iii
Sammanfattning	v
Preface	vii
1 Introduction	1
1.1 Background	2
1.2 Aims and scope of the thesis	4
1.3 Structure of the thesis	4
2 Anchorage to concrete	7
2.1 Different fasteners	7
2.2 Failure modes	9
2.2.1 Tensile load	10
2.2.2 Shear load	15
3 Finite element modelling of concrete	19
3.1 Nonlinear behaviour of concrete	19
3.2 Concrete material models	22
3.2.1 Basic concepts	22
3.2.2 Concrete damaged plasticity in ABAQUS	28
3.2.3 Concrete material model in ADINA	33
3.3 Dynamic explicit integration	37
3.3.1 Explicit integration in ABAQUS	38

3.3.2	Explicit integration in ADINA	39
3.3.3	Quasi-static analysis	40
4	Design codes	41
4.1	Design according to CEN	42
4.1.1	Steel failure	43
4.1.2	Concrete cone failure	44
4.1.3	Concrete pry-out failure	47
4.1.4	Pull-out failure	48
4.1.5	Combined shear and tensile load	48
4.2	ACI 349-6	49
4.3	Design considerations for nuclear facilities	53
5	Verification examples	57
5.1	Notched unreinforced concrete beam	57
5.2	Headed stud	65
5.2.1	Finite element model	67
5.2.2	Results	69
5.3	Expansion anchor	76
5.3.1	Finite element model	77
5.3.2	Results	78
6	Analysis of anchor plates at Forsmark nuclear facility	83
6.1	Anchor plates at Forsmark nuclear facility	83
6.2	General aspects of the finite element models	85
6.3	M-type anchor plate	86
6.3.1	Design calculations	87
6.3.2	Finite element model	88
6.3.3	Static analysis	89
6.3.4	Failure envelopes	101
6.3.5	Dynamic analysis	104

6.4 Expansion anchor plates	108
6.4.1 Design calculations	109
6.4.2 Finite element model	110
6.4.3 Static analysis	111
6.4.4 Failure envelopes	122
6.4.5 Dynamic analysis	128
7 Conclusions	131
7.1 Considerations regarding finite element analysis of anchorage to concrete	131
7.2 Capacity assessment of anchor plates	133
7.2.1 Static analysis	133
7.2.2 Failure envelopes	134
7.2.3 Dynamic analysis	135
7.3 Further research	135
Bibliography	137
A Design codes	141
A.1 Further design procedures according to CEN/TS 1992-4:2010	141
A.2 Design of the M3 anchor plate subjected to a bending moment according to SIS-CEN/TS 1992-4-1:2010	149
B Photos	157
B.1 Photos of anchor plates	157

@Seismicisolation

Chapter 1

Introduction

In Sweden approximately 50 % of the electricity production comes from nuclear power. The remaining demand is primarily covered by hydropower, but also by wind power and other renewable energy sources. Today, Sweden has in total 10 active nuclear reactors distributed over three facilities: Forsmark, Oskarshamn and Ringhals. The facilities at Forsmark and Ringhals are operated by Vattenfall AB while the facility at Oskarshamn is operated by E.ON Sverige AB. These 10 reactors make Sweden the country with most nuclear reactors per capita in the world, according to the World Nuclear Association, and therefore the nuclear industry is of great importance. Along with the nuclear reactor facilities, a number of other facilities are also necessary for the operation of the nuclear reactors. A summary of all nuclear facilities is presented in Fig. 1.1.

The Swedish nuclear reactors were put into service during the late 1970s and early 1980s and were designed with a expected lifetime of 40 years. Therefore, during their operation the maintenance of the nuclear reactors have been performed with the expected life time as a goal. Further, there have for a long time been a decision to phase out nuclear power in Sweden, but this have changed during the last years. Today, it has been decided to increase the service time and capacity of the Swedish reactors. Hence, large investments are required in order to extend the lifetime of the old reactors. As an effect, some of the nuclear reactors have been partly closed during the cold winter months, with high electricity prices as a result. These prices have been historically high and have influenced both the industry and the households to a great extent. In addition, the Swedish government decided in the year 2010 that the old reactors may be replaced with new ones in the future.

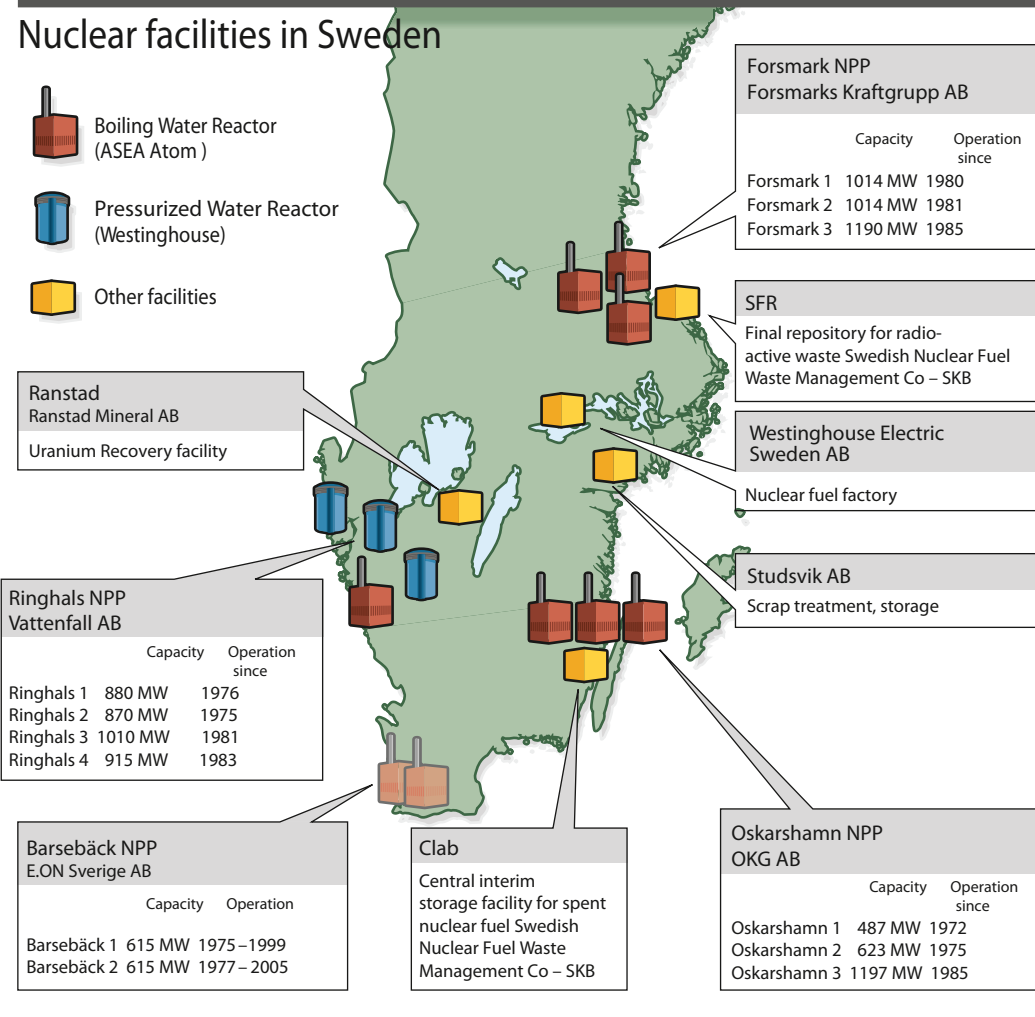


Figure 1.1: Summary and distribution of nuclear facilities in Sweden. Reproduction from (Ministry of the Environment Sweden, 2007).

1.1 Background

The demand for electricity has during the last years slowly increased in Sweden, and since the phase out of the nuclear power has been suspended, a decision to upgrade and uprate the existing nuclear reactors have been taken. An uprate of nine of the nuclear reactors has previously been made shortly after they were put into service. This was mainly performed through a more efficient use of the existing margins, better methods of analysis and improved fuel design. These methods of increasing the output effect meant that no major modifications had to be made to the facilities, whereas the planned upcoming uprate is of a different scale and therefore demands major modifications. In fact, the scale of the uprates are unique and nothing similar has been made in any other country. For the three reactors at Forsmark nuclear facility, studied in this thesis, the planned uprate is between 20-25

% of the current power level. As mentioned, an uprate of this scale affect many of the systems which therefore require modifications to withstand the increased loads. One of these systems is the water based coolant system designed to remove residual heat from the reactor core through a piping system (Ministry of the Environment Sweden, 2007).

The piping system mentioned above is only one of many piping systems needed at a nuclear facility; others include the piping between the reactor and the turbine and other cooling systems. Common to all these piping systems is that they are mainly supported through the use of anchor plates installed in the structural concrete of the facility. Due to the extensive length of piping, a huge number of anchor plates are required in order to support it. Anchor plates are also used to support other technical and structural equipment. All in all, this results in several thousands of anchor plates at each individual nuclear reactor facility. For example, the layout of anchor plates inside a typical containment vessel can be seen in Fig. 1.2. The dimensions of these anchor plates normally vary between 100-500 mm and they can be anchored to the concrete through different type of anchors. Because of the uprate, most of these anchor plates have to be verified for the new loads from the piping systems affected by the uprate.

No existing design code for anchorage to concrete is available in Sweden, hence design codes from the US have often been used. In some cases the old anchor plates are not sufficient when the new loads are applied in accordance to design methods. Therefore, there is a need to investigate the amount of conservatism included in the design methods which are often based on empirical equations. Furthermore, a European technical specification has recently been published, which in the future is planned to become an European standard. Hence, the anchor plates have to be verified against the design procedures given in the European technical specification.

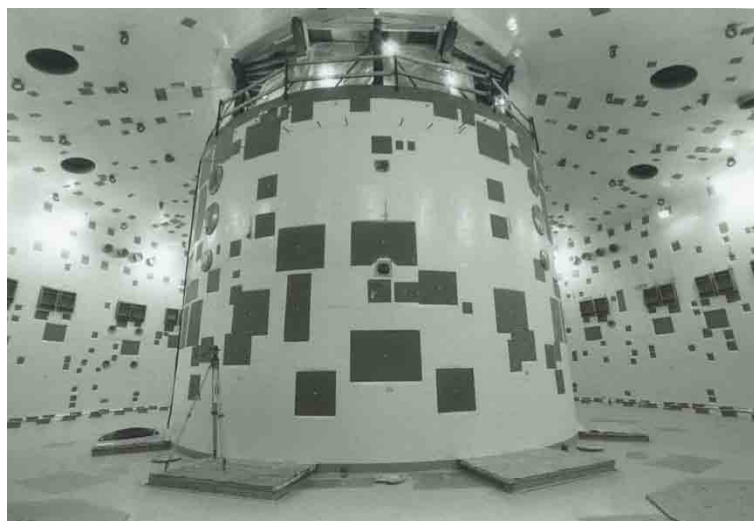


Figure 1.2: Anchor plates inside a typical nuclear containment vessel during the construction phase.

1.2 Aims and scope of the thesis

The aim of this master thesis was to do a capacity assessment of anchor plates located at nuclear facilities through numerical analysis. The examples chosen in this thesis are from the nuclear facility at Forsmark in Sweden. The numerical analyses were performed through the use of the finite element method, where the main analysis tool was the commercial software ABAQUS. Some of the analyses were also performed with the software ADINA, to compare the results from the two programs. A purpose of this thesis was to examine whether the two finite element programs are able to describe the common concrete failure modes associated with anchorage to concrete; mainly concrete cone failure. For the capacity assessment, mainly two types of anchor plates were studied; one plate anchored to the concrete through headed studs and one general design of post-installed anchor plates. The post-installed plates were assumed to be anchored to the concrete through sleeve-type expansion anchors. The main purpose of the capacity assessment was to investigate whether an overcapacity is present when comparing the numerical results to the results obtained from the design codes. Several load combinations were studied, with the intention to study the interaction between the different loads. With the result form these analyses, failure envelopes were developed to show the convenience of failure envelopes as an aid in the design process. This is especially the case when anchor plates are subjected to complex load combinations.

The theory of the material models used for the numerical analyses are given, as well as some of the other numerical techniques used. The numerical material models were calibrated against experimental data found from the literature, since no experiments were included in the scope of this project. Design calculations were only made according to the upcoming Eurocode SIS-CEN/TS 1992-4 (2009), but the methods included in it are also compared to the ones in the US design code ACI 349-6 (2007). Further, the analyses only cover the case of uncracked and unreinforced concrete. Most of the analyses were performed as static load cases, but to show that dynamic load cases can be analysed through the finite element method, a few dynamic load cases are presented as well. The static load cases were limited to cover tensile loads, bending moments and combinations of the two, as well as moments in two perpendicular directions.

1.3 Structure of the thesis

To give an overview of the structure in the thesis, the contents of the respective chapter are given below.

In chapter 2, the most commonly used anchor types are briefly presented. Followed by a description of the different failure modes that are associated with anchorage to concrete, with an emphasis on the concrete cone failure.

The numerical methods used, are presented in chapter 3 together with a short de-

scription of concrete as a structural material. First the basic concepts of the non-linear material models used to describe concrete are explained. Then the material models from ABAQUS and ADINA, used for the analyses in this thesis, are presented. At last, the explicit time integration scheme used to solve the problems is explained.

In chapter 4, the most relevant design procedures from SIS-CEN/TS 1992-4 (2009) are presented. These are compared to their corresponding methods in ACI 349-6 (2007), although no equations from the later is given. The general design code, DRB:2001 (2002), that controls the construction of nuclear facilities in Sweden is then introduced to give the reader an overview of aspects associated with nuclear facilities.

To verify the numerical material models, a series of verification examples are given in chapter 5. These include a notched unreinforced concrete beam, a single headed stud and a single sleeve-type expansion anchor. Parametric studies are performed in order to calibrate the material models.

In chapter 6, the result from the analyses of the chosen anchor plates are presented and discussed. As previously mentioned, the results include static load cases, from which failure envelopes are developed and presented, and a few dynamic load cases.

The conclusions from this study are presented in chapter 7 together with suggestions for further research.

@Seismicisolation

Chapter 2

Anchorage to concrete

There are many different types of fastening systems used for anchorage to concrete, both cast-in-place and post installed systems. These systems transfer and distribute loads from the various equipment anchored to the concrete. This is usually achieved through three different types of load transfer mechanisms, or a combination of them.

- Mechanical interlock.
- Frictional interlock.
- Chemical bond.

Mechanical interlock transfers the load through a bearing interlock between the fastener and the concrete. Load transfer through friction is accomplished by applying a radial expansion force between the fastener and the concrete, which results in frictional forces in the tangential direction. The chemical bond appears after a chemical reaction which creates an adhesive bond between the fastener and the concrete. The three different load transfer mechanisms can be seen in Fig. 2.1 (Eligehausen et al., 2006).

In this thesis the emphasis will be on fasteners which utilise mechanical and frictional interlock, from now on called mechanical fasteners. Despite this, the most commonly used fasteners are briefly presented in this chapter. Then, the different failure modes associated with anchorage to concrete, due to tensile and shear loads, are explained. In this thesis, no difference is made between the words anchors, bolts, fasteners and studs unless nothing else is specified, although a difference is made in some of the literature.

2.1 Different fasteners

Fig. 2.1 shows the three different load transfer mechanisms for fasteners commonly used for anchorage to concrete. The most commonly fasteners are described below.

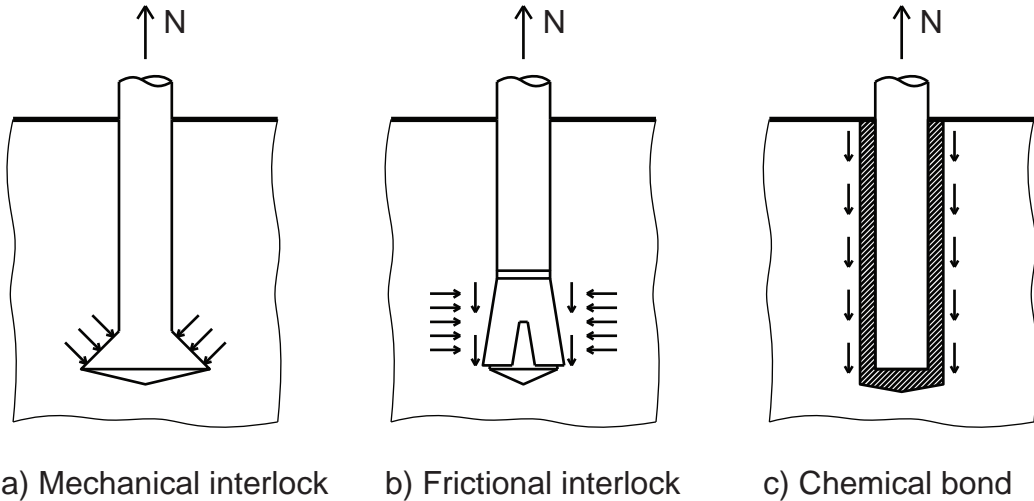


Figure 2.1: The most common load transfer mechanisms of fasteners.

Headed studs The studs are commonly welded to a steel plate, which is attached to the formwork and cast into concrete. The load is transferred to the concrete by a mechanical interlock between the steel plate and the concrete (Eligehausen et al., 2006).

Undercut anchors Like the headed studs, the undercut anchors develop a mechanical interlock to the concrete, even though they are post-installed. To accomplish this interlock, a cylindrical hole with a notch in the bottom is drilled. Once the anchor is inserted into the hole, the bearing element of the anchor unfolds in the notch and the mechanical interlock is developed. There are other types of undercut anchors which are not mentioned in this thesis, for example of other types see Eligehausen et al. (2006). Fortunately the fundamental mechanics of these types are just the same as for the aforementioned type (Eligehausen et al., 2006).

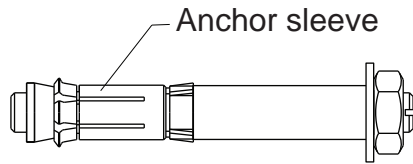


Figure 2.2: A typical design of an undercut anchor.

Screw anchors The screw anchor develops a mechanical interlock to the concrete through the threading of the screw. To allow the thread to penetrate the concrete, the screw material is hardened and installed in a drilled hole. The drilled hole is usually deeper than the length of the screw, in order to provide space for the decay products of the thread-cutting process (Eligehausen et al., 2006).

Mechanical expansion anchors The mechanical expansion anchors interact with the concrete mainly through a frictional interlock. The expansion anchors can be divided into two different groups.

- Torque-controlled.
- Displacement-controlled.

Both type of expansion anchors develop the frictional interlock through an expansion sleeve. For the torque-controlled expansion anchor, this is achieved by drawing one or more cones into the expansion sleeve, as the torque is applied. The cones forces the expansion sleeve to expand against the concrete and the frictional interlock is developed. For the displacement-controlled anchors a cone is either driven into the expansion sleeve or the expansion sleeve is driven onto an expansion cone. This is accomplished by the use of a setting tool and a hammer, hence they are named displacement-controlled (Eligehausen et al., 2006).

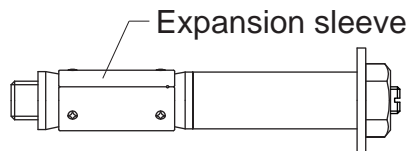


Figure 2.3: A typical design of torque-controlled sleeve-type expansion anchor.

Bonded anchors Many different bonded anchor systems are available, similar for all of them are that they interact with the concrete through a chemical interlock. There are mainly two different types of systems.

- Capsule anchors.
- Injection anchors.

The capsule anchors consist of a capsule containing the bonding material, which during the installation is crushed. This enables the bond material to leak out in the pre-drilled hole and create a chemical bond between the base material and the anchor. For the injection system the bond material is injected into a pre-drilled hole. When the anchor is inserted into the same hole, a chemical interlock is developed between the anchor and the concrete. The bonding materials are of course also of different types, but usually consist of polymer resins, cementitious materials or a combination of the both (Eligehausen et al., 2006).

2.2 Failure modes

As mentioned above, the emphasis in this thesis is on mechanical fasteners. Therefore, only the failure modes associated with the mechanical fasteners are presented in this section.

2.2.1 Tensile load

Five different types of failure modes are normally related to mechanical fasteners loaded in tension, they are all depicted in Fig. 2.4. The emphasis of this section is on concrete cone failure, since all of the analyses performed in this thesis are assumed to fail primarily in concrete cone failure. While the other failure modes are only described briefly.

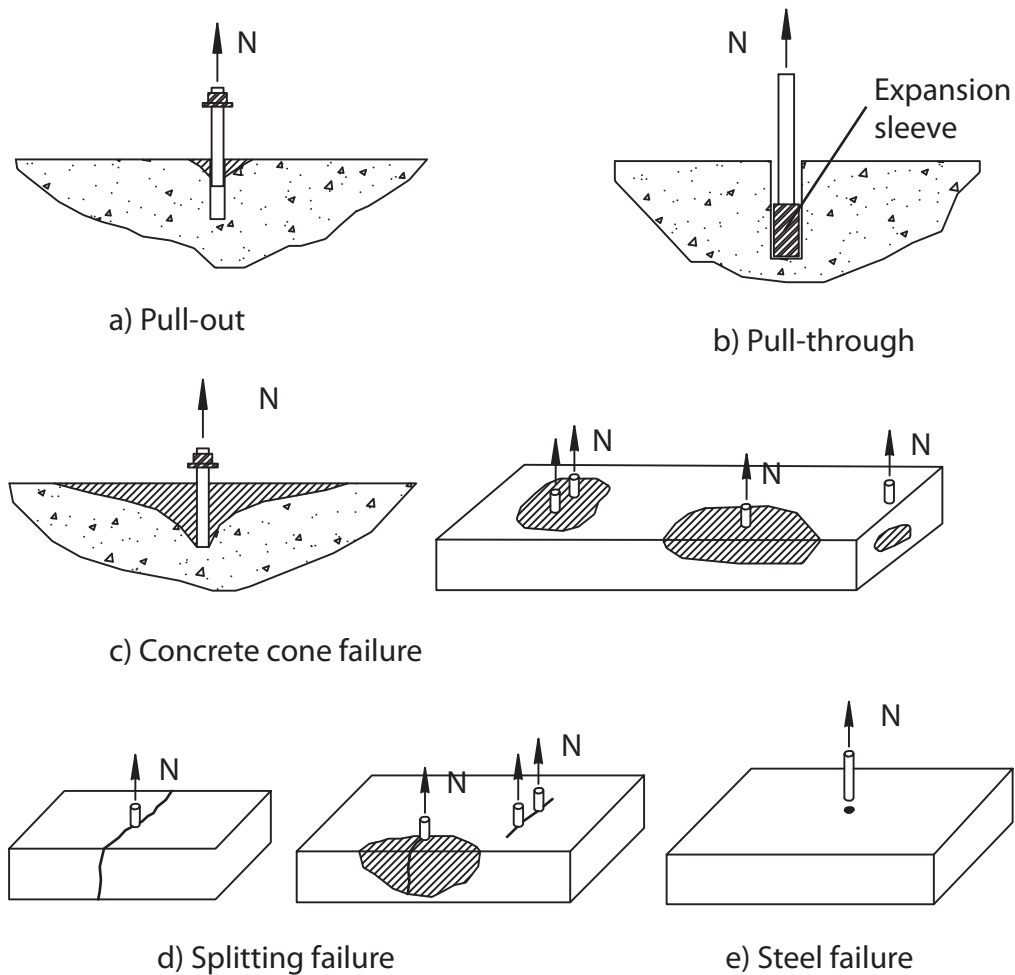


Figure 2.4: Failure modes associated with tensile loading of mechanical fasteners.
Reproduction from (Eligehausen et al., 2006).

Steel failure Steel failure occurs when the maximum capacity of the steel, loaded in tension, is reached while the concrete remains undamaged. This is a ductile failure mode and is rarely observed for mechanical fasteners, unless the embedment depth is very deep (Eligehausen et al., 2006).

Pull-out and pull-through failure The pull-out failure mode is a failure where the anchor is pulled out of the hole. For a headed anchor, this implies that the

pressure between the head and the concrete becomes higher than the compressive strength of the concrete. As the anchor is pulled out of the hole the, surrounding concrete is damaged, but only in the vicinity of the anchor. This failure mode can be avoided by enlarging the bearing area, i.e. using a larger head. For fasteners such as the mechanical expansion anchors, the pull-out failure mode is bit different. Since there is no head developing the mechanical interlock with the concrete, the pull-out starts when the tensile force becomes larger than the friction force between the concrete and the fastener. Therefore, there is no major crushing of the concrete associated with the pull-out failure mode of a non-headed fastener. The fastener instead slides out of the hole. For expansion anchors with an expansion sleeve, pull-through failure may occur. A pull-through failure implies that the expansion cone is pulled through the expansion sleeve (Eligehausen et al., 2006).

Splitting failure The splitting failure implies that the concrete member, which the fastener is anchored to, splits because of a propagating crack. This often occurs when the concrete member is relatively small in comparison to the fastener, if the fasteners are installed in a line close to one another, or if the fastener is installed close to an edge. The failure load associated with the concrete cone failure is normally larger than the splitting failure load. Nevertheless, it is important to keep this failure mode in mind when designing anchorage to concrete (Eligehausen et al., 2006).

Concrete cone failure Concrete cone failure is characterised by a concrete break-out body, shaped like a cone. The full tensile capacity of the concrete is used when failure occurs through concrete cone failure. This failure mode is fairly common for many type of fasteners, as long as the steel capacity of the fastener is not exceeded. Fasteners which utilise mechanical interlock with the concrete exhibit concrete cone failure, given that the bearing area is large enough so that pull-out failure do not occur. If the fasteners works through frictional interlock, it fails due to concrete cone failure if the expansion force is large enough and pull-through failure do not occur. For fasteners that employ chemical bond, concrete cone failure in its pure form only occurs for fasteners with small embedment depth. As the embedment depth increases the failure changes to a mixed-mode failure, with a shallow cone failure close to the surface and bond failure over the rest of the embedment depth. There are many aspects that may alter the shape and capacity of the cone failure. For example, a group of fasteners placed closely, joined together and loaded in tension may result in a reduced failure load compared to the load obtained if the failure loads of all the single fasteners are summarised. This occurs since the cone break-out bodies of each fastener intersect, leading to a reduced size of the resulting break-out body. If a fastener is placed close to an edge and loaded in tension, the concrete cone may not fully develop before the crack reaches the edge of the concrete member. This failure is called blow-out, and is related to the cone failure. It normally exhibits a lower failure load than the fully developed concrete cone. More of these kind of aspects will be given in chapter 4, where the design methods are explained (Eligehausen et al., 2006).

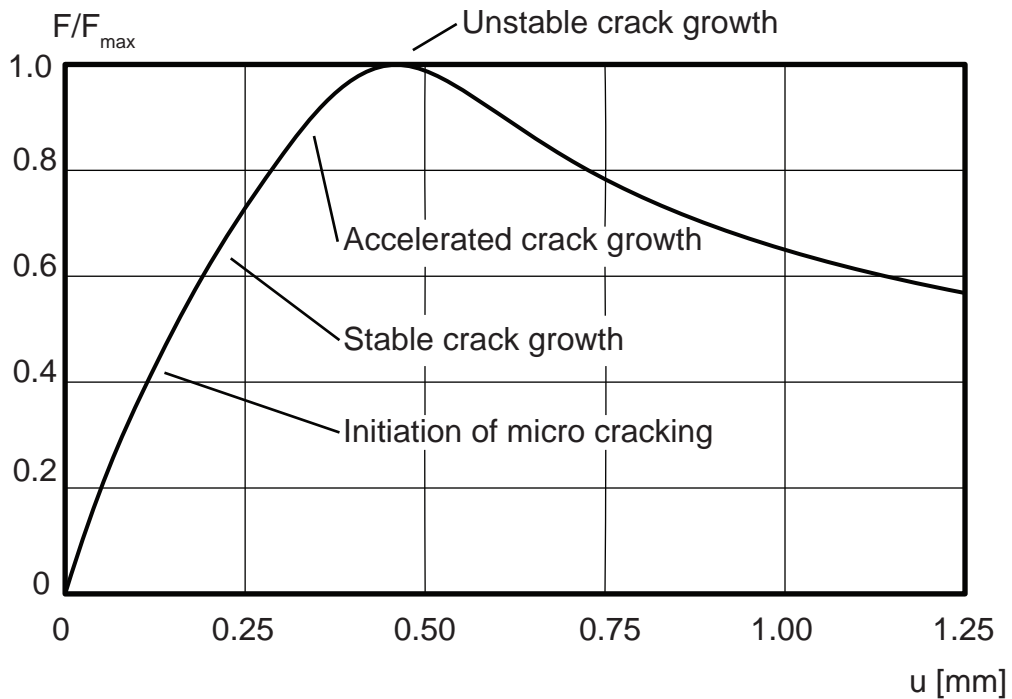


Figure 2.5: Typical load–displacement curve of a single headed stud failing due to concrete cone failure. Reproduction from (Eligehausen et al., 1989).

The development of a concrete cone can be seen in Fig. 2.5, which describes a typical load-displacement curve for a headed stud loaded in tension. The failure starts with the initiation of micro cracks in the circumference of the head, which then develop into discrete cracks as the load increases. The crack growth is stable up to loads close to the peak load where the crack growth accelerates and becomes unstable. The peak load is reached for a relative crack length of 25–50 % of the crack length of the final cone, depending on the embedment depth.

Experimental studies have shown that the slope of the fracture surface of the cone is not constant over the depth or the circumference of the fastener. It also varies from test to test. At an average, the angle measured from the horizontal plane lies between 30° and 40° . This angle can be seen in Fig. 2.6 which shows a typical cone shaped break-out body. The angle also tends to increase with increasing embedment depth. Compressive stress acting perpendicular to the load increases the angle, while tensile stress decreases the angle (Eligehausen et al., 2006).



Figure 2.6: Concrete break-out cone. Photo from the test series presented in Nilsson and Elfgren (2009).

Since the concrete cone failure depends on the tensile behavior of concrete, many investigations have been made on how it is influenced by the macroscopical material properties of concrete. One such study was made by Ozbolt (1995) through numerical analyses. Two cases were considered, one with constant fracture energy while the tensile strength was varied and one with constant tensile strength while the fracture energy was varied. The remaining variables, such as embedment depth, were kept the same in all analyses. It was shown that the tensile strength of concrete do not significantly affect the failure load of the concrete cone failure, see Fig. 2.7(a). However, the failure load appeared to have strong dependence on the fracture energy, see Fig. 2.7(b), i.e. the post failure behavior of concrete. Among others, the same conclusions have been drawn by Eligehausen and Clausnitzer (1983) through numerical studies and Sawade (1994) through experimental studies.

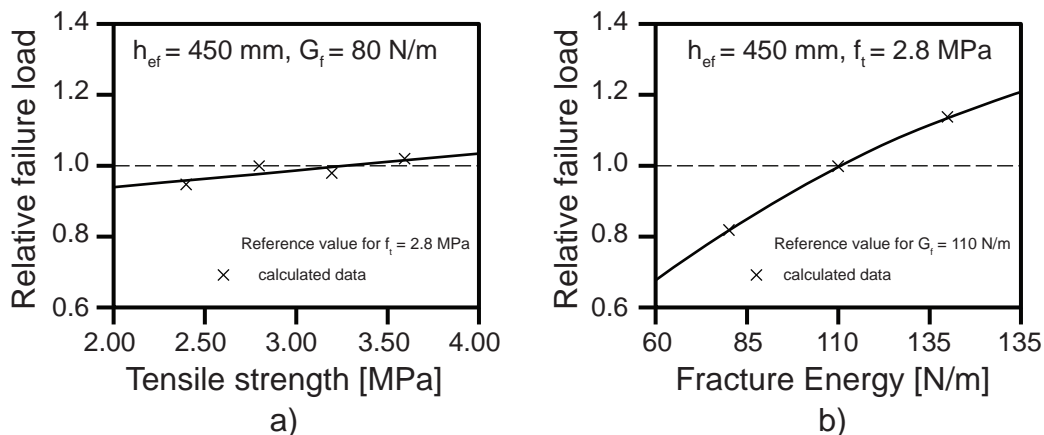


Figure 2.7: Numerical study on the effect of material properties on concrete cone failure. Reproduction from (Ozbolt, 1995).

In Eq. (2.1) the general form of an empirical equation for approximating the concrete cone failure load F_u of a single fastener can be seen. It is derived from numerous test results of headed studs, expansion anchors and undercut anchors (Eligehausen et al., 1989).

$$F_u = a_1 \cdot (f_c)^{a_2} \cdot (h_{ef})^{a_3} \quad [\text{N}] \quad (2.1)$$

The expression $(f_c)^{a_2}$ is a convenient way of representing the tensile strength with the compressive strength f_c , which is a value normally used for design applications. In the equation f_c should be given in [MPa]. A typical value for a_2 is 0.5. The expression $(h_{ef})^{a_3}$ takes into account how the embedment depth h_{ef} influences the failure load. In the equation h_{ef} should be given in [mm]. A typical value of a_3 is 1.5, which implies that the failure load do not increase proportionally to the area of the failure surface. The factor a_1 is used to calibrate the equation and to ensure dimensional correctness (Eligehausen et al., 1989).

Another equation for calculating F_u is proposed in Eligehausen et al. (1989), which is analytically derived for a headed stud through the use of linear fracture mechanics. It assumes that the failure surface of the cone is axisymmetric and discrete. The equation is given in Eq.(2.2) and can be used to calculate the entire load curve of the cone failure.

$$F_u = \sqrt{E \cdot G_f} \cdot h_{ef}^{1.5} \cdot f(a/l_b) \quad [\text{N}] \quad (2.2)$$

where,

- E is the elastic modulus [GPa]
- G_f is the fracture energy [Nm/m^2]
- a is the current length of the failure surface [mm]
- l_b is the final length of the failure surface of the cone [mm]

The factor $f(a/l_b)$ depends on the crack length, for a cone with an angle of 37.5° the failure load is reached for an relative crack length $a/l_b = 0.45$. The factor then assumes the value 2.1.

Fig. 2.8 shows a comparison between Eq.(2.1) and Eq.(2.2) with different embedment depths, for the values $a_1 = 15.5$, $a_2 = 0.5$, $a_3 = 1.5$ and $f(a/l_b) = 2.1$, along with experimental results. It can be seen that both equations agree quite well with the experimental results. Although, as stated above, the failure load of the concrete cone failure depends on the fracture energy, Eq.(2.1) has been chosen for the design methods described in section 4.1.2. The reason is that the fracture energy is a difficult parameter to determine and that it is not normally used in typical design calculations. While on the other hand, the compressive strength of concrete is a widely used material properties and is fairly easy to determine.

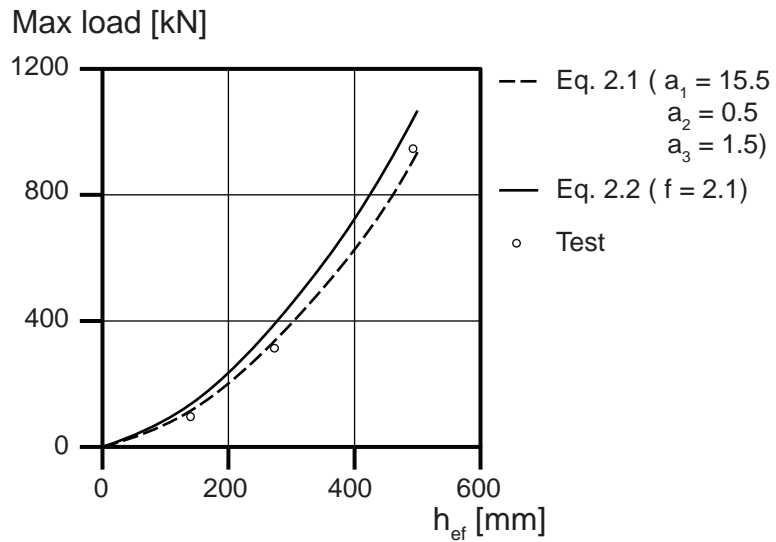


Figure 2.8: Comparison of different equations for approximating the failure load of concrete cone failure. Reproduction from (Eligehausen et al., 1989).

2.2.2 Shear load

There are primarily four different failure modes associated with shear loading of mechanical fasteners. They are all discussed below and depicted in Fig. 2.9. In some cases these failure modes are preceded by crushing of the concrete close to the surface in front of the fastener. This is called concrete spalling, see Fig. 2.9a), if the embedment depth of the fastener is shallow the ultimate failure may be governed by this phenomenon (Eligehausen et al., 2006).

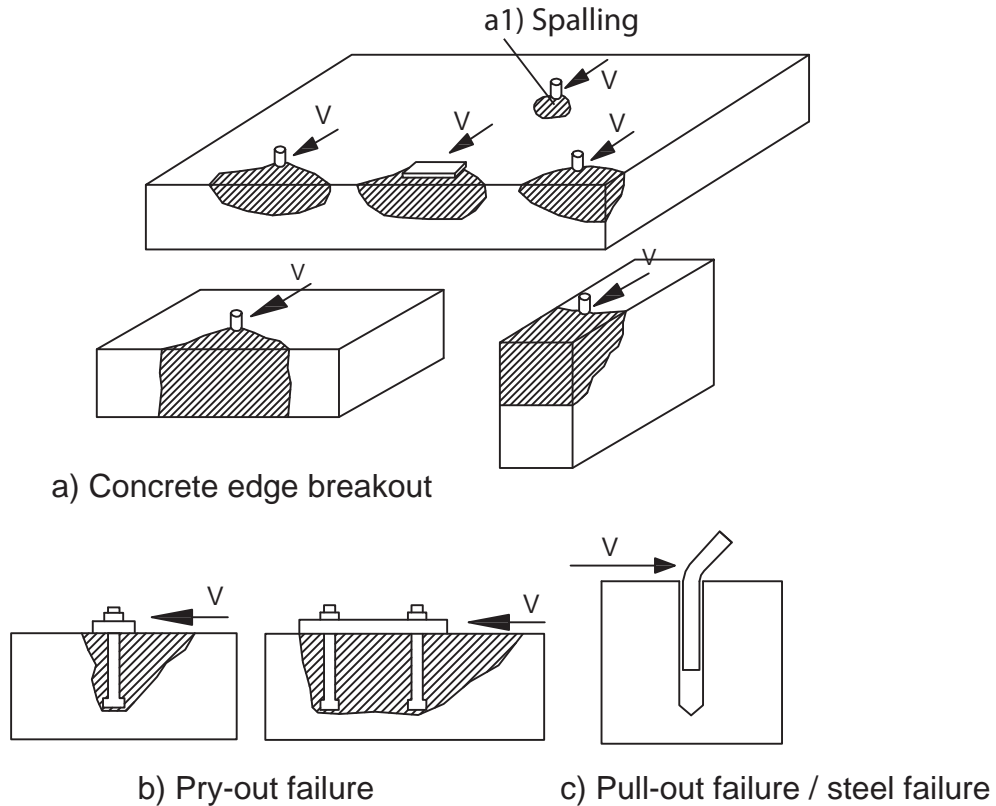


Figure 2.9: Failure modes associated with shear loading of mechanical fasteners. Reproduction from (Eligehausen et al., 2006).

Steel failure Steel failure is always preceded by concrete spalling and represents the upper capacity limit of a fastener failing due to shear loads. Given that the embedment depth is large enough and that the steel is strong enough, the fastener may be able to resist additional loading after concrete spalling has occurred. After concrete spalling has occurred, the lever arm between the load application point and the bearing resultant is increased. This results in increasing flexural stresses in the fastener, which ultimately fails due to bending in combination with shear and tensile stresses (Eligehausen et al., 2006).

Concrete edge failure Anchors close to an edge and subjected to a shear load perpendicular to the edge, may result in a concrete edge failure. The shape of this failure is semi-conical and depicted in Fig. 2.9a). The fracture surface propagates from the fastener towards the edge at an angle of approximately 35° . This failure mode is similar to the concrete cone failure due to tensile loading. There are a few aspects which may reduce the failure load substantially. It is possible for a group of fasteners, loaded in shear, to develop a common failure mode shaped like a cone. This will, as mentioned above, significantly reduce the failure load in comparison to the sum of the single fasteners in a group loaded in shear. The failure load will also be reduced for fasteners located near a corner or for fasteners installed

with limited depth and for fasteners with adjacent edges parallel to the shear load direction (Eligehausen et al., 2006).

Pry-out failure Anchors subjected to shear loads may, if the embedment depth is relatively small, start to rotate as the load is applied. This means that a pry-out fracture surface develops behind the anchor, see Fig. 2.9b). The pry-out failure mode does not require a free edge in the vicinity of the anchor. A group of anchors may develop a common pry-out failure mode which often results in a reduced failure load compared to that of a single anchor in a group (Eligehausen et al., 2006).

Pull-out failure This failure mode is almost only valid for expansion anchors, and develops if the frictional forces between the anchor and the concrete are not sufficiently large, see Fig. 2.9c) (Eligehausen et al., 2006).

@Seismicisolation

Chapter 3

Finite element modelling of concrete

In this section, a few different aspects concerning finite element modelling of concrete encountered during this study are presented. These include the concrete material models used to describe the structural behaviour of concrete and the different time integration schemes used to solve the problems. First a short description on concrete as a structural material is given.

3.1 Nonlinear behaviour of concrete

Concrete is a composite material, the material matrix consists of aggregates enclosed by cement paste. Mechanically, concrete is considered to be a homogenous and isotropic material, given that the sample looked upon is considerably larger than the aggregate. For normal concrete, the strength is determined by the cement paste and the bond between the cement paste and the aggregate. The aggregate itself is often very strong and only affects the properties of the concrete indirectly. One of the main characteristics of concrete is the difference in ability to resist tensile and compressive stresses; normally the tensile strength is approximately a tenth of the compressive strength. Another important behaviour is its brittle failure due to tensile loading, in which no plastic deformation nor lateral contraction precedes the failure. Both the aggregate and the cement paste are more brittle than the concrete; this is because the crack is forced to propagate around the aggregate (Björnström et al., 2006).

Since concrete is a composite material, it is not possible to describe a general behaviour of concrete. There are many ways to alter its behaviour, for example with chemical agents to obtain a stronger concrete or with polymer fibers to obtain a more ductile behaviour. The concrete described in this section is to be considered as “normal” concrete.

Tension Until tensile failure is reached, concrete is in most material models assumed to act linear elastic, although some minor plastic deformation occurs. The cracking of concrete is initiated by the formation of micro cracks, see Fig. 3.1. These

start to develop when the stress is close to the tensile strength of the material. When the tensile strength is reached the micro cracks start to localize to a limited area called the fracture process zone, thereafter micro cracking only occurs within this zone. As the deformation increases, the micro cracks in the fracture process zone increase in number and start to merge with each other. This lead to lower stresses in the fracture process zone and the material exhibits a softening behaviour. The ultimate failure occurs when the micro cracks eventually merge into a real crack that splits the fracture process zone (Björnström et al., 2006).

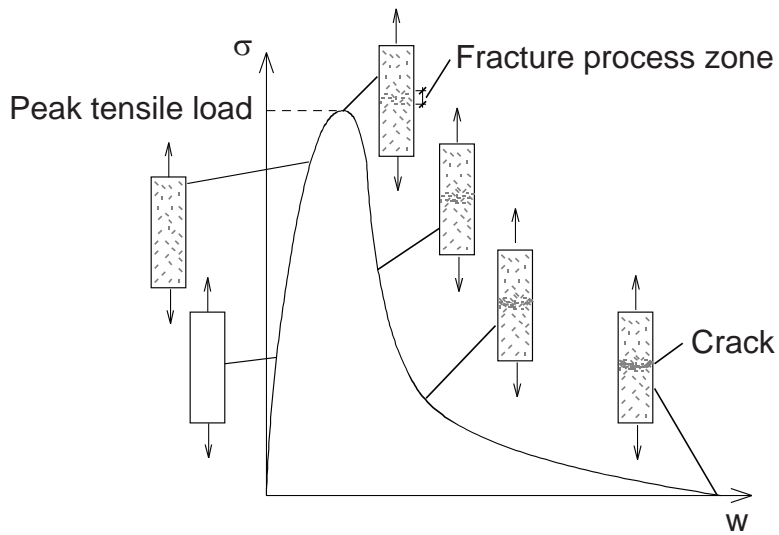


Figure 3.1: Development of a macro crack under uniaxial tensile loading. Reproduction from (Malm, 2006).

Compression The compressive failure of concrete under low confining pressure is also of a brittle nature but the failure becomes more ductile as the concrete is subjected to a higher confining pressure. As the confining pressure increases so does the compressive strength. If the concrete is subjected to a pure hydrostatic pressure, no peak strength can be observed. Under uniaxial compressive loading, concrete acts linear elastic up to approximately 30-60 % of its compressive strength. After that, some small plastic deformation starts to occur due to bond cracks between the aggregate and the cement paste. This leads to a degradation of the stiffness of the material. When the peak load is reached, the increasing number of bond cracks leads to cracking of the material matrix. This leads to a softening response until the material is completely crushed (Malm, 2006). A typical stress-strain curve for the compressive behaviour of concrete can be seen in Fig. 3.2.

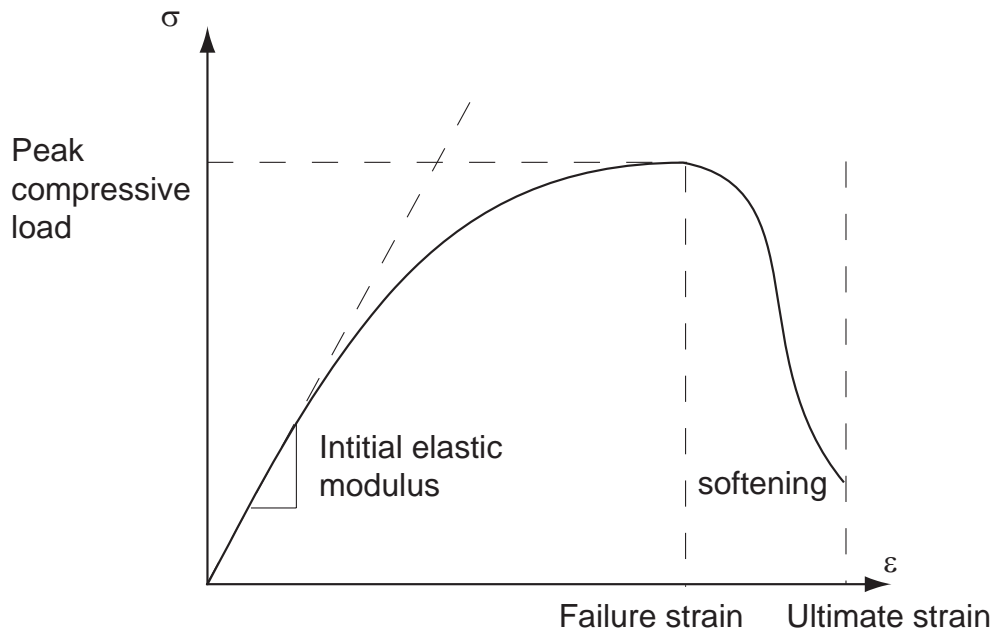


Figure 3.2: Typical uniaxial compressive behaviour of concrete. Reproduction from (Malm, 2006).

Multiaxial behaviour A typical biaxial failure envelope for concrete under a plane stress state is shown in Fig. 3.3. It can be seen that tensile cracking occurs in the first, second and fourth quadrant. The direction in which the crack occurs is determined by the principal tensile stress; a crack grows perpendicular to the principal tensile stress. The third quadrant describes a state of biaxial compression. From the figure it can be seen that the compressive stress increases significantly under biaxial compression; up to 25 % of the uniaxial compressive strength. It can also be observed that a state of simultaneous compression and tension (second and fourth quadrant) reduces the tensile strength (Malm, 2006).

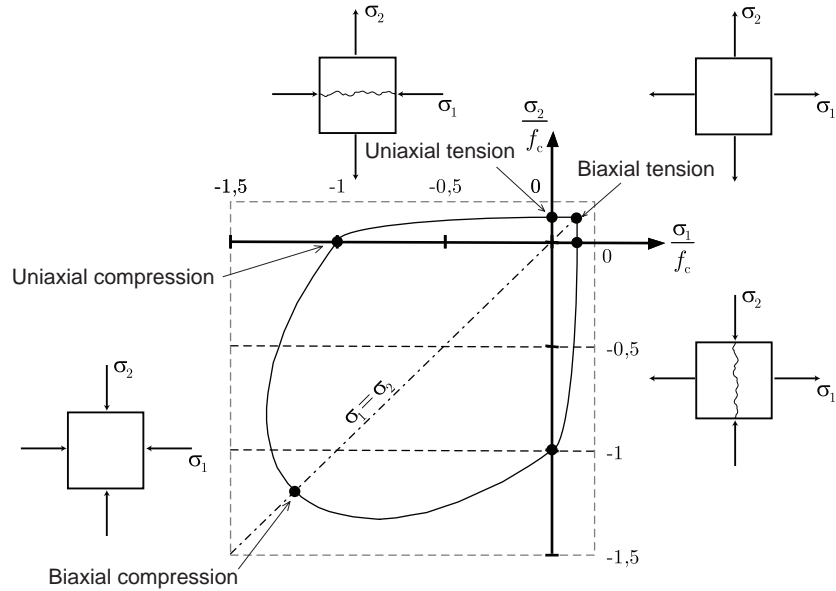


Figure 3.3: Yield surface of concrete for plane stress conditions. Reproduction from (Malm, 2006).

Under triaxial compressive loading, the failure involves either tensile cracks parallel to the maximum compressive stress or a shear failure mode. Concrete subjected to triaxial compression exhibits a major increase in ductility and strength, compared to a state of uniaxial compression (Wight and MacGregor, 2009).

3.2 Concrete material models

Numerous material models for concrete have been developed during the years and most of the commercial finite element software available today has its own material model for concrete. Although different from each other, most of them are based on a combination of non-linear fracture mechanics, plasticity theory and/or damage theory. In this thesis two different material models are used; the Concrete Damaged Plasticity model in ABAQUS and the Concrete material model in ADINA. The theory and concepts of these two material models are described below.

3.2.1 Basic concepts

Fracture mechanics The post tensile failure behaviour of concrete is often described by fracture mechanics. According to fracture mechanics, failure can occur through three different failure modes or combinations of them. The failure modes can be seen in Fig. 3.4, they are tensile (mode I), shear (mode II) and tear (mode III). For concrete, mode I is the only failure mode which can occur in its pure form.

Mode III is very rare but a combination of mode I and II is often observed for concrete (Malm, 2006).

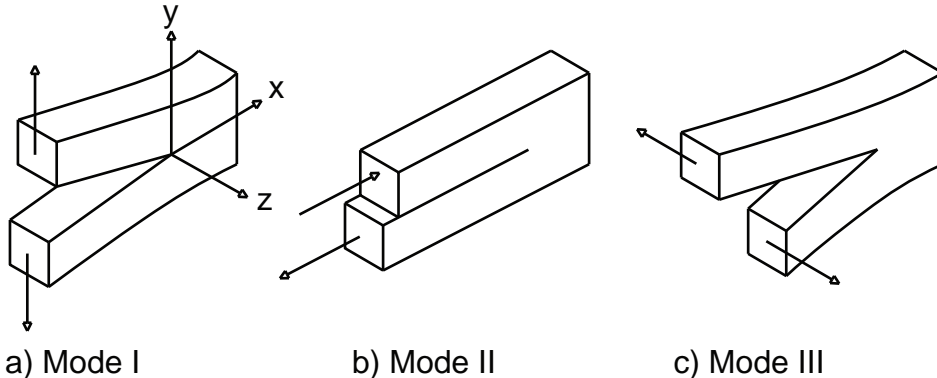


Figure 3.4: The three different failure modes of fracture mechanics. Reproduction from (Björnström et al., 2006).

To determine whether a crack initiates and propagates, the fracture energy G_f of the material has to be considered. Each of the above mentioned failure modes have its own fracture energy. The fracture energy is a material property, which describes the energy consumed when a unit area of a crack is completely opened.

In linear elastic fracture mechanics, failure (mode I) is considered to be reached when the maximum principal stress σ_1 equals the tensile strength f_t of the material. In this approach a crack is considered to be fully opened when failure is reached, i.e. no softening behaviour. Another way of explaining this is that the elastic strain energy built up in the material, which would be released if unit area of a crack were to open, has to be greater than the materials fracture energy. This is the simplest form of fracture mechanics and it is only valid if the material is linear elastic and the crack tip is sharp, which is not the case for concrete (Björnström et al., 2006).

To be able to describe the tensile behaviour of concrete, a non-linear fracture mechanic approach has to be adopted. There are basically two different concepts to achieve this; the discrete crack approach and the crack band approach, often called the smeared crack approach (Elfgren, 1989). Since both of the material models used in this study are most similar to the smeared crack concept, the discrete crack approach is only briefly mentioned.

A crack in the discrete crack model either splits an element in two or divides the nodes of two elements. There are many different discrete crack models, but the fundamentals of them are often similar. The first developed models were based on a principle called cohesive cracks, which is similar to linear elastic fracture mechanics. The difference is that a tension softening behaviour has been incorporated into the model, see Fig. 3.5. This is accomplished by defining the fracture process zone as a fictitious crack ahead of the pre-existing macro crack. The fictitious crack is made of cohesive elements, which lose their stress transferring ability as the crack opening displacement w increases, i.e. the material softens. A stress-displacement relation is used to describe this softening behaviour; the area under the softening

curve represents the fracture energy. The thickness of the fracture process zone is assumed to be negligible, hence the name discrete crack (Elfgren, 1989).

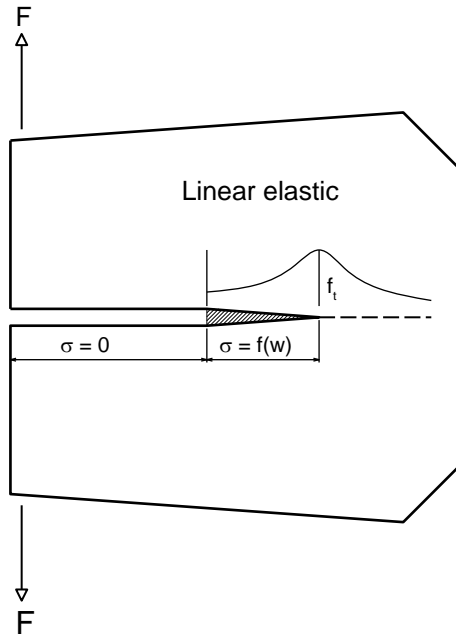


Figure 3.5: Discrete crack model with tension softening. Reproduction from (Elfgren, 1989).

In the smeared crack approach, the fracture process zone is assumed to exist over a finite width h , for example the size of a finite element, called a crack band. When a crack occurs, the elements within this crack band lose their stiffness as described by the softening curve of concrete shown in Fig. 3.1. Since the crack occurs over a finite width, the softening curve has to be described as a stress-strain relation. This strain softening curve is dependant on the chosen width of the crack band; a wider crack band results in a steeper strain softening curve, which may lead to an unstable model. The inelastic crack opening strain ε , is related to the crack opening displacement w and the fracture energy as $\varepsilon = w/h$ (Elfgren, 1989). When the tensile strength f_t is reached, a crack is initiated perpendicular to the maximum principal stress direction. This has the implication that the isotropic material is changed to an orthotropic material. As the crack starts to propagate, there are two different concepts to determine the direction of the propagation; fixed and rotating cracks. The differences between the two are explained below and can be seen in Fig 3.6.

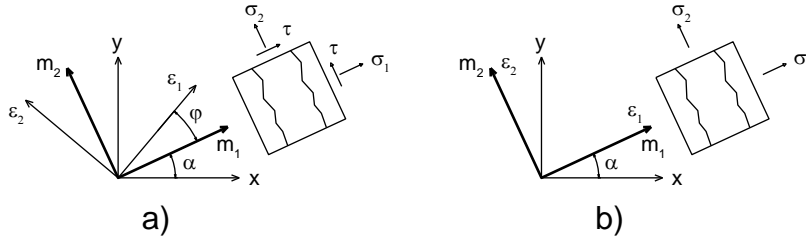


Figure 3.6: Example of a) a fixed crack model and b) a rotated crack model. Axes x and y represent the local coordinate system. The axis m_1 is the weak material direction while m_2 is the strong material direction. The axis m_1 is always perpendicular to the crack. Reproduction from (Malm, 2006).

In the fixed crack approach the direction of the crack never changes, even if the principal stress direction does. If the principal stress direction changes, shear stress is induced on the crack faces. To avoid unrealistic results a shear retention factor is introduced to the model, which reduces the shear modulus as the crack opening strain increases. A typical formulation for a fixed crack model, including both tension softening and shear retention, is given in Eq. (3.1) (Elfgren, 1989).

$$\begin{bmatrix} \Delta\sigma_{11} \\ \Delta\sigma_{22} \\ \Delta\sigma_{12} \end{bmatrix} = \begin{bmatrix} \frac{\mu E}{1 - \nu^2 \mu} & \frac{\nu \mu E}{1 - \nu^2 \mu} & 0 \\ \frac{\nu \mu E}{1 - \nu^2 \mu} & \frac{\mu E}{1 - \nu^2 \mu} & 0 \\ 0 & 0 & \beta G \end{bmatrix} \begin{bmatrix} \Delta\varepsilon_{11} \\ \Delta\varepsilon_{22} \\ \Delta\varepsilon_{12} \end{bmatrix} \quad (3.1)$$

where,

- μ is the parameter that controls the tension softening.
- β is the shear retention factor.
- σ is the stress in different directions.
- E is the elastic modulus.
- G is the shear modulus.
- ν is the Poisson's ratio.

In the rotated crack approach the direction of the crack changes as the principal stress direction change and the two always coincide. The direction of the rotated crack is always perpendicular to the tensile principal stress. The result of this is that no shear stress is induced on the crack faces, i.e. there is no need for shear retention. Instead an implicit shear modulus has to be calculated to keep the co-axiality between the principal stress and strain (Elfgren, 1989). It has been shown by Malm (2006) that rotated crack models sometimes overestimate the capacity of the analysed structure and yields results far from the expected; especially for reinforced concrete structures.

Plasticity theory Although normally used for ductile materials, such as metals, plasticity theory can also be used as an approximation of the behaviour of brittle

materials under certain circumstances. As to concrete, plasticity theory has been successful in describing its behaviour in compression, but for problems including tension and shear it often face difficulties. Thus, the procedure is often to let plasticity theory describe the compression zone, while tensile stresses are described with fracture mechanics. However, constitutive models derived from plasticity theory have been developed that govern the entire non-linear behaviour of concrete, including failure due to either tension or compression. One such model is the plastic-damage model developed by Lubliner et al. (1989), this model serves as the basis for the *Concrete damaged plasticity model* in the commercial finite element software ABAQUS; which is used in this study and described further in section 3.2.2. The classical formulation of plasticity theory is described by three essential parts; a yield criterion, a hardening rule and a flow rule (Lubliner et al., 1989).

The yield criterion is described as a yield surface to account for biaxial and multiaxial effects. The most commonly known yield surface is the von Mises yield criterion, which is suitable for steel materials. For concrete and other brittle materials, a combination of the Drücker-Prager and the Mohr-Coulomb yield criterion is, according to Lubliner et al. (1989), a good approximation of the yield surface. These can be seen in Fig. 3.7 for plane stress condition, compared to the yield surface of concrete. Apart from the yield surface, a failure surface is also needed to define when ultimate failure is reached. Normally the yield surface is defined by the material strength at the point where the material starts to act non-linear, while the failure surface is defined by the ultimate strengths. In pure tension, the failure and yield surfaces coincide since concrete is assumed to be elastic up to the tensile strength (Malm, 2006).

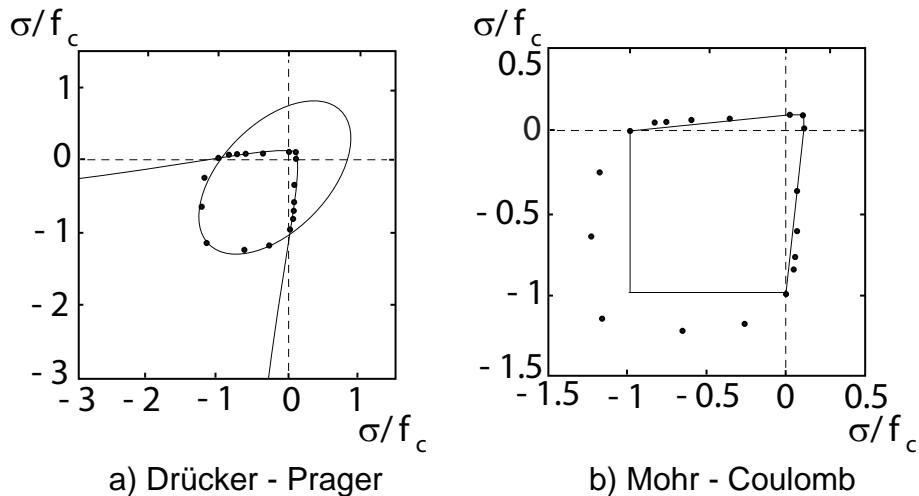


Figure 3.7: Yield surfaces for biaxial conditions. Reproduction from (Malm, 2006).

The hardening rule can be used to describe both the hardening and the softening of concrete, in both tension and compression. The principal idea of a hardening rule is to describe how the stress depends on the plastic strains, i.e. the material behaviour beyond the point of yielding. A hardening rule also introduces history dependence to the material. There are many different hardening rules available; the simplest is

called isotropic hardening. The isotropic hardening describes the plastic behaviour by letting the yield surface increase in size, while its shape remains, see Fig. 3.9. The hardening is in most cases described as perfectly plastic (no increase in stress after yielding), as linearly increasing or as an increasing power law, see Fig. 3.8. The increase in stress with increasing plastic strain is governed by the hardening variable h , which starts to affect the material after the yield stress is reached (Bower, 2009).

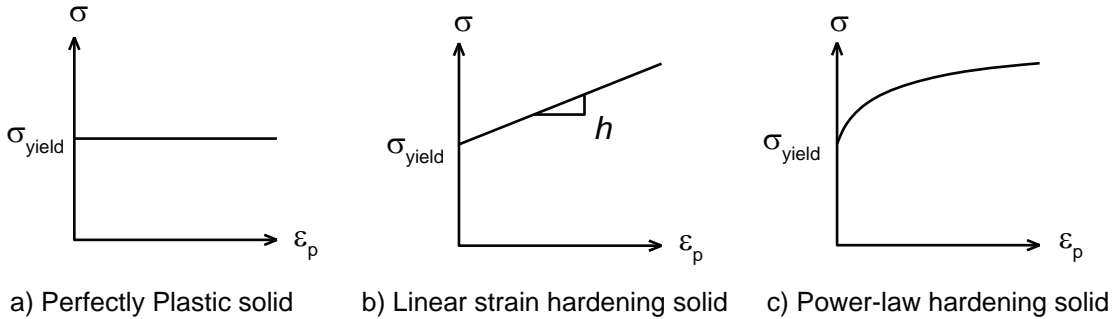


Figure 3.8: Different types of isotropic hardening rules. Reproduction from (Bower, 2009).

When the material is subjected to cyclic loading the isotropic hardening rule is normally not sufficient. Instead a so called kinematic hardening rule is often used. The kinematic hardening rule translates the yield surface in stress space as a result of plastic strains, without changing its shape or size. If the material is deformed due to tension, the yield surface is translated towards the increasing strain i.e. the material hardens in tension. This also has the effect that the material softens in compression. This is schematically shown in Fig. 3.9 (Bower, 2009).

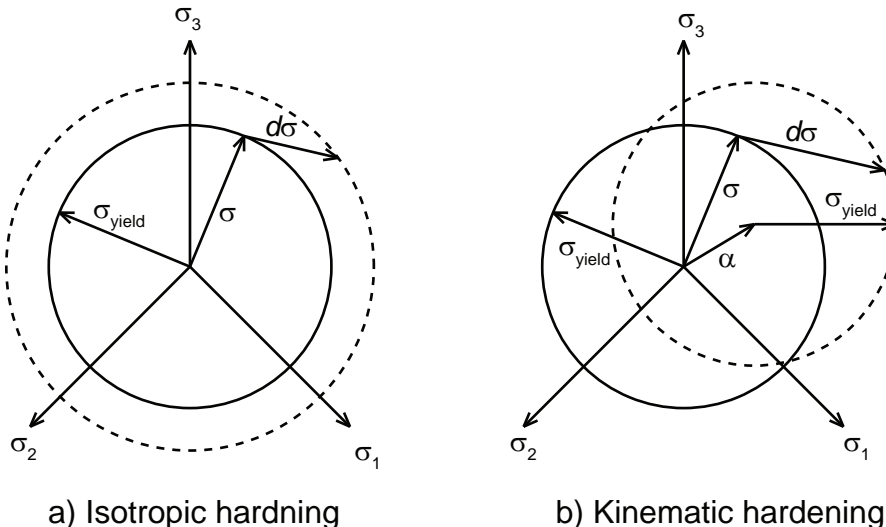


Figure 3.9: Hardening rules. Reproduction from (Bower, 2009).

In Fig. 3.8 and Fig. 3.9 the parameters are as follows,

- σ is stress in an arbitrary direction.
- ε_p is plastic strain in an arbitrary direction.
- σ_{yield} is the yield strength.
- h is the isotropic hardening variable.
- $d\sigma$ is the stress beyond yielding.
- α describes the kinematic hardening.

The last essential part of the plasticity theory is the flow rule. The flow rule determines the relationship between the stress and the plastic strains under multiaxial conditions. Given the current stress and the current state of hardening, the flow rule is used to determine the increase of plastic strain obtained from a small increase of stress. There are many different flow rules available, but most of them can be divided into either associated flow or non-associated flow. An associated flow rule is derived from the yield surface, while a non-associated flow rule uses two separate functions to describe the flow rule and the yield surface (Malm, 2006).

Damage theory The macroscopical behaviour of concrete in damage theory is represented by a set of damage variables which alter the elastic and plastic response of the model. Most damage models are very similar to plasticity theory, with the difference that there is no residual damage after unloading in the material, i.e. no plastic deformation occurs. This is not realistic for concrete and to overcome this limitation, the stiffness reduction from damage theory is often coupled with the plastic deformation from plasticity theory. In this manner some permanent deformation remains after unloading (Malm, 2006).

3.2.2 Concrete damaged plasticity in ABAQUS

Concrete damaged plasticity is one of three available concrete material models in ABAQUS. The two other material models, *Concrete Smeared Cracking* and *Brittle Cracking*, are both based on the smeared crack approach of fracture mechanics. The concrete damaged plasticity model is based on a coupled damage plasticity theory from the models proposed by Lubliner et al. (1989) and Lee and Fenves (1998). Although primarily intended for analysis of concrete, it is also suitable for other quasi-brittle materials such as soils and rocks. Regarding concrete, it can be used to describe all types of structures, both unreinforced and reinforced. It is intended for concrete under no or low confining pressure; concrete under high confining pressure is out of the scope of the material model. The model can be used to analyze structures subjected to monotonic, cyclic and dynamic loading and is available in both ABAQUS/Standard and ABAQUS/Explicit (Hibbit et al., 2010).

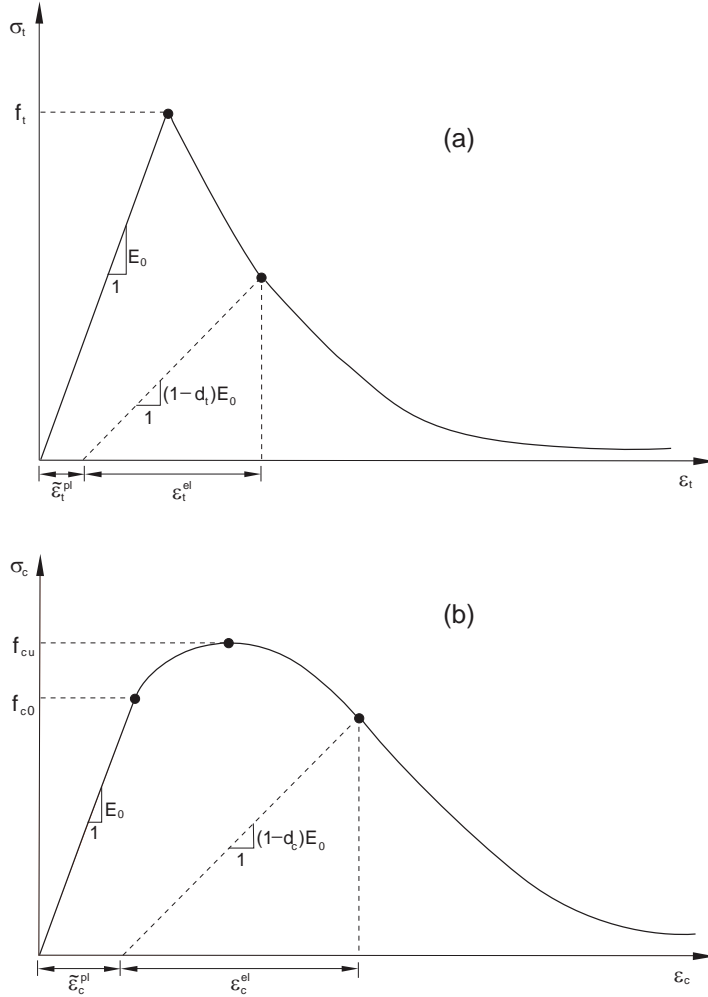


Figure 3.10: The uniaxial behaviour in both tension (a) and compression (b). Reproduction from (Hibbit et al., 2010).

The uniaxial behaviour of the material model can be seen in Fig. 3.10. It is described as a stress-strain relationship, in which the non-linear behaviour of concrete is implemented through plastic damage variables, one for tension and one for compression. The plastic damage variables resemble the hardening variables of plasticity theory, in that they never decrease and increase if and only if plastic deformation occurs. These variables are coupled to a scalar tensile damage parameter d_t and a scalar compressive damage parameter d_c , to account for the stiffness degradation exhibited by concrete. The stress-strain relationship, which in fact is a stress-plastic strain relationship, is governed by Eq. (3.2). In principal, Eq. (3.2) is the same in tension and compression, the only difference is in the evolution of the respective plastic damage variable.

$$\sigma_t = (1 - d_t)E_0(\varepsilon_t - \tilde{\varepsilon}_t^{pl}) \quad (3.2a)$$

$$\sigma_c = (1 - d_c)E_0(\varepsilon_c - \tilde{\varepsilon}_c^{pl}) \quad (3.2b)$$

where,

- σ is the Cauchy stress.
- E_0 is the initial elastic modulus.
- ε is the strain
- $\tilde{\varepsilon}^{pl}$ is the equivalent plastic strain in tension or compression.

Under uniaxial conditions cracks propagate perpendicular to the stress direction, which results in that the load-carrying area reduces as the crack propagates. This means that the effective stress increases; in fact the scalar damage parameters can be considered as the percentage of the sectional area which is still transferring stress. The uniaxial behaviour has to be given to ABAQUS when defining the material model. It is given as tabular functions of stress and inelastic strain for the compressive part, and as either stress and cracking strain or stress and cracking displacement for the tensile part. The scalar damage parameters are given in the same manner. The input data are then converted to the stress–plastic strain relationships used in the material model, by the following equations.

For the compressive side, Eq. (3.3) is used to convert the inelastic strains $\tilde{\varepsilon}_c^{in}$ given to the program to plastic strains.

$$\tilde{\varepsilon}_c^{pl} = \tilde{\varepsilon}_c^{in} - \frac{d_c}{1 - d_c} \frac{\sigma_c}{E_0} \quad (3.3)$$

For the tensile side the stress can, as mentioned above, either depend on cracking strain or crack displacement; it is recommended to use the displacement alternative to avoid mesh dependencies. The crack displacements u_t^{ck} given to the program is converted to plastic displacement u_t^{pl} through Eq. (3.4). In Eq. (3.4) the variable l_0 is equal to unity, i.e. $l_0 = 1$.

$$u_t^{pl} = u_t^{ck} - \frac{d_t}{1 - d_t} \frac{\sigma_t l_0}{E_0} \quad (3.4)$$

At each integration point, the cracking displacement is associated with a characteristic length which converts the displacements to strains. It should also be noted that the plastic strains can never decrease nor assume negative values (Hibbit et al., 2010).

These uniaxial concepts are then generalized to multiaxial conditions. The multiaxial evolution of the plastic damage variables are based on the work of Lee and Fenves (1998). Further, the model uses a yield criterion first proposed by Lubliner et al. (1989) and later modified by Lee and Fenves (1998). In biaxial compression the yield function reduces to the Drücker–Prager yield criterion, in fact the yield surface proposed by Lubliner et al. (1989) is in principle a combination of the Mohr–Coulomb and the Drücker–Prager yield criterions. The modifications made to the yield surface by Lee and Fenves (1998) takes into account the different evolution of strength under tension and compression. In Fig. 3.11, the yield surface for plane stress conditions can be seen.

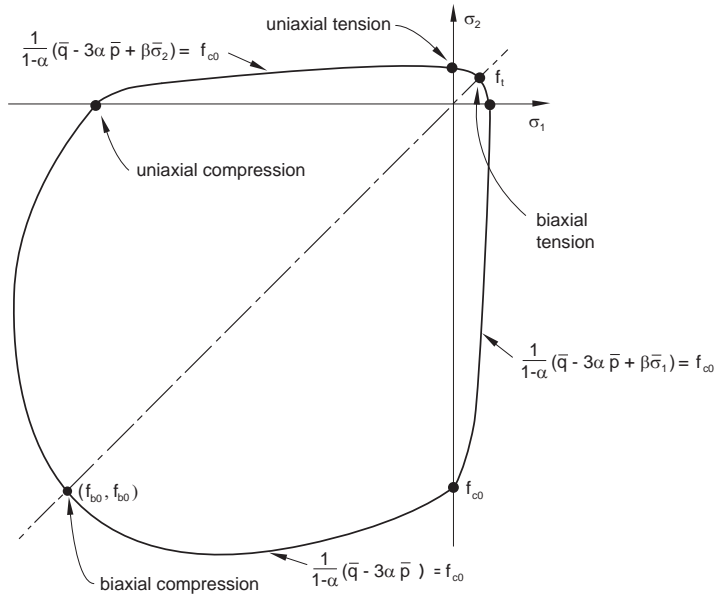


Figure 3.11: The biaxial yield surface for plane stress conditions. Reproduction from (Hibbit et al., 2010).

where,

\bar{p} is the effective hydrostatic pressure.

\bar{q} is the Mises equivalent effective stress.

α is a dimensionless coefficient. $\alpha = \frac{f_{b0} - f_{c0}}{2f_{b0} - f_{c0}}$

β is a dimensionless coefficient. $\beta = \frac{\bar{\sigma}_c(\tilde{\varepsilon}_c^{pl})}{\bar{\sigma}_t(\tilde{\varepsilon}_t^{pl})}(1 - \alpha) - (1 + \alpha)$

f_t is the initial uniaxial tensile yield stress.

f_{c0} is the initial uniaxial compressive yield stress.

f_{b0} is the initial equibiaxial compressive yield stress.

$\bar{\sigma}_t(\tilde{\varepsilon}_t^{pl})$ is the effective tensile cohesion stress.

$\bar{\sigma}_c(\tilde{\varepsilon}_c^{pl})$ is the effective compressive cohesion stress.

The concrete damaged plasticity model uses a non-associated flow rule. The flow potential G is described by the Drücker–Prager hyperbolic function, shown in Eq. 3.5.

$$G = \sqrt{(\epsilon\sigma_{t0} \tan \psi)^2 + \bar{q}^2} + \bar{p} \tan \psi \quad (3.5)$$

where,

ϵ is the eccentricity.

ψ is the dilation angle.

The flow potential is illustrated in Fig. 3.12. As the eccentricity approaches zero, the flow potential approaches a straight line, i.e. the eccentricity defines the rate at which the function approaches the asymptote shown in the figure. If the dilat-

tion angle is equal to the material inner friction angle, then the flow rule becomes associative (Hibbit et al., 2010). In a physical sense, the dilation angle describes the roughness of the crack and shear stress transfer ability between two adjacent crack surfaces. A low dilation angle gives a low shear resistance, while a high value gives a high shear resistance. This can be observed in Fig.3.12, where \bar{p} can be interpreted as the normal stress and \bar{q} as the shear stress. With an increasing value of ψ , a higher shear stress is received for a constant normal stress. This implies that the shear resistance increases as the dilation angle increase. In some sense, the dilation angle corresponds to the shear retention factor in a smeared crack fracture mechanics model (Malm, 2009).

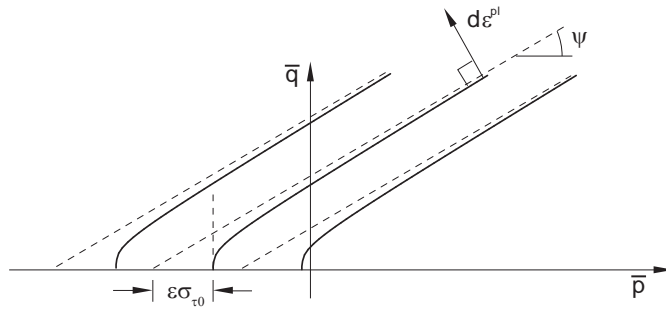


Figure 3.12: The hyperbolic Drucker–Prager flow potential. Reproduction from (Hibbit et al., 2010).

Since the concrete damaged plasticity model is primarily intended for dynamic and cyclic load conditions, the rather complex load reversal behaviour of concrete has to be included into the model. This is achieved through a combination of stiffness recovery factors, w_t and w_c , and the scalar damage parameters d_t and d_c described above. The stiffness recovery factors are a sort of weight factors, which control the recovery of the tensile and compressive stiffness upon load reversal. The default behaviour is no loss in compressive stiffness when a tensile crack closes, $w_c = 1$, and complete loss of stiffness if the load changes from compression to tension, $w_t = 0$, once crushing micro cracks have occurred. These factors are then used to calculate a scalar degradation factor d according to Eq. (3.6), which reduces the elastic modulus. A typical load cycle can be seen in Fig. 3.13 (Hibbit et al., 2010).

$$(1 - d) = (1 - s_t(w_t)d_c)(1 - s_c(w_c)d_t) \quad (3.6)$$

where,

s_t, s_c are functions of the current stress state and the respective stiffness recovery factor. $0 < s < 1$

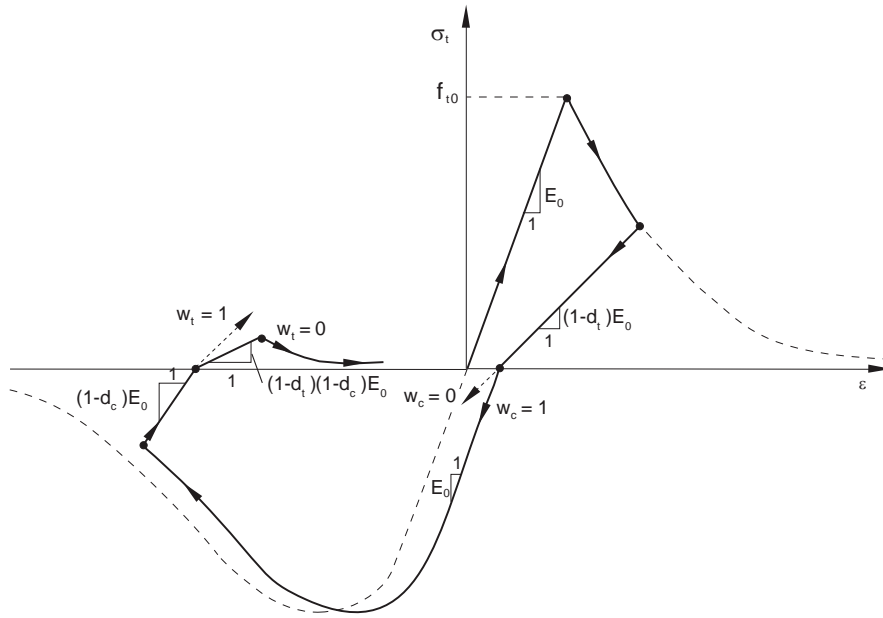


Figure 3.13: A typical uniaxial load cycle, with default stiffens recovery. Reproduction from (Hibbit et al., 2010)

3.2.3 Concrete material model in ADINA

The concrete material model in ADINA is based on the smeared crack approach of fracture mechanics. It can only be used with 2D-solid and 3D-solid elements. The main characteristics of the model is a tensile failure at a relatively small maximum principal stress, crushing failure at high compressive stresses and strain softening after the crushing failure to an ultimate strain at which the material fails completely. These characteristics are, besides concrete, applicable to many other materials such as a variety of rocks. All the complex behaviour aspects of concrete are not covered by the model which instead only intends to describe the most important aspect so that an effective and easy to use material model is obtained (Bathe, 2009).

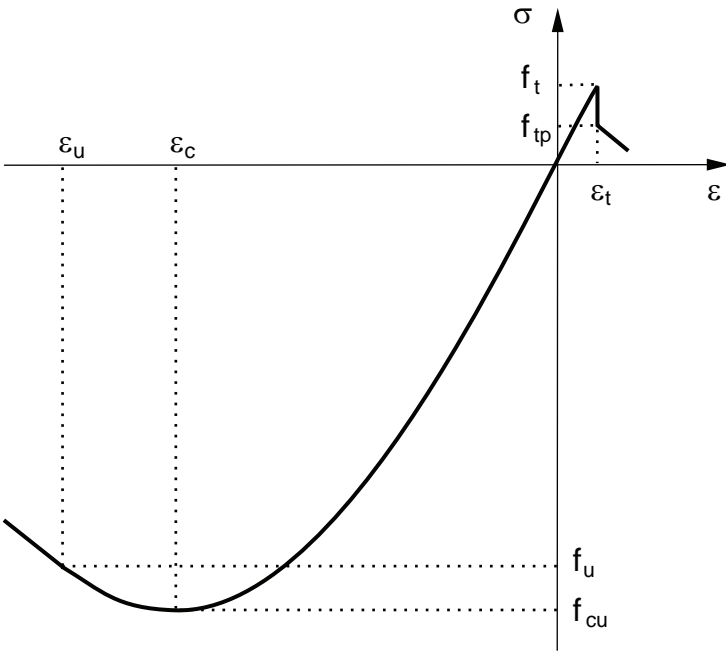


Figure 3.14: The uniaxial behaviour of the material model. Reproduction from (Bathe, 2009).

The uniaxial behaviour of the material model can be seen in Fig. 3.14 as a stress-strain relationship. This relationship assumes monotonic load conditions; for unloading the initial elastic modulus E_0 is used. In tension, the uniaxial behaviour is linear elastic up to the tensile strength f_t . The compressive side of the uniaxial behaviour is governed by Eq. 3.7. As the stress reaches the ultimate compressive strength f_u , ultimate failure of the material is assumed.

$$\sigma = \frac{\left(\frac{E_0}{E_s}\right) \left(\frac{\varepsilon}{\varepsilon_c}\right) \sigma_c}{1 + A \left(\frac{\varepsilon}{\varepsilon_c}\right) + B \left(\frac{\varepsilon}{\varepsilon_c}\right)^2 + C \left(\frac{\varepsilon}{\varepsilon_c}\right)^3} \quad (3.7)$$

where,

- σ is the uniaxial stress
- f_{cu} is the maximum uniaxial compressive stress
- ε is the uniaxial strain
- ε_c is the uniaxial strain corresponding to f_{cu}
- E_s is the secant modulus corresponding to the maximum uniaxial compressive stress, $E_s = f_{cu}/\varepsilon_c$

The coefficients A , B and C are given in Eq. 3.8.

$$A = \frac{\left[\frac{E_0}{E_u} (p^3 - 2p^2) \frac{E_0}{E_s} - (2p^3 - 3p^2 + 1) \right]}{(p^2 - 2p + 1)p} \quad (3.8a)$$

$$B = \left[2 \frac{E_0}{E_s} - 3 - 2A \right] \quad (3.8b)$$

$$C = \left[2 - \frac{E_0}{E_s} + A \right] \quad (3.8c)$$

where,

ε_u is the uniaxial strain corresponding to f_u

E_u is the secant modulus corresponding to the ultimate uniaxial compressive stress, $E_u = f_u/\varepsilon_u$

p is a coefficient, $p = \varepsilon_c/\varepsilon_u$

As the tensile stresses reaches the tensile strength f_t , a crack starts to develop. The material model uses a fixed crack approach of the smeared crack concept, i.e. as a crack is initiated the direction is constant and perpendicular to the principal stress direction at crack initiation. A crack is then represented by a failure plane at the given integration point at which failure has occurred. The stress transfer across the failure plane is given as a tension softening stress-strain relationship and is shown in Fig. 3.15.

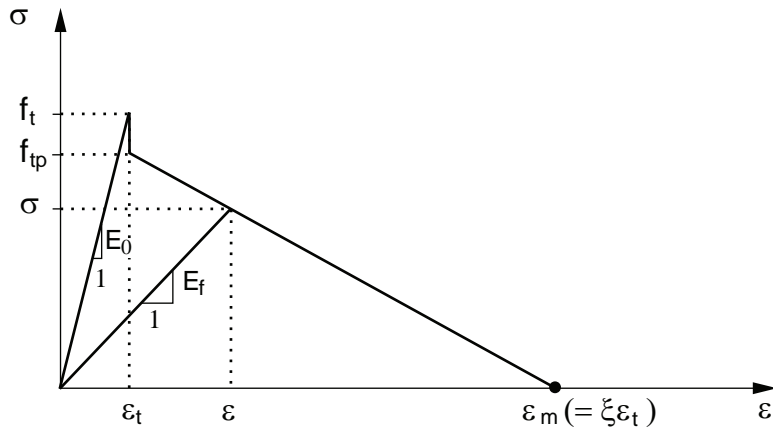


Figure 3.15: Post tensile cracking behaviour of the material model. Reproduction from (Bathe, 2009).

The post-cracking cut-off tensile strength f_{tp} is an optional parameter, and if not given to the program it is set equal to f_t . The elastic modulus E_f is used for unloading of the stresses normal to the failure plane, and is evaluated by the program. The ultimate strain ε_m is determined through the parameter ξ , which in turn depends on the fracture energy G_f and the element size. The parameter ξ is associated with each integration point of an element, as can be seen in Fig. 3.16, and is calcu-

lated according to Eq. 3.9. Fig. 3.16 also shows the principle of the failure plane associated with each integration point.

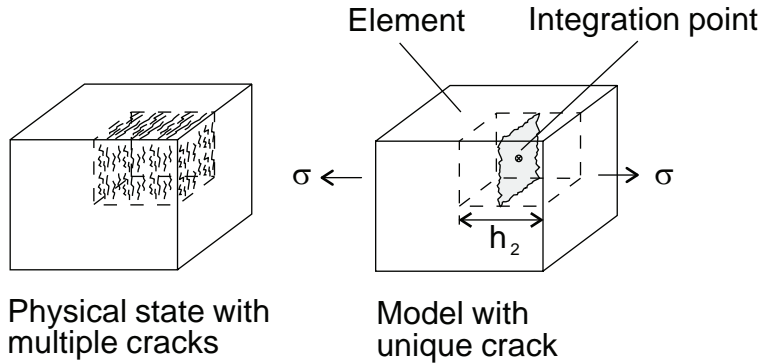


Figure 3.16: Tensile cracking of an element. Reproduction from (Bathe, 2009).

$$\xi = \frac{2E_0G_f}{f_t^2 h_2} \quad (3.9)$$

As the material model is based on a fixed crack approach, a shear retention factor is needed to avoid unrealistic results. The evaluation of the shear retention factor η_f is shown in Fig. 3.17, and is used to reduce the shear stiffness across the failure plane as the crack grows. The parameter η_s determines the residual shear stiffness left after a crack is fully opened, and is given by the user.

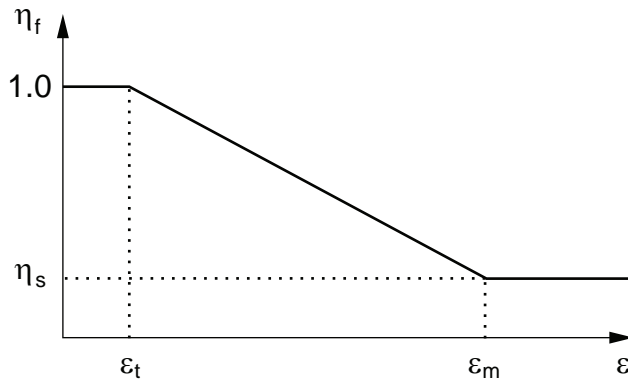


Figure 3.17: Development of the shear retention factor with increasing strain normal to the failure plane. Reproduction from (Bathe, 2009).

To describe the multiaxial behaviour of concrete, failure surfaces are used to alter the uniaxial material strength with the current stress state. The altered material strengths are then used with the uniaxial governing equations described above. The default biaxial failure surface for plane stress conditions is shown in Fig. 3.18 in comparison with an experimentally obtained failure surface.

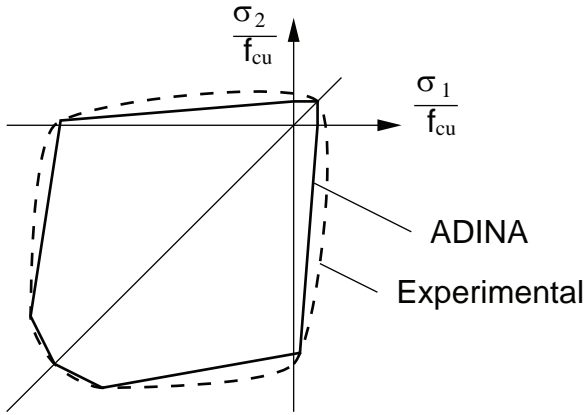


Figure 3.18: Biaxial failure surface for plane stress conditions. Reproduction from (Bathe, 2009).

3.3 Dynamic explicit integration

Finite element analysis of concrete structures are often associated with convergence problems. To avoid these, most of the analyses made during this study are performed with a dynamic explicit solver. Normally, a dynamic explicit procedure is intended for high-speed dynamic events, but its large deformation theory also makes it suitable for quasi-static events which undergo severe deformation. The basic idea behind the procedure is that a large number of small time increments are used to solve the problem. Each of these time increments are relatively inexpensive to solve, which results in a computationally efficient solution scheme. The procedure is built around a central-difference time integration rule. A central-difference scheme is in principle quite simple, it uses the known values at time increment t , for which dynamic equilibrium is satisfied, to calculate the accelerations and velocities so that the solution can advance to time increment $t + \Delta t$. In explicit analysis, the central-difference scheme is always used in combination with “lumped” mass matrices. Consequently, no coupled equations need to be solved and no stiffness matrices need to be assembled and updated during the analysis (Hibbit et al., 2010).

The major advantage of using an explicit solver is that it allows the solution to proceed without any convergence iterations and, as mentioned above, that no stiffness matrices need to be formed. This is the basis of the computational efficiency of the solver and the major reason why no convergence issues are exhibited. The explicit formulation also simplifies the treatment of contact iterations, which can be defined in a very general manner. Furthermore, the computational time needed to solve a problem only increase linearly with the size of the model, while the solution time for an implicit solver increases more rapidly with the model size. Hence the explicit solver is very suitable for large problems. However, it should be noticed that explicit solvers only deliver accurate results as long as the time increment is

smaller or equal to the stable time increment of the model. This limits the problems appropriate to those with a relatively short time span, as the computational time needed is proportional to the time period of the event.

When using explicit solvers certain aspects have to be taken into account. One aspect is the stability of the solution limited by the stable time increment Δt_{cr} , as mentioned above. If Δt is greater than Δt_{cr} the explicit integration fails and if Δt is too small the calculations become too expensive. The stable time increment Δt_{cr} depends on the highest eigen-frequency of the finite element model. It can, according to Cook et al. (2001) be noted that this eigen-frequency must be smaller than the eigen-frequency of any unassembled and unsupported element in the finite element model. Therefore, Δt_{cr} can often be approximated by Eq. (3.10), although this is an unconservative approximation. Eq. (3.10) is often only valid for undamped systems, depending on the formulation of the central-difference.

$$\Delta t_{cr} = \frac{L_{min}}{c} \quad (3.10)$$

where,

- L_{min} is the smallest element dimension of the mesh.
 c is the wave speed in the material (speed of sound).

The physical interpretation of Eq. (3.10) is that Δt has to be small enough so that information does not propagate further than the distance between adjacent nodes during a single time increment (Cook et al., 2001).

Another limitation of the explicit solvers is the type of elements that can be used in order to maintain the computational efficiency of the solver. A general rule is to use elements with as few integration points as possible. The reason is that the internal forces of the model are calculated by summing the contribution of each element. As the number of integration points per element increase so does the computational time to calculate the contribution from each element. For example the use of a reduced four node element instead of a fully integrated four node element quarters the computational cost. The calculation of these internal forces make up a large portion of the computational time needed per increment, i.e. keeping the number of integration points per element to a minimum significantly reduces the overall computational time needed to solve the system (Cook et al., 2001).

There are many different explicit integration methods available. Two of the most common are the *Half-Step Central Difference* and the *Classical Central Difference* formulations, which are used in ABAQUS and ADINA respectively.

3.3.1 Explicit integration in ABAQUS

In ABAQUS an explicit integration solver is available in ABAQUS/Explicit, the solver is based on half-step central difference formulation. The displacement u in a half-step method is advanced from time step i to $i + 1$, through the acceleration

\ddot{u} at time step i and the velocity \dot{u} at time step $i - 1/2$, hence the name half-step. The governing equations of the half-step method are given in Eq. (3.11).

$$u(i+1) = u(i) + \Delta t \dot{u}(i + \frac{1}{2}) \quad (3.11a)$$

$$\dot{u}(i + \frac{1}{2}) = \dot{u}(i - \frac{1}{2}) + \Delta t \ddot{u}(i) \quad (3.11b)$$

$$\ddot{u}(i) = M^{-1}(F(i) - I(i)) \quad (3.11c)$$

where,

M is the lumped mass matrix.

F is the applied load.

I is the internal force.

The basic principle of the solution algorithm is as follows. The accelerations are calculated at the current time step at the beginning of each increment. These accelerations are then used to calculate the velocities at the midincrement, which in turn are used to calculate the displacements at the end of the increment. After this the internal force contribution from each element are calculated and summarized for the whole model and the process starts over (Hibbit et al., 2010).

3.3.2 Explicit integration in ADINA

The explicit solver in ADINA uses a classical central difference formulation. In a classical central difference it is assumed that the accelerations at time step i can be approximated according to Eq. (3.12).

$$\ddot{u}(i) = \frac{1}{\Delta t}(u(i+1) - 2u(i) + u(i-1)) \quad (3.12)$$

and that the velocities can be approximated according to Eq. (3.13).

$$\dot{u}(i+1) = \frac{1}{2\Delta t}(u(i+1) + u(i-1)) \quad (3.13)$$

The system is governed by the dynamic equilibrium equation, which is given in Eq. (3.14).

$$M\ddot{U}(i) + C\dot{U}(i) = F(i) - I(i) \quad (3.14)$$

where,

C is the lumped damping matrix.

By substituting Eq. (3.12) and Eq. (3.13) into Eq. (3.14) an equation is obtained which can be used to advance the solution from $u(i)$ to $u(i+1)$ (Bathe, 2009).

3.3.3 Quasi-static analysis

Since most of the analyses in this study are static problems, the dynamic explicit solvers have to be adjusted to solve static problems. Using a dynamic solver to solve a static problems is often referred to as quasi-static analysis. This is accomplished by allowing the system to be exposed to dynamic properties such as velocities and accelerations, but applying the boundary conditions and loads so that the dynamic effects are kept at a minimum. This can for example be achieved by applying the load as a low velocity in a deformation controlled analysis. A control to find out whether quasi-static conditions are valid for a analysis is to compare the internal energy of the system to the kinetic energy of the system. When comparing these quantities the internal energy should be significantly greater than the kinetic energy during the entire analysis. For large and complicated models it is also important to look at the distribution of the energy over the entire model, so that no element is subjected to high kinetic energy. This is important since a single small element subjected to high kinetic energy wont effect the energy of the entire model. Further, the mass inertia effects should also be low through the entire analysis. Quasi-static analysis is often used when the advantages of the explicit solvers are sought to solve static problems which might undergo large deformations or exhibit convergence problems.

Chapter 4

Design codes

The design of mechanical fasteners may be performed according to several different design codes and technical specifications. There is no Eurocode available for the design of fasteners at the time of this thesis; however, there is a European Technical Specification available that contain design procedures. It is called SIS-CEN/TS 1992-4 (2009), from now on called TS, where Part 2 includes recommended design procedures for cast-in-place headed fasteners. Part 4 includes design procedures for post-installed fasteners with a mechanical interlock mechanism, such as friction. The US design code, ACI 349-6 (2007), also includes design methods for fasteners in concrete. In section 4.2 these methods will be compared with those defined in TS.

The equations presented in TS are empirically derived and corresponds to the design method called the CC-method (Concrete Capacity method) (Eligehausen et al., 2006). The earlier used method for the design of fasteners was relatively time consuming since a circular failure surface was assumed. The circular shape resulted in complex area calculations of merged failure surfaces of groups of fasteners. To overcome this complexity, the CC-method was developed by Fuchs et al. (1995) where the failure surface is assumed to have a rectangular shape. Despite this simplification, the results from the CC-method show good agreement with the old methods and experiments (Fuchs et al., 1995).

There are several different types of European standards where the harmonised standards are superior to all the others and starts with the letters EN. All Eurocodes are harmonised standards, but as mentioned above there is no Eurocode available for fasteners in concrete. An European Technical Specification, called CEN/TS, is a type of pre-standard and is valid until a harmonised standard is published. ETAG stands for European Technical Approval Guideline and is a document describing how to evaluate different products in order to obtain a European Technical Approval, called ETA, for a specific product. If no harmonised standard is available, then the most relevant of the three aforementioned standards should be used.

Section 4.1 will explain the design procedures from TS that correspond to the failure modes for the structures examined in this thesis. These are steel failure, concrete cone failure, pull-out failure and pry-out failure. All the other verifications required in TS can be found in appendix A.1. The load case where tensile and shear loads

act on the fastener at the same time, will also be covered. Some of the coefficients in the design equations for cast-in-place (e.g. headed studs) and post-installed (e.g. expansion anchors) fasteners differ. The coefficients for each type of fastener will be given in connection to the equations.

Since nuclear power facilities can be subjected to extreme loads, the last section of this chapter will discuss the special regulations specified in the Swedish code for nuclear facilities DRB:2001 (2002).

4.1 Design according to CEN

As mentioned above, the design methods for mechanical fasteners are divided into two parts in TS. Before the presented methods may be used for the design, all forces and moments acting on a fastener shall be determined by a linear elastic analysis. All verifications that TS require for both tensile and shear loads are specified below. But as mentioned before, all the equations will not be given in this section.

For a cast-in-place headed fastener, there are seven different verifications specified, but all are not required for every fastener. A distinction is made between fasteners with or without supplementary reinforcement. For fasteners without supplementary reinforcement the following verifications are required.

- Steel failure of fastener
- Pull-out failure of fastener
- Concrete cone failure
- Splitting failure
- Blow-out failure

For anchorage with supplementary reinforcement the following two additional verifications are required.

- Steel failure of reinforcement
- Anchorage failure of reinforcement

A significant difference is that the supplementary reinforcement should be designed to resist the total tensile load on the fastener. This means that the concrete cone verification is neglected, and instead the two verifications for supplementary reinforcement are added.

Three different design methods, A-C, are stated in TS to calculate the resistance of a post-installed fastener or a group of fasteners. Method B and C are based on simplified approaches and will not be covered in this thesis. Method A is similar to the specified design procedure for cast-in-place headed anchors and require that four different failure modes are verified.

- Steel failure of fastener
- Pull-out failure of fastener
- Concrete cone failure
- Splitting failure

All tensile failure modes are explained in section 2.2.1 and depicted in Fig. 2.4. Notice that the blow-out failure mode is explained in the concrete cone failure section.

As for cast-in-place anchors loaded in tension, a distinction is made between shear loaded fasteners positioned in concrete with or without supplementary reinforcement. For a fastener or a group of fasteners in concrete without supplementary reinforcement the following verifications are required.

- Steel failure without lever arm
- Steel failure with lever arm
- Concrete pry-out failure
- Concrete edge failure

However, if supplementary reinforcement is present in the concrete member, two additional verifications are required.

- Steel failure of supplementary reinforcement
- Anchorage failure of supplementary reinforcement

Shear loaded post-installed fasteners require the same verifications as cast-in-place headed fasteners without supplementary reinforcement loaded in shear. The shear failure modes are all explained in section 2.2.2.

4.1.1 Steel failure

According to both Part 2 and 4 of TS, the characteristic resistance of a tensile loaded fastener, in case of steel failure, should be determined according to the relevant European technical specification. It is also specified that the method should be based on the ultimate strength of the steel. In ETAG 001 Annex C, Eq. (4.1) is given for the characteristic resistance of a fastener in case of steel failure.

$$N_{R,ks} = A_s \cdot f_{uk} \quad [N] \quad (4.1)$$

where,

- A_s is the tensile stress area of the bolt [m^2]
 f_{uk} is the ultimate steel strength [Pa]

This equation is valid for both cast-in-place headed anchors and post-installed fasteners loaded in tension. A difference is made between the tensile stress area and

the cross-sectional area of a bolt, where the tensile stress area considers reduction of the area due to for example threading.

There is no equation given in TS for the characteristic resistance in case of steel failure due to shear loading. Instead it refers to the relevant European Technical Specification. In ETAG 001 Annex C, Eq. (4.2) is given for the case of steel failure without lever arm.

$$V_{Rk,s} = 0.5 \cdot A_s \cdot f_{uk} \quad [N] \quad (4.2)$$

where,

- A_s is the tensile stress area of the bolt [m^2]
- f_{uk} is the ultimate steel strength [Pa]

Note that Eq. (4.2) is not valid for fasteners with a reduced sectional area along the length of the fastener. Therefore, the presented equation cannot be applied to a fastener of expansion type. Instead, for such a fastener the characteristic resistance can be found in the relevant ETA. Furthermore, the characteristic resistance, calculated according to Eq. (4.2) or found in the relevant ETA, should be reduced by a factor 0.8 if the fastener is made of steel with low ductility.

4.1.2 Concrete cone failure

The characteristic resistance in case of concrete cone failure is determined by the same equation for both cast-in-place headed fasteners and post-installed fasteners. A distinction is also made whether the concrete is cracked or not. The specified Eq. (4.3) is given in TS and should be used when designing fasteners considering concrete cone failure.

$$N_{R,kc} = N_{R,kc}^0 \cdot \Psi_{A,N} \cdot \Psi_{s,N} \cdot \Psi_{re,N} \cdot \Psi_{ec,N} \quad [N] \quad (4.3)$$

$N_{R,kc}^0$ is the characteristic resistance of a single fastener which is not influenced by adjacent fasteners or edges of the concrete member and may be determined by Eq. (4.4). The equation is based on Eq. 2.1, but the factors have been modified to be suitable for design work.

All the coefficients and how to calculate them, will be given in the following.

$$N_{R,kc}^0 = k_{cr} \cdot \sqrt{f_{ck,cube}} \cdot h_{ef}^{1.5} \quad [N] \quad (4.4)$$

where,

- k_{cr} is 8.5 for headed fasteners in cracked concrete and 11.9 in uncracked concrete. For non-headed fasteners k_{cr} is 7.2 in cracked concrete and 10.1 in uncracked concrete [-]
- $f_{ck,cube}$ is the characteristic concrete cube strength [MPa]
- h_{ef} is the effective embedment depth of the fastener [mm]

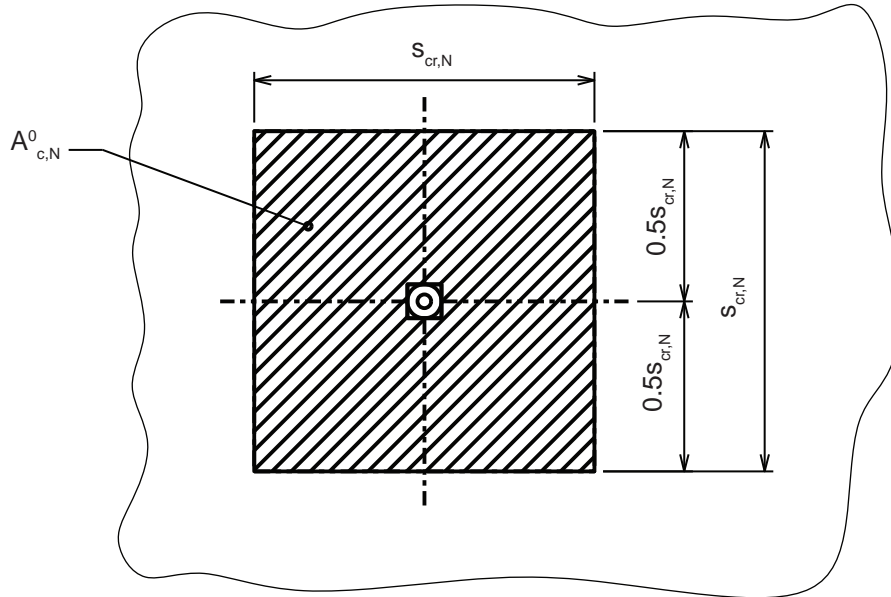
The effect of axial spacing and edge distance on the characteristic resistance is taken into account by Eq. (4.5).

$$\Psi_{A,N} = \frac{A_{c,N}}{A_{c,N}^0} \quad [-] \quad (4.5)$$

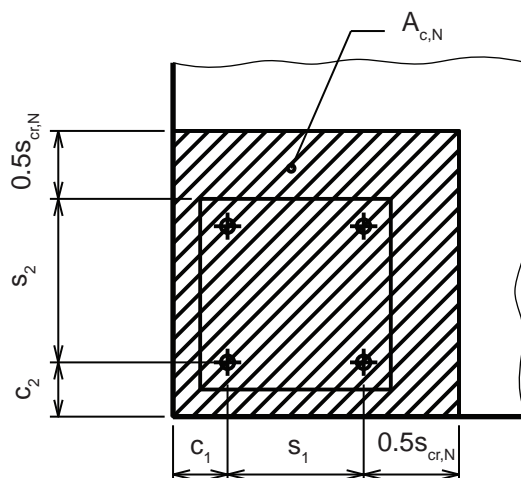
where,

$A_{c,N}$ is the actual projected area, see Fig. 4.1 [m^2]

$A_{c,N}^0$ is the reference projected area, $s_{cr,N} \cdot s_{cr,N}$. Where $s_{cr,N} = 3 \cdot h_{ef}$, see Fig. 4.1 [m^2]



a) Reference projected area



b) Example of an actual projected area

Figure 4.1: Example of an actual projected break out area of a simple group of fasteners. Reproduction from (SIS-CEN/TS 1992-4, 2009).

Fasteners with a limited distance to one or more edges may receive a disturbance in the concrete cone stress distribution. To account for these effects Eq. (4.6) should be used. For a fastener with several adjacent edges, the smallest edge distance should be used.

$$\Psi_{s,N} = 0.7 + 0.3 \cdot \frac{c}{c_{cr,N}} \leq 1 \quad [-] \quad (4.6)$$

where,

- c is the smallest edge distance [m]
- $c_{cr,N}$ is the characteristic edge distance in order to assure the characteristic resistance of a single fastener, $c_{cr,N} = 1.5 \cdot h_{ef}$ [m]

The factor $\Psi_{re,N}$ takes shell spalling effect into account, which may arise if a dense reinforcement is present and the embedment depth is less than 100 mm. However, in the following cases one may calculate the characteristic resistance of a fastener with $\Psi_{re,N} = 1$.

1. The reinforcement spacing is ≥ 150 mm, this is valid for any reinforcement diameter.
2. The reinforcement spacing is ≥ 100 mm, this is valid for reinforcement diameters ≤ 10 mm.

$$\Psi_{re,N} = 0.5 + \frac{h_{ef}}{200} \leq 1 \quad [-] \quad (4.7)$$

where,

- h_{ef} is the embedment depth [mm]

If a tensile load acts eccentric on a fastener or a group of fasteners, the factor $\Psi_{ec,N}$ must be determined according to Eq. (4.8). If the tensile load is eccentric in two directions $\Psi_{ec,N}$ must be determined separately in both directions. The product of the two factors should then be used in Eq. (4.3).

$$\Psi_{ec,N} = \frac{1}{1 + 2 \cdot \frac{e_N}{s_{cr,N}}} \leq 1 \quad [-] \quad (4.8)$$

where,

- e_N is the eccentricity of the tensile load [mm]

4.1.3 Concrete pry-out failure

The characteristic resistance in case of pry-out failure may be calculated according to Eq. (4.9). The pry-out failure mode always occur in the opposite direction to the shear force in the concrete member.

$$V_{Rk,cp} = k_3 \cdot N_{Rk,c} \quad [N] \quad (4.9)$$

In TS, the factor k_3 is not specified, instead it refers to the relevant European Technical Specification. One relevant technical specification is ETAG 001 Annex C, where k_3 is defined as 1.0 for fasteners with $h_{ef} < 60$ mm and 2.0 for fasteners with

$h_{ef} \geq 60$ mm. Another option where k_3 can be found is in the relevant ETA. The characteristic resistance $N_{Rk,c}$ should be determined according to Eq. (4.3).

Eq. (4.9) applies to a single fastener or a group of fasteners. However, in some cases the direction of the acting shear load, on the individual fasteners in a group, may alter. In such a case Eq. (4.9) do no longer apply for the whole group and instead the most unfavorable fastener should be verified against Eq. (4.9). For example, this is the case when a torque is applied to a group of fasteners.

4.1.4 Pull-out failure

As mentioned in section 2.2.1, the failure mode in case of a pull-out failure is a bit different between a headed fastener and a non-headed fastener. Hence, the specified design procedures for the two type of fasteners are not equal. According to TS, Eq. (4.10) may be used to calculate the characteristic resistance in case of pull-out failure for a cast-in-place headed fastener.

$$N_{R,kp} = 6 \cdot A_h \cdot f_{ck,cube} \cdot \Psi_{ucr,N} \quad [\text{N}] \quad (4.10)$$

where,

A_h is the load bearing area of the fastener [m^2]

$f_{ck,cube}$ is the characteristic concrete cube strength [Pa]

$\Psi_{ucr,N}$ is 1.0 for fasteners in cracked concrete and 1.4 for fasteners in non-cracked concrete [-]

No design procedure is defined in TS for a post-installed non-headed fastener; instead it refers to the relevant European technical specification. However, there is no existing equation for the design of non-headed fasteners in any technical specification at time of this thesis. Instead, the characteristic resistance of the fastener has to be derived by approval tests. In the respective European technical approval, called ETA, the results of such tests are specified for each fastener, and may be used as the characteristic resistance.

4.1.5 Combined shear and tensile load

A distinction is made between fasteners where steel failure is decisive for both tensile and shear load and where one of the concrete failure modes is decisive. In the case of steel failure Eq. (4.11) should be satisfied.

$$\beta_N^2 + \beta_V^2 \leq 1 \quad [-] \quad (4.11)$$

For all the other failure modes, either Eq. (4.12) or Eq. (4.13) should be satisfied. In which β_N and β_V should be taken as the largest values received from the different failure modes.

$$\beta_N + \beta_V \leq 1.2 \quad [-] \quad (4.12)$$

$$\beta_N^{1.5} + \beta_V^{1.5} \leq 1 \quad [-] \quad (4.13)$$

where,

- β_N is $N_{Ed}/N_{Rd} \leq 1$ [-]
- β_V is $V_{Ed}/V_{Rd} \leq 1$ [-]
- N_{Ed} is the applied tensile load [N]
- N_{Rd} is tensile resistance [N]
- V_{Ed} is the applied shear load [N]
- V_{Rd} is shear resistance [N]

In Fig. 4.2, Eq. (4.11) to (4.13) for combined shear and tensile load are depicted.

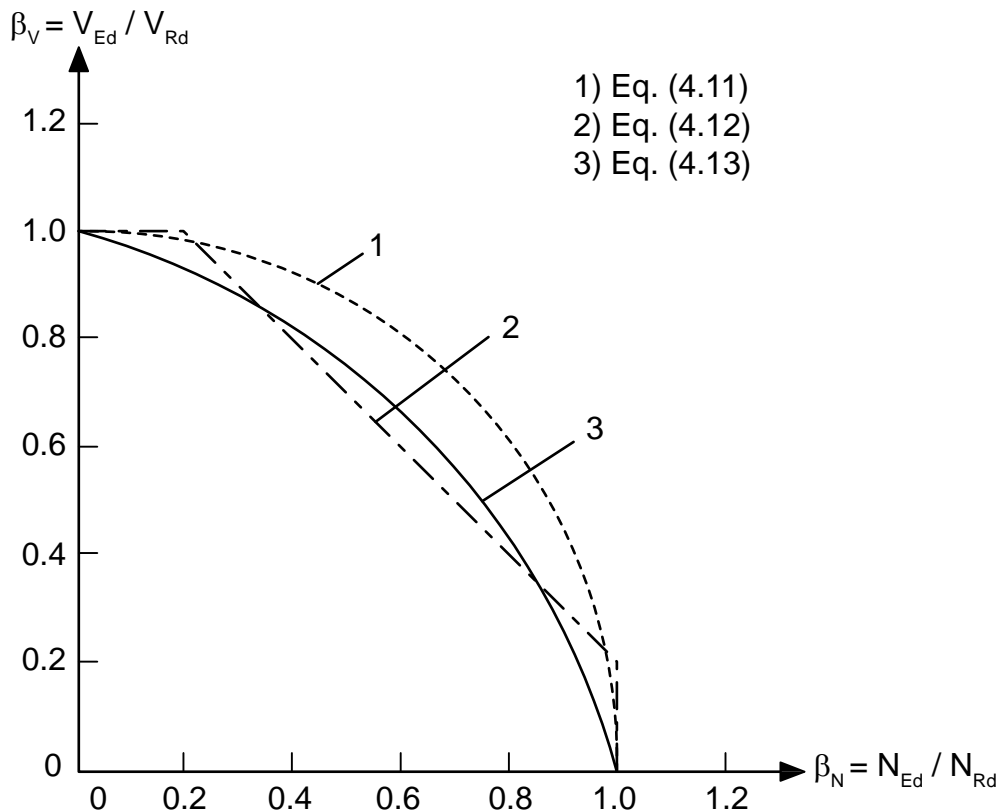


Figure 4.2: Interaction expressions according to TS. Reproduction from (SIS-CEN/TS 1992-4, 2009).

4.2 ACI 349-6

The design procedures for fasteners presented in ACI 349-6, from now on called ACI, are based on the exact same method as those in TS. However, in Europe this method

is called the CC-method (Concrete capacity method) while it is called the CCD-method (Concrete capacity design method) in the US (Eligehausen et al., 2006). The structure of ACI is partially different from that in TS. Instead of subdividing cast-in-place fasteners and post-installed fasteners into different parts, as in TS, ACI present the equations for both type of fasteners in the same section of the code. Some of the coefficients in the equations differ with the result that the characteristic resistance is more or less conservative. The required verifications are mainly identical to those in TS but some are treated in a different manner, the required verifications are:

- Steel strength of anchor in tension
- Steel strength of anchor in shear
- Concrete breakout strength of anchor in tension (called concrete cone failure in TS)
- Concrete breakout strength of anchor in shear (called concrete edge failure in TS)
- Pull-out strength of anchor in tension
- Concrete side-face blowout strength of anchor in tension (called blow-out failure in TS)
- Concrete pry-out strength of anchor in shear

Splitting failure is not a required verification in ACI. Instead, this failure mode is taken into account by specifying minimum values for edge distances, spacings and concrete member thicknesses to preclude splitting failure. There is however a possibility to perform product specific tests, if lower minimum values are wanted. These tests should be performed according to the guidelines in ACI. The specified values are valid if no supplementary reinforcement is provided to prevent splitting failure of the concrete member.

TS specify a required verification considering the steel strength of an anchor loaded in shear with a lever arm. This verification is not mentioned in ACI, and no equivalent restrictions for this failure mode is given.

The differences between the equations in TS, presented in section 4.1.1 to 4.1.5, and ACI are given below. It should also be noted that the safety philosophy differs between the two design codes. This may for example apply to the material properties and the load effects defined in respective design code. Therefore, even more differences than presented below may be present.

Steel strength in tension and shear The equation given in ACI is identical to the one specified in TS, see Eq. (4.1). Both are based on the ultimate steel strength and the tensile stress area of the bolt. However, two limitations are given in ACI concerning the ultimate steel strength; it should not be taken greater than the smaller of $1.9f_{yk}$ or 862 MPa. This limitation has been introduced to ensure a proper behaviour of the bolts during service loads, i.e. no yielding of the steel.

Regarding shear load, no equation is presented in ACI for the steel strength of an anchor loaded with a lever arm. But a distinction is still made between cast-in-place headed anchors, cast-in-place headed bolts and hooked bolts. Where an anchor is welded without threading, whereas a bolt always has a threaded part. The presented equation for cast-in-place headed anchors subjected to a shear load, is equivalent to the equation for anchors loaded in tension presented in TS. Further, the same limitations regarding the ultimate steel strength as mentioned above applies. This means that the equation differs from the presented equation in TS, which has an additional coefficient of 0.5, see Eq. (4.2). For cast-in-place headed bolts and hooked bolts the equation are analogous to the one specified in TS but with a factor 0.6 instead, which results in a less conservative characteristic resistance. However, this is compensated by the limitations of the ultimate steel strength.

Just as in TS, the characteristic resistance in case of steel failure, due to shear and tensile load, for an anchor of expansion sleeve type must be determined by product specific tests. This also applies to anchors with internal threading and anchors which do not have a constant cross-section along the length.

Concrete breakout strength of an anchor The equations given for characteristic resistance in case of concrete cone failure are almost equal in ACI and TS, but there are some differences. The coefficient in the equation for the characteristic resistance of a single fastener, not influenced by adjacent edges, is 10.0 for cast-in-place headed anchors and 7.0 for post-installed anchors in ACI. In TS this coefficient do not only consider the type of bolt, but also whether the concrete member is cracked or uncracked. To compensate for this, ACI includes an additional coefficient, which considers whether the concrete member is cracked or not; for the exact values see ACI 349-6 (2007). However, the resulting product of the coefficients differ just slightly from those presented in Eq. (4.3). A comparison of the characteristic resistance for a single cast-in-place headed fastener in uncracked concrete is depicted in Fig. 4.3.

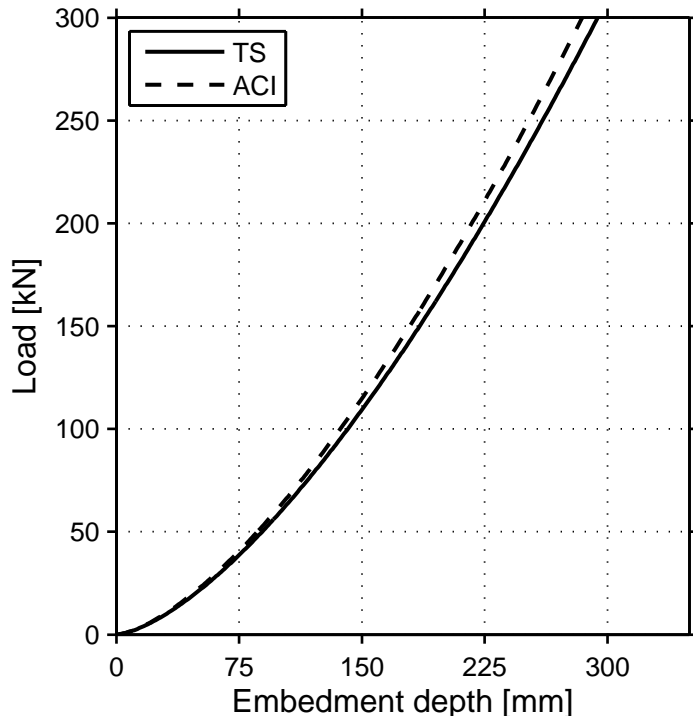


Figure 4.3: Comparison of the characteristic resistance according to TS and ACI for concrete breakout.

The projected areas of the failure surface, both the reference projected and the actual projected areas, are calculated in ACI with the same procedure as in TS.

The coefficients that take eccentricity and adjacent edges into account are identical in ACI and TS, see Eq. (4.6) and (4.8) respectively. A coefficient that accounts for shell spalling effects is included in TS, see Eq. (4.7). ACI does not include such a coefficient and is not specifying any other restrictions considering this type of effects. However, for post-installed fasteners intended for use in an uncracked concrete member without supplementary reinforcement, a coefficient is included in the equation to limit the risk of splitting, see ACI 349-6 (2007). In TS, the splitting risk is instead taken into account by a separate verification, see appendix A.1.

Concrete pry-out strength of an anchor in shear The equations given to determine the concrete pry-out strength of a fastener is almost identical in TS and ACI, see Eq. (4.9). However, the limit of the embedment depth differ for the coefficient k_3 in the equation; in ACI the limit is $h_{ef} = 65$ mm while the corresponding limit value in TS is 60 mm, as can be seen in the aforementioned equation. Since the concrete cone resistance is included in this equation, the slight differences, mentioned above, will also affect the total pry-out strength.

Pull-out strength of anchor in tension The method to determine the characteristic resistance in case of pull-out failure according to TS differ whether the

fasteners are of post-installed non-headed type or cast-in-place headed type. For a post-installed fastener with no head, the resistance is very dependent on the design. Therefore, no equation has been derived for this type of bolt and instead the resistance has to be determined by approval tests. This applies in both TS and ACI, where the approval tests should be performed according to the given guidelines in the respective design code. For the cast-in-place headed type, equations are given in both TS and ACI. These equations are almost equal, with the only difference that the constant is 8.0 in ACI and 6.0 in TS, see Eq. (4.10). The lower value in TS has been chosen to limit the displacement of fasteners placed in cracked concrete members where the crack width may alternate during its life time (Eligehausen et al., 2006).

Combined tensile and shear load Three different expressions are given in TS for fasteners subjected to combined tensile and shear load. However, according to ACI, only Eq. (4.12) has to be satisfied; the other two equations are omitted.

4.3 Design considerations for nuclear facilities

DRB:2001 (2002) is the Swedish design standard valid for existing nuclear facilities at the time of this study. The purpose of DRB is to complement the Swedish design standard BKR 2010 (2011), which give general guidelines on the design procedure. In principle, DRB suggest modifications and limitations to the general guidelines in BKR so that the design procedure is more appropriate for nuclear facilities. According to DRB and BKR, concrete structures should be designed according to BBK 04 (2004) and steel structures according to BSK 07 (2007). However, none of the above mentioned design standards give any specific design methods for anchorage to concrete. Hence, the procedure has been to borrow the design methods from other codes and use the general guidelines from the Swedish standards. Often, the design methods from ACI, described in section 4.2, have been used. For general structural design with the transition to Eurocodes in Sweden, the old Swedish standards are no longer valid. Before Eurocode is implemented for regulating the design of nuclear facilities or a new version of DRB is published, the principles of DRB have to be applied. When the Eurocodes come into effect, the design procedures from SIS-CEN/TS 1992-4 (2009) described in section 4.1 are appropriate to use; even if they do not have the status of an Eurocode yet. This section will describe the basic principles of DRB and how the guidelines in it could be used in the design procedure of anchorage to concrete.

There are some new concepts introduced in DRB that are not present in BKR and some of the concepts from BKR are modified. The safety classes in BKR only take into account the risk of damage to person while DRB also regards economical aspects. The safety classes in DRB are:

B1 limited risk of severe damage

B2 some risk of severe damage

B3 vast risk of severe damage

In the Swedish design standards the safety factors reduce the material properties with increasing safety class. Normally, Eurocodes do not use safety classes, but according to the national annex EKS 8 (2011) they can be implemented into the Eurocodes by reducing the load for safety class one and two with a factor 0.83 and 0.91 respectively. According to DRB, all structures of a nuclear facility should be designed in safety class B3 if any risk for radiological damage is present.

A new concept called event class is introduced in DRB to categorise different events depending on the probability that they will occur. These event classes are then associated with the different requirements given in DRB, for example bearing capacity or survivability.

H1 normal operations

H2 disturbance of the normal operations

H3 smaller accident

H4 accidents that affect the structural integrity

H5 hypothetical accidents

The design procedure in DRB is based on the partial coefficient method where both the material properties f and the design loads F are reduced or increased through partial coefficients. The design requirement is given in Eq. (4.14).

$$R_d(a, f) \geq S_d(F, a) \quad (4.14)$$

where,

R_d is the resistance

S_d is the load effect

a is the geometrical properties of the structure

The load effect on the structure is obtained from the different load combinations given in DRB. Load combinations are given for three different limit states; the serviceability state, the ultimate limit state and the accident limit state. A difference is also made between the containment vessel and the other buildings on the facility. For the other buildings, the load combinations for each limit state are associated with the event classes as: the serviceability state and the ultimate limit state (H1–H2) and the accident limit state (H3–H5). As an example on which type of loads that needs to be taken into consideration, one such load combination will be described.

Since many of the anchor plates are used as supports for the piping system, an interesting load combination is number seven, concerning pipe failure in the accident limit state and event class H4. The load combination is given in Tab. 4.1.

Table 4.1: Load combination seven in DRB for all buildings except the containment vessel.

		Partial coefficient	Reduction factor
Permanent loads			
Dead load	D	1.0	—
Normal water pressure	H_{gw}	1.0	—
Soil pressure	H_{gc}	1.0	—
Tendon load	P_{sp}	1.0	—
Variable loads			
Live load	L	1.0	ψ
Changes in the water pressure	H_{gw}	1.0	ψ
Changes in the soil pressure	H_{gc}	1.0	ψ
Snow load	S	1.0	ψ
Wind load	W_q	1.0	ψ
Accident loads			
Transient pressure changes in the pipe	P_a	1.0	—
Transient temperature changes due to P_a	T_a	1.0	—
Jet blast force due to pipe failure	R_{rj}	1.0	—
Missile load due to pipe failure	R_{rm}	1.0	—
Loads acting on the support due to pipe failure	R_{rr}	1.0	—
Loads due to exceptional water pressure due to pipe failure	H_{tf}	1.0	—

The value of the load reduction factors ψ is taken from the relevant design code. If the load combinations are to be used together with the Eurocodes the safety factor mentioned above is also inserted on each load type. In the old Swedish standard, the safety factor is instead used to reduce S_d .

@Seismicisolation

Chapter 5

Verification examples

In this chapter the two material models chosen for the modelling of concrete will be verified against experimental results; partly to verify that they are able to describe the complex behaviour of concrete and partly to calibrate the models. Both of the material models include non-conventional concrete material properties, especially the concrete damaged plasticity model in ABAQUS, and calibration of the models is therefore of great importance.

5.1 Notched unreinforced concrete beam

The purpose of this verification example is to determine whether the two material models are able to describe a simple tensile failure in a concrete member and to compare them to each other. Further, it will be used to study how different definitions of the tension softening part of the uniaxial behaviour of concrete effects the response of the member. It will also compare the response between a static analysis and a quasi-static analysis.

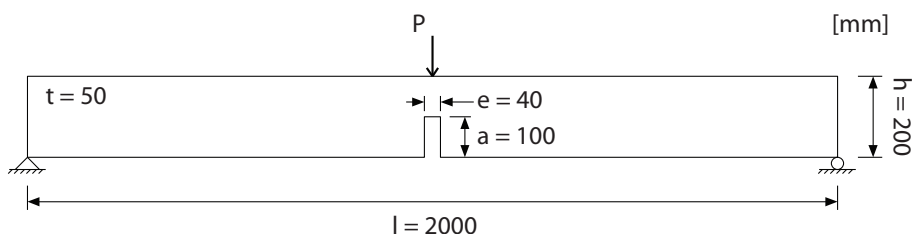


Figure 5.1: Geometry of the notched beam.

The verification example consists of simply supported unreinforced concrete beam. To ensure a pure mode I failure, i.e. tensile failure, a notch has been placed at the mid span of the beam. The dimensions of the beam can be seen in Fig. 5.1. This beam has previously been examined experimentally by Petersson (1981), who used it to evaluate the fracture energy of different mixes of concrete. It has also been

examined analytically in several other papers and is used as a benchmark example in the ABAQUS documentation (Hibbit et al., 2010). The material properties of the beam are given in Tab. 5.1.

Table 5.1: Material properties of the notched beam.

Density	ρ	2400	kg/m ³
Elastic modulus	E	30	GPa
Poisson's ratio	ν	0.2	-
Compressive strength	f_c	30	MPa
Tensile strength	f_t	3.33	MPa
Fracture energy	G_f	137	Nm/m ²

Since the beam fails in bending, which is dominated by tensile stresses, a simplified bilinear compression curve up to the compressive strength has been used. Three different tension softening descriptions seen in Fig. 5.2, will be evaluated; a linear, a bilinear and an exponential function according to Cornelissen et al. (1986). However, it is only possible to define linear tension softening in ADINA.

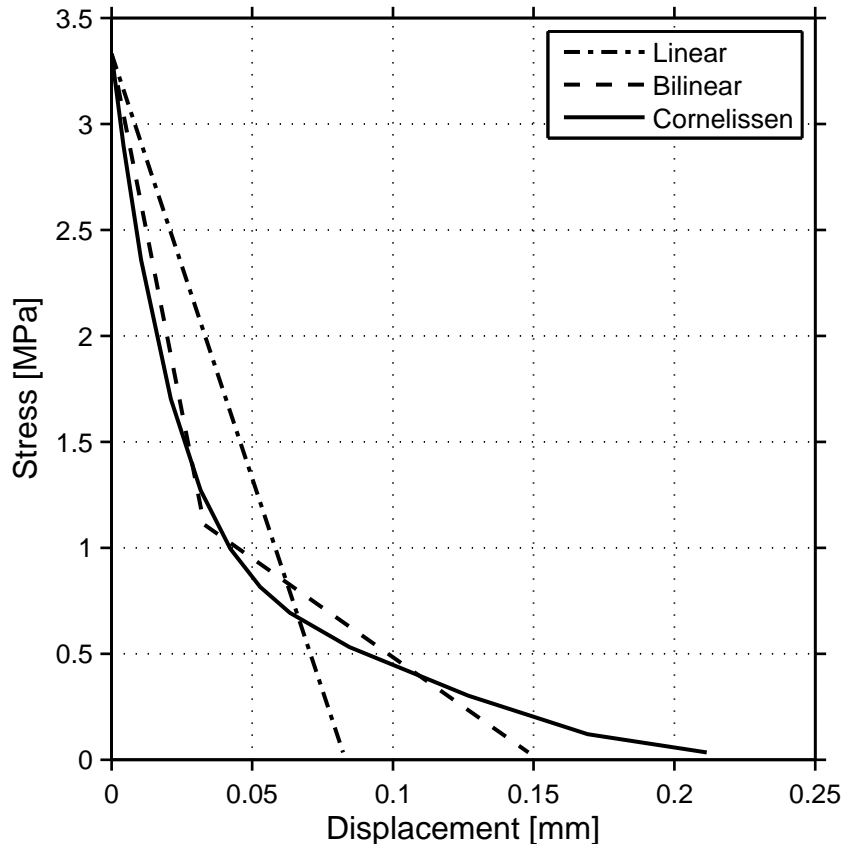


Figure 5.2: The three different tension softening functions used.

In the concrete damaged plasticity model, there are many parameters that are spe-

cific for the material model and that must be defined. The dilation angle ψ , is chosen as 38° , a ψ between 30° and 40° is often a reasonable value according to Malm (2009), but the correct value of ψ can vary from different load cases and compositions of the analysed concrete. A lower value of ψ leads to a more brittle behaviour of the concrete. Therefore, the influence of ψ on the result are evaluated further in the verification examples in section 5.2 and 5.3. Another parameter that may influence the result significantly is the tensile damage parameter d_t , in this example it is defined as a linear function of the crack displacement w with $d_{t,max} = 0.95$ for the ultimate crack opening displacement. The effect of different formulations of d_t will be examined further in section 5.2.

Symmetry conditions have been utilised when creating the models so that only half the beam is analysed. The models are built up by quadrilateral plane stress elements, with a size of 10 mm. In ABAQUS, a four node element with reduced integration is used (CPS4R), while a nine node element with full integration is used in ADINA. All analyses are deformation controlled, which means that the load is applied as a forced displacement at the load application point. For the quasi-static analyses this displacement is applied as a low velocity to further minimize the dynamic effects.

In the tests by Petersson (1981) an ultimate load of approximatley 80 kN is reached for a displacement of 0.4 mm. The load–displacement curve from Petersson (1981) can be seen in Fig. 5.3 along with the results from the analyses preformed in ABAQUS/Explicit with the three different tension softening definitions.

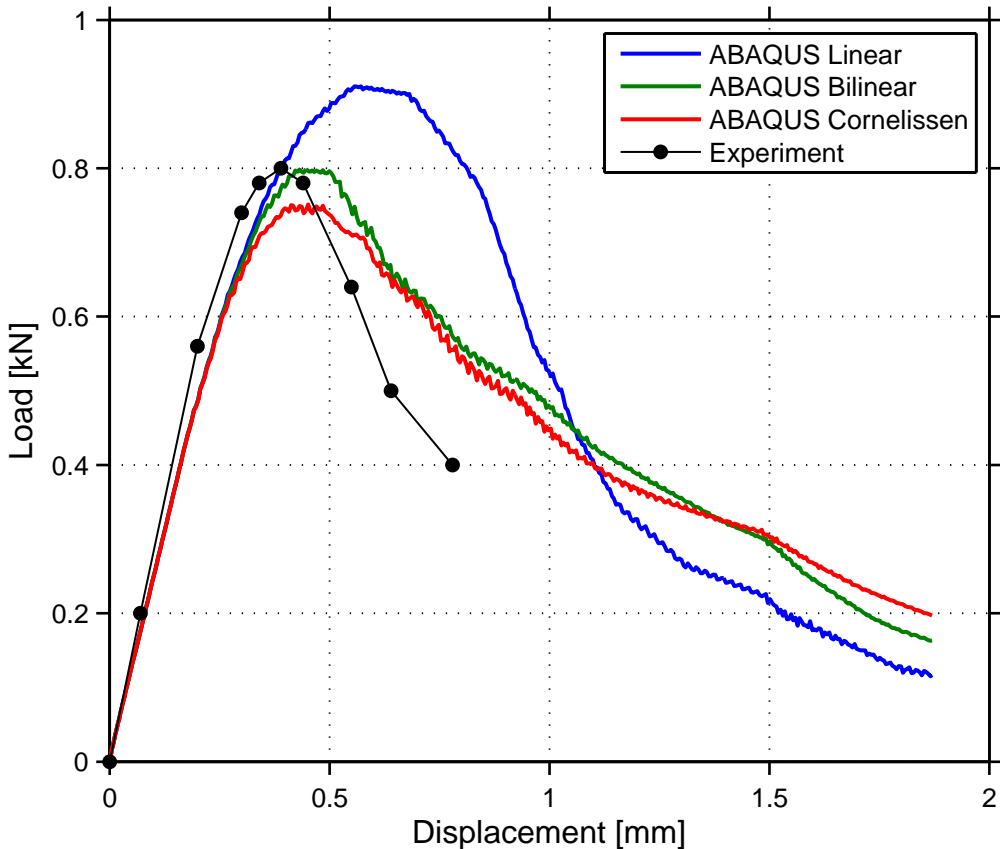


Figure 5.3: Load–displacement curves from test by Petersson (1981) and quasi-static finite element analyses in ABAQUS.

Both of the analyses made in ABAQUS with bilinear and exponential tension softening shows very good agreement with the experimental results; although they exhibit a slightly too soft response. According to Hibbit et al. (2010), the too soft response might be explained by the fact that Petersson (1981) used a much sharper notch than that of the finite element models. The analysis with linear tension softening overestimates the failure load and the deformation at which failure occurs. The initial response is however similar to that of the other two analyses.

To show that the quasi-static solutions, shown in Fig. 5.4, describe the static problem correctly, the problem has also been solved with static solvers. Results from the static solutions for bilinear tension softening are presented in Fig. 5.3 and compared to the respective quasi-static solution.

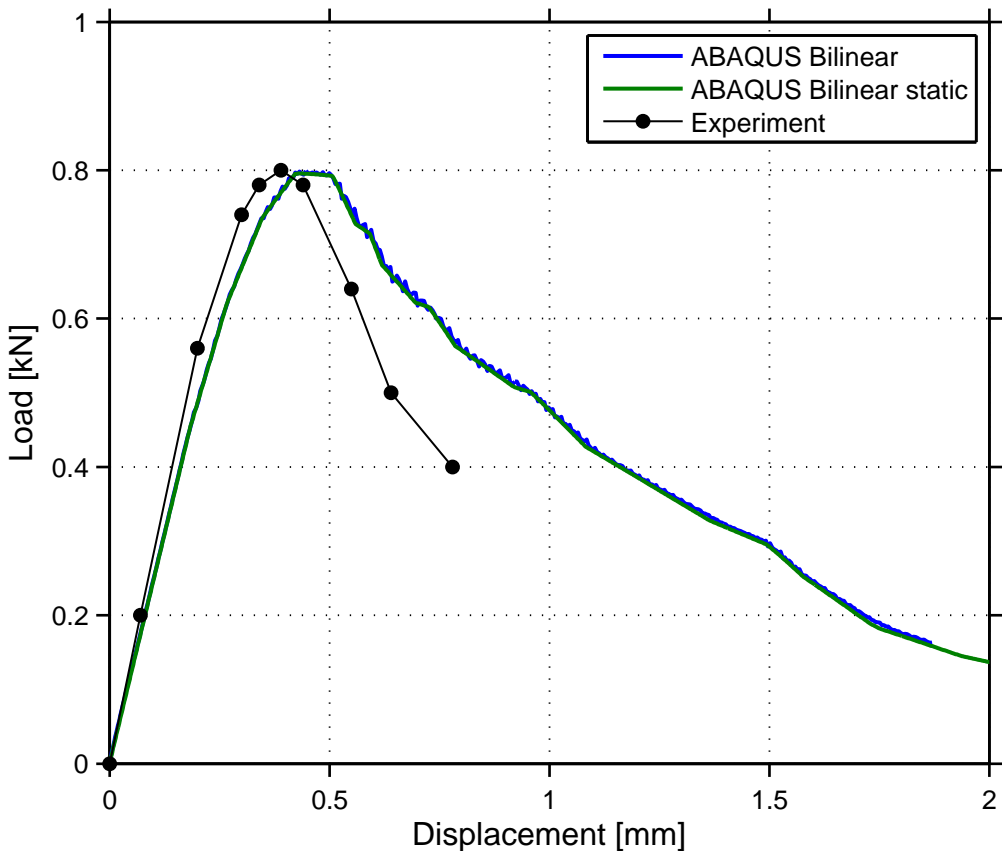


Figure 5.4: Comparison of static versus quasi-static solutions in ABAQUS.

The quasi-static solutions exhibit small dynamic effects, which can be seen in the small oscillations of the load–displacement curve, when compared to the static solution. The failure load and overall response of the structure is however almost identical for the two different solution schemes. Static analyses have been made for all analysis cases, the results excluded in Fig. 5.4 can be seen in Tab. 5.2 in comparison with the quasi-static results. From the results in Tab. 5.2 it can be seen that the quasi-static solutions often give a slightly higher failure load and mid deflection than the static solutions. This is probably due to the small oscillations in the load–displacement curves observed for the quasi-static solutions.

At the start of this project, severe convergence problems were encountered in the analyses made with the currently available version of ADINA (8.6.3). Furthermore, the response of the beam was too stiff and a very high resistance was obtained. As a comparison to the ADINA analyses, the finite element software SOLVIA was used. In principle, the material models in ADINA and SOLVIA are based on the same equations and the two programs have a lot of other similarities as well; in fact, SOLVIA originates from ADINA. After being in contact with ADINA R&D an error was discovered in the concrete material model, which meant that a crack was not allowed to propagate through an entire element. In the new release of ADINA (8.7.4) this error had been adjusted, results from the fixed material model is presented in

Fig. 5.5 together with results from ABAQUS and SOLVIA. All analyses presented in Fig. 5.5 are performed with a static solver. A comparison of the concrete material models in ADINA 8.6.3 and 8.7.4 is shown in Fig. 5.6, where the unrealistic response of the unaltered material model is obvious.

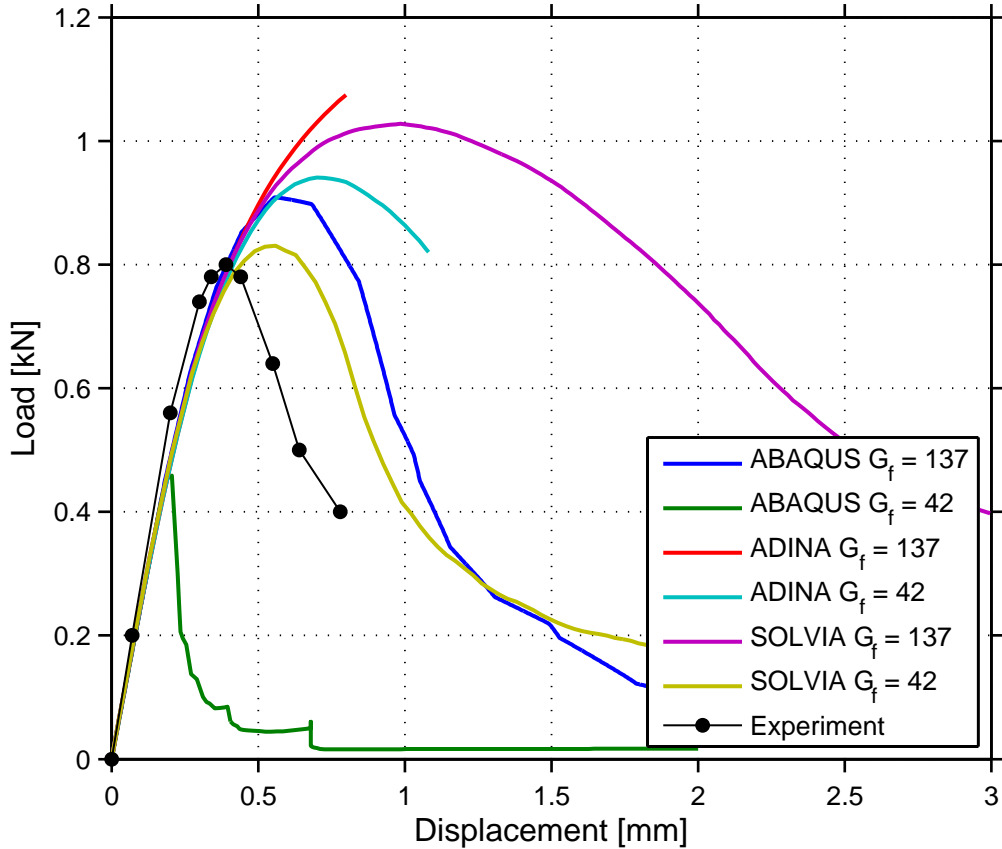


Figure 5.5: Comparison of results from ABAQUS, ADINA and SOLVIA with experimental results.

The unreinforced notched beam must be considered as a very simple example, whereas no convergence problems should arise. Hence, the analyses presented are performed with basic settings regarding convergence tolerances. The analyses in ADINA that ends prematurely could probably be deformed further through changes in the tolerances. In the ADINA analysis with $G_f = 137 \text{ Nm/m}^2$, the ultimate failure could not be observed and the analysis ended at a too high load. The fracture energy was defined through the use of Eq. (3.9), where the parameter ξ is based on the length over one integration point, i.e. approximately a third of the element length. To further investigate the material model, a analysis with a ξ based on the whole element length was also performed. As a reference, the new value of ξ corresponds to a $G_f = 42 \text{ Nm/m}^2$ if Eq. (3.9) is used with a length associated with an integration point. Although, a ultimate failure could be observed in this analysis, the ultimate failure load was too high and the unloading of the beam could not be followed. As a comparison, analogous analyses were performed with SOLVIA, as mentioned above.

However, in these analyses four node elements were used since these gave best convergence. This means that the same ξ used in the ADINA analyses could not be used in SOLVIA. In the SOLVIA analysis with a $G_f = 137 \text{ Nm/m}^2$, the response was similar to the corresponding analysis in ADINA. Although, the ultimate failure load is lower and no convergence problems were encountered, the failure load is still too high compared to the experimental results. As an additional comparison, an analysis was also performed in SOLVIA with a $G_f = 42 \text{ Nm/m}^2$. The results from the analysis showed a response and a failure load which agrees very well with the experimental data. In Fig. 5.5, the corresponding static analysis from ABAQUS with linear tension softening is presented, as a comparison. Further, an equivalent analysis but with a $G_f = 42 \text{ Nm/m}^2$ was also performed in ABAQUS. This analysis showed a very brittle and unstable behaviour.

The purpose with these analyses was to compare the programs with each other, not to fit the results to the experimental data. A more accurate result would probably be obtained if the load application and boundary conditions were described more accurately. In the analyses, the loads were applied to a single node in the symmetry plane. As a result, interlocking of the elements in the vicinity of the load may have occurred. In addition, hourgassing may be present in the ADINA and SOLVIA analyses, whereas ABAQUS includes hourglass control to reduce this phenomenon. This may explain the high failure loads obtained with ADINA and SOLVIA. A better way of describing the load application would be to instead distribute the load over a couple of elements. This would especially reduce the interlocking effects.

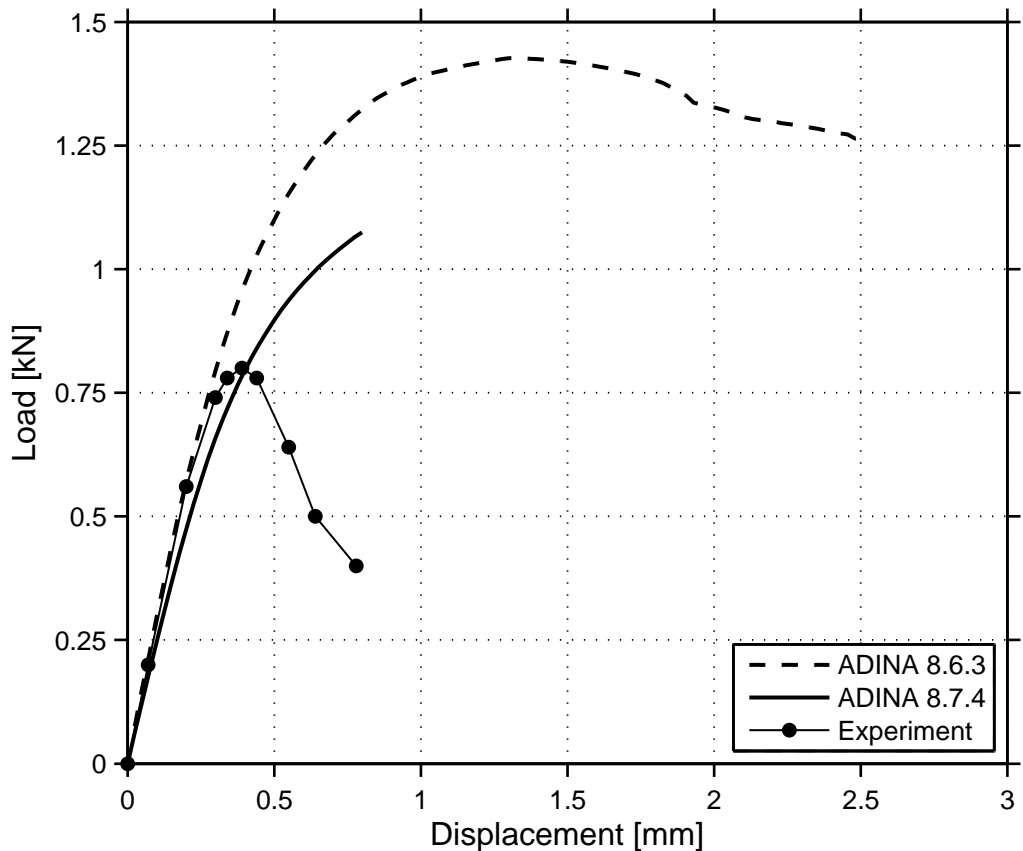


Figure 5.6: Results from ADINA before and after the fixed material model.

A summary of the failure loads from all analyses is presented in Tab. 5.2.

Table 5.2: Failure loads and corresponding mid deflections. Note that the values presented for ADINA are not for the ultimate failure, see Fig. 5.5.

	Failure load [N]		Mid deflection [mm]	
	Static	Quasi-static	Static	Quasi-static
Experiment by Petersson (1981)	800	—	0.4	—
ABAQUS with linear tension softening	909	911	0.56	0.56
ABAQUS with bilinear tension softening	795	799	0.43	0.45
ABAQUS with exponential tension softening	741	751	0.48	0.45
ADINA with linear tension softening	1075	—	0.8	—
SOLVIA with linear tension softening	1028	—	0.99	—

In conclusion, this verification example shows that ABAQUS is able to describe the behaviour of concrete very well. Whereas, the material models in ADINA and SOLVIA can be a bit unreliable, although, if used with care they can give accurate results. What also should be mentioned is that material models based on the principles of fracture mechanics often exhibit a too stiff behaviour, thus, the phenomenon shown in Fig. 5.5 is not unique for ADINA and SOLVIA. Further, it shows that quasi-static solutions obtained through the use of a dynamic solver are able to describe a static event accurately. Best agreement with the experimental results is achieved when a bilinear or exponential definition of the tension softening is used. The most accurate results should be obtained from the exponential function, which resembles the real behaviour of concrete best. However, the results obtained when using bilinear tension softening agree just as well with the experiment as the exponential function and is easier to work with. Therefore, the bilinear alternative will be used for the following analyses in this thesis. Because of the unreliability exhibited by both ADINA and SOLVIA, all further analyses will only be performed with ABAQUS.

5.2 Headed stud

In this verification example, the material models will be verified against experimental data from tests made on a single headed stud failing due to a concrete failure mode. The purpose is to show that both material models are able to describe the concrete cone failure mode and to calibrate them against the test results. The calibration results from this example will then be used in the calculations of the headed stud anchor plates in section 6.3.

An experiment performed by Nilsson and Elfgren (2009) has been chosen. The experiment was performed as a pre-study for a proposed project for the Swedish nuclear industry. As a part of a planned increase of the effect in the Swedish nuclear power facilities it was decided that all the anchor plates used as support for the piping systems should be verified. The proposed project aimed at finding new and less conservative design methods, compared with the currently used ones. Further, it was to study the influence of surface reinforcement on the failure load and failure mode. In the pre-study, a total of 66 tests were performed on single headed studs for different support conditions, slab sizes and top surface reinforcement ratios for both cracked and uncracked concrete. The tested stud had a diameter of 30 mm while the head had a diameter of 45 mm. For this verification example, the simplest test setup has been chosen; an uncracked slab without any top surface reinforcement and with supports on the four corners of the top surface. The load is applied as a pure tensile load. The test setup can be seen in Fig. 5.7.

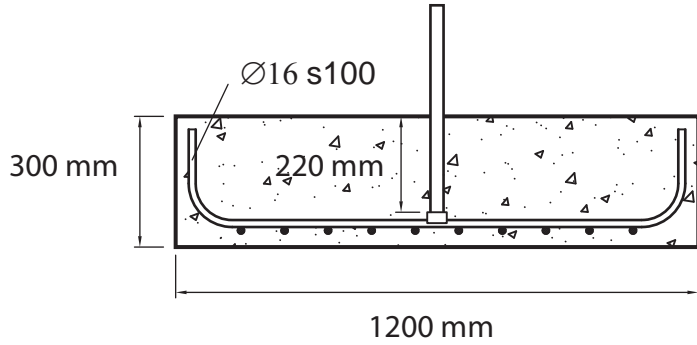


Figure 5.7: Geometry of the test setup. Reproduction from (Nilsson and Elfgren, 2009).

A steel quality with an ultimate strength $f_{uk} = 800$ MPa and a yield strength $f_{yk} = 640$ MPa was used for the studs. The reinforcement was of quality B500B, which means a yield strength $f_{yk} = 500$ MPa. In the slab, a concrete of quality C25/30 was used, but for the test chosen for this verification example the concrete was only allowed to harden during nine days. The material properties of the C25/30 concrete are therefore not fully developed and have to be reduced when comparing the test results with hand calculations and numerical studies. Equations for reducing the material properties are available in EC 2 (2004) and given in Eq. 5.1 to Eq. 5.4.

$$f_c(t) = \beta_{cc}(t) \cdot f_c \quad (5.1)$$

$$f_t(t) = \beta_{cc}^\alpha(t) \cdot f_t \quad (5.2)$$

$$E(t) = (f_c(t)/f_c(t))^{0.3} \cdot E \quad (5.3)$$

$$\beta_{cc}(t) = \exp(0.38(1 - \sqrt{28/t})) \quad (5.4)$$

where,

- f_c is the compressive strength after 28 days
- f_t is the tensile strength after 28 days
- E is the elastic modulus after 28 days
- f_c is the compressive strength after t days
- f_t is the tensile strength after t days
- E is the elastic modulus after t days
- α is a coefficient. $\alpha = 1$ for $t < 28$ and $\alpha = 2/3$ for $t \geq 28$

According to De Schutter and Taerwe (1997), it can be assumed that the fracture energy G_f at early ages of concrete develops proportional to the tensile strength. The material properties for both 28 day and 9 day concrete of quality C25/30 are

given in Tab. 5.3. The material properties of the 28 day concrete corresponds to the mean values given in EC 2 (2004). No definition of G_f is given in EC 2 (2004), the value presented for the 28 day concrete in Tab. 5.3 was instead taken from MC 90 (1993), which can be found in Malm (2006).

Table 5.3: Material properties of a C25/30 concrete after 9 and 28 days.

		9 days	28 days	
Density	ρ	2400	2400	kg/m ³
Elastic modulus	E	28.4	31	GPa
Poisson's ratio	ν	0.2	0.2	-
Compressive strength	f_c	24.7	33	MPa
Tensile strength	f_t	1.94	2.6	MPa
Fracture energy	G_f	48.6	65	Nm/m ²

5.2.1 Finite element model

Since severe discontinuities are expected with following convergence issues, all analyses are solved quasi-statically and performed with explicit solvers. 3D models of the test have been built in which two symmetry planes have been utilised so that only a quarter of the problem has to be analysed. This significantly reduces the computational time needed to solve the problem. The quarter model used can be seen in Fig. 5.8.

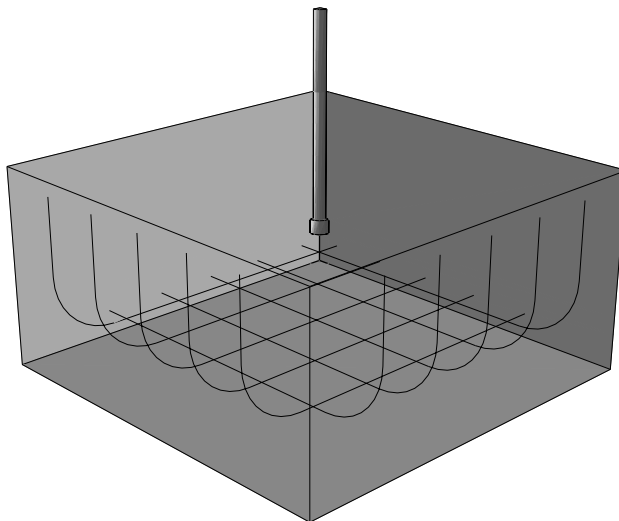


Figure 5.8: Finite element model used for analysis.

Boundary conditions are applied to the entire circumference of the top surface at which all translational degrees of freedom are constrained. These boundary conditions differ from the ones of the test setup, but should not affect the overall response

of structure since it is only pinned at the circumference and still allowed to rotate. Consequently, the stress distribution in the slab should not be substantially affected by the difference in boundary conditions while the proposed modification simplifies the numerical model. The analyses are deformation controlled and the stud is therefore subjected to a forced displacement. Since the analyses are quasi-static, a velocity of 0.0075 m/s has been used to avoid as much dynamic effects as possible. The reinforcement is modeled with truss elements and full bond between the reinforcement and the concrete is assumed, i.e. no bond slip may occur. The interaction between the stud and the concrete is considered as hard in the normal direction, which means that the surfaces of the two cannot penetrate each other. In the tangential direction, frictionless behavior has been assumed; which is a conservative simplification.

A global element size of approximately 20 mm has been used to be able to follow the crack propagation. The elements around and in the stud are smaller, so its circular shape can be described properly. 8 node linear brick elements have been used in both the slab and the stud. An element with reduced integration called C3D8R has been used, this means that the element only has one integration point. The mesh used in ABAQUS can be seen in Fig. 5.9.

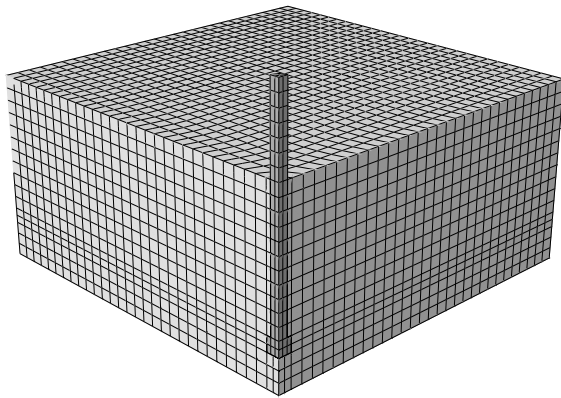


Figure 5.9: Mesh used for the analysis in ABAQUS.

The general material properties for the 9 day concrete stated above are used in the models. Further, a bilinear tension softening curve is used in accordance with the results from the verification example in section 5.1. In the concrete damaged plasticity material model in ABAQUS, parametric studies will be performed on the dilational angle and the tension damage parameter to determine which values are appropriate to use. Elsewhere, a dilational angle of 10° and a linear function for the damage parameter with max damage 0.95 is used. The compressive behaviour in ABAQUS has been defined as a tabular function, according to the stress-strain relation for non-linear structural analysis given in section 3.1.5 of EC 2 (2004), see Fig 5.10. This function assumes that the compressive behaviour is linear elastic up to 40 % of the compressive strength. All steel parts, the stud and the reinforcement, are modeled with an elastic perfectly plastic material model with their respective yield strengths.

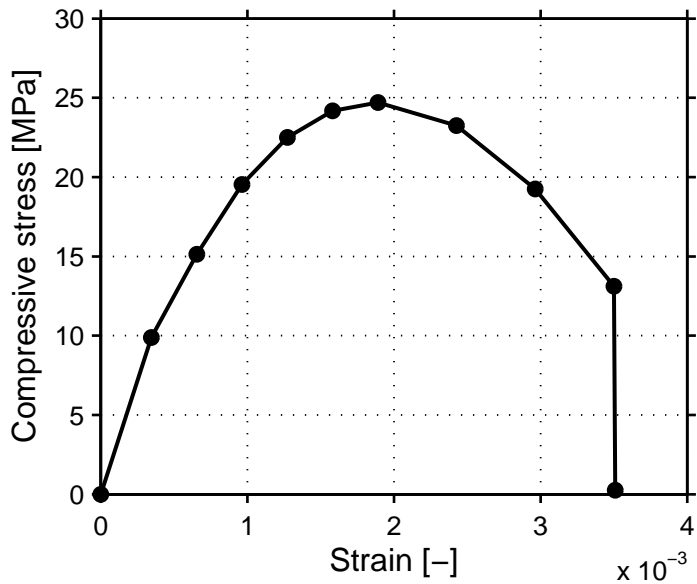


Figure 5.10: Compressive stress-strain behaviour according to EC 2 (2004) for 9 day concrete of quality C20/25.

5.2.2 Results

The result from the experiment is presented in Tab. 5.4 together with the failure loads obtained from hand calculations according to SIS-CEN/TS 1992-4 (2009) described in section 4.1. The hand calculations are made with the same material properties used in the finite element models and without any partial coefficients nor safety factors.

Table 5.4: Failure loads from the experiment and hand calculations.

	Cone failure [kN]	Pull-out failure [kN]	Steel failure [kN]
Experiment	179.1	—	—
CEN/TS	193	182	509

As can be seen in Tab. 5.4 the hand calculation results in pull-out failure being the decisive failure mode, although the difference between pull-out failure and cone failure only is 6%. This should be seen as an indication that the true failure mode probably is a combination of the two, and that the deciding failure mode might change between different tests due to the stochastic nature of concrete. The reason why pull-out failure may be the decisive failure mode, is the small bolt head used. This leads to that all the load acting on the bolt is transferred to the concrete over a small area. In Nilsson and Elfgren (2009), two similar test setups were also analysed, which only differed from the chosen test in their boundary conditions. Instead of only being supported at the four corners of the top surface, they were supported with

a circular support ring on the top surface. One test was made with a rubber ring between the support and the concrete and one without the rubber ring. The failure load from these tests only differed 3 % and 8 % from the chosen test, respectively. This further validates the simplification of the boundary conditions made in the finite element analyses.

The experimental results and concrete cone failure load from the hand calculations can be seen in Fig. 5.11 together with load curves from one finite element analysis from ABAQUS.

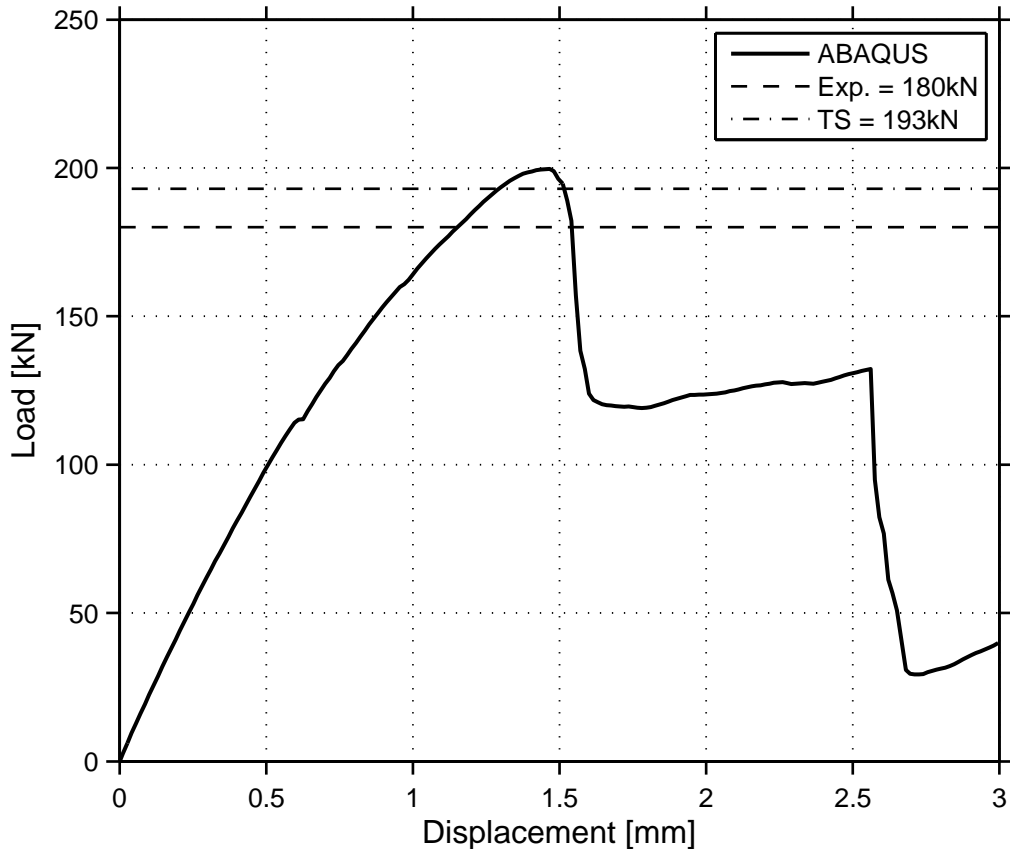


Figure 5.11: Load-displacement curve from ABAQUS in comparison with experimental results and hand calculations.

As can be seen in the figure, the finite element result corresponds very well with both the experiments and the hand calculations. The difference is only 11 % compared to the experimental results and only 3.6 % compared to the hand calculated concrete cone failure load.

To confirm that the results shown in Fig. 5.11 are not mesh dependent and that they converge towards the experimental results, a mesh refinement study has been performed. In the study, the global element size has been halved, i.e. elements with an approximate size of 10 mm have been used. The results from the study are shown in Fig. 5.12, compared with the experimental results. To speed up the calculation

a higher velocity has been used for the refined mesh size, than for the normal mesh size. This lead to some minor dynamic effects in the results, i.e. small oscillations in the load–displacement curve. The curves for the refined meshes showed in Fig. 5.12 have been smoothed to better represent a static solution.

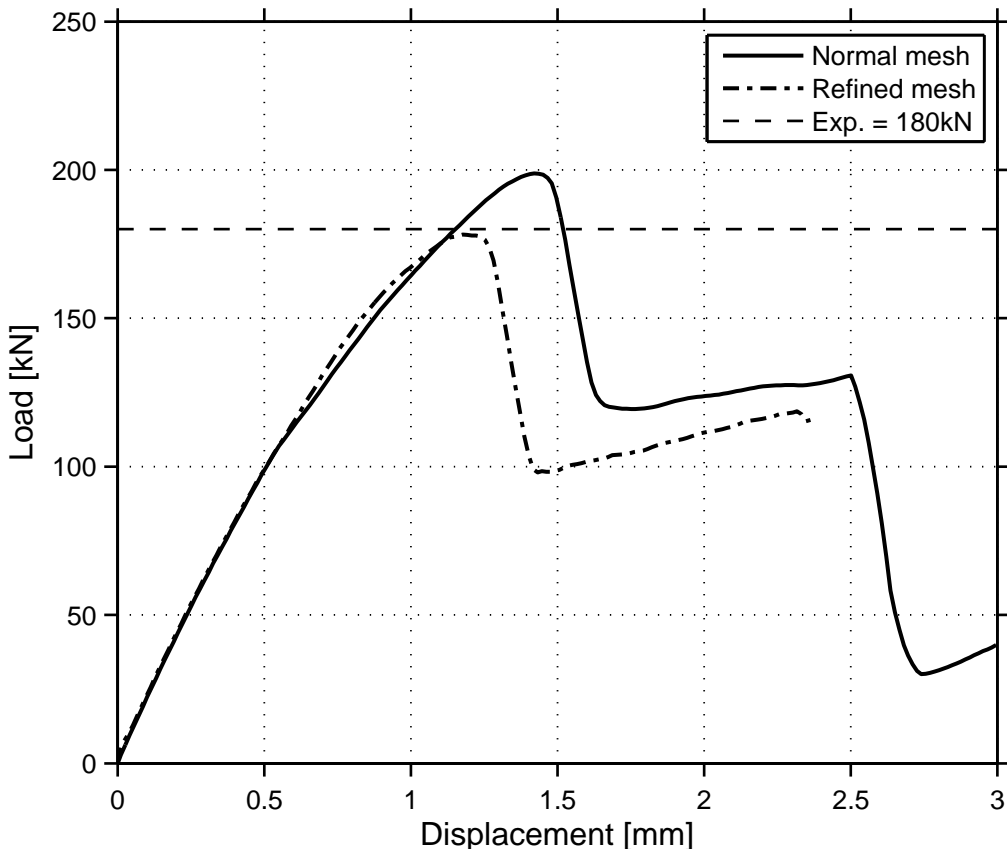


Figure 5.12: Results from the mesh refinement study.

The mesh refinement study shows that the ABAQUS model gives an almost identical failure load compared to the experiment for the refined mesh. This shows the the model converge towards the experimental results as the mesh is refined.

As previously mentioned, the concrete damaged plasticity model in ABAQUS contains several input parameters that cannot be found among the typical material properties used to describe concrete, hence these parameters have to be chosen with great care in every new problem analysed. Two of these parameters, the dilation angle and the tension damage parameter, have been investigated through parametric studies, as mentioned above. The dilation angle has to assume a value larger than 0° and smaller than the inner friction angle of the material, which is 56.3° for concrete. In the parametric study of the dilation angle, the following values have been tested; 5° , 10° , 15° , 20° , 30° , 40° and 50° . The result from the parametric study is shown in Fig. 5.13.

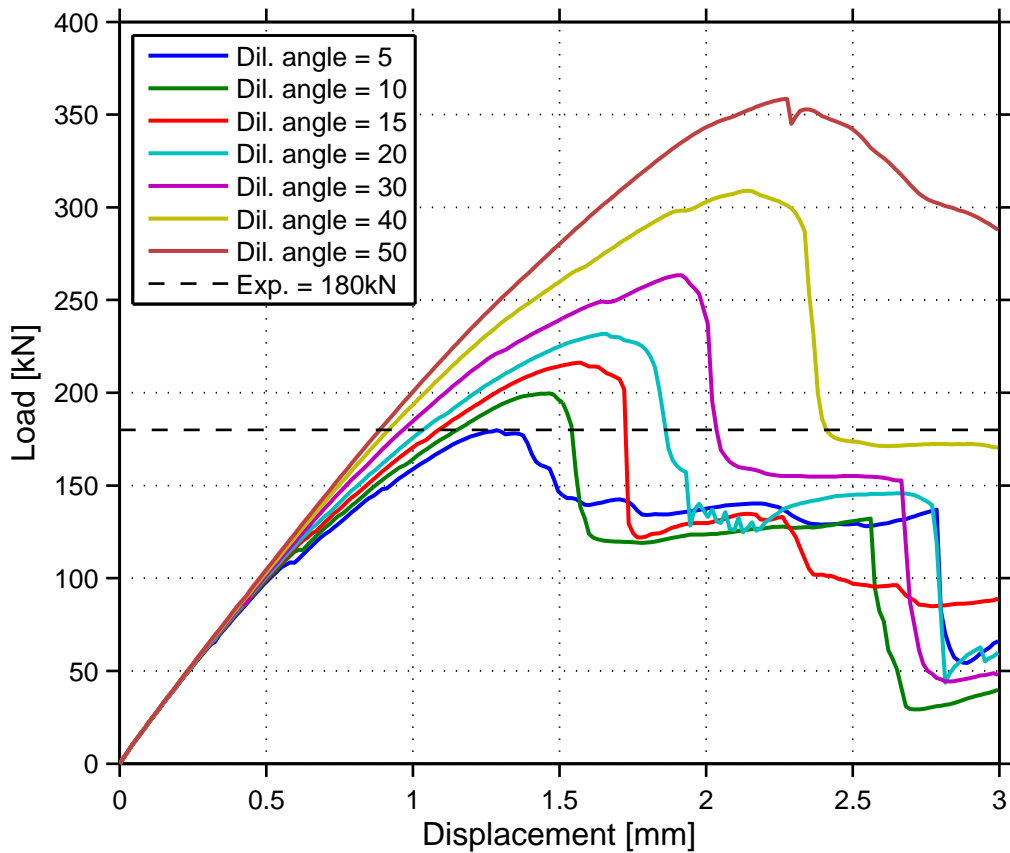


Figure 5.13: Parametric study of the dilation angle in ABAQUS.

High values of the dilation angle leads to a severe overestimation of the failure load and a slightly more ductile post-failure, as seen in Fig. 5.13. This is especially seen in the result obtained for a dilation angle equal to 50° . Good agreement with the experimental result is achieved for dilation angles between 5° and 20° , which at maximum differs about 30 % from the experimental results. But as shown in the mesh refinement study, the failure load decreases and approaches the experimental result as the mesh is refined. However, a dilation angle equal to 5° show a post-failure behaviour that differs from the other analyses with low values of the dilation angle and is more ductile. This may be an indication that failure mode has changed into a more pronounced pull-out failure.

The dilation angle is a property related to the shear resistance of the concrete. Since the shear resistance is increased as concrete hardens, it is reasonable to assume a low dilation angle for a young concrete; as the 9 day concrete used in the experiments. As previously mentioned, a normal value for the dilation angle is between 30° and 40° .

In the next parametric study, different formulations of how the tensile damage parameter varies with the crack displacement have been tested. It has also been tested to omit the damage parameter, which should give accurate results as long as the

load case is monotonic. Otherwise, three different linear functions with a maximum damage of 0.90, 0.95 and 0.99 have been tested. Additionally, a bilinear function has been tested, which has been defined so that the stress–plastic displacement relationship calculated according to Eq. (3.4) resembles that of the stress–crack displacement as good as possible. This lead to a maximum damage of 0.74 for the bilinear function. The four different damage formulations can bee seen in Fig. 5.14.

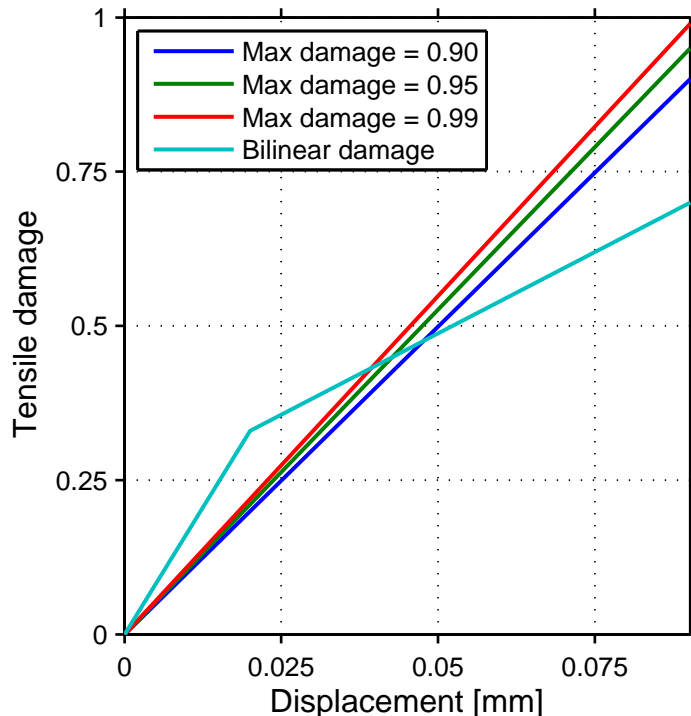


Figure 5.14: The different formulations of the tensile damage parameter used in the parametric study.

Since the concrete cone failure is governed by the tensile strength of concrete and no other compressive failure is expected, the compressive damage parameter is omitted from the analyses and its influence is not studied in any analysis in this thesis. A dilation angle of 10° has been used in the parametric study. The results are shown in Fig. 5.15.

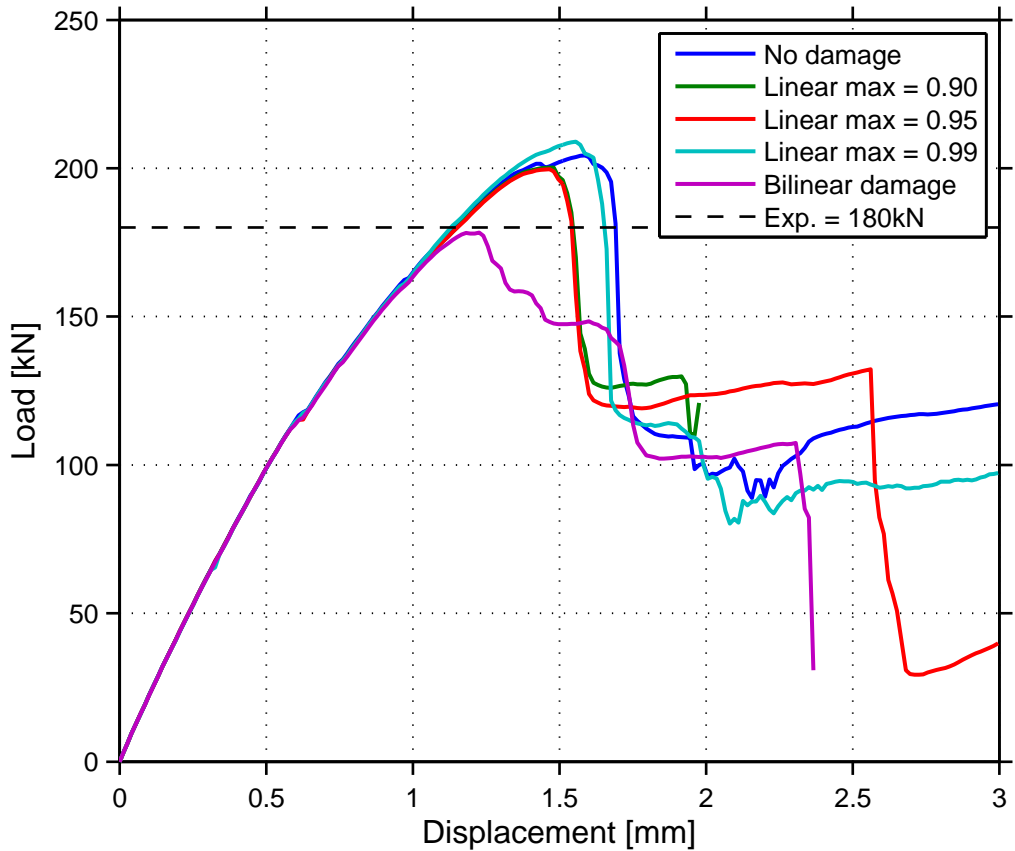


Figure 5.15: Parametric study of the tension damage parameter in ABAQUS.

The results from the analyses with linear damage definition and with no damage give almost identical results, while the bilinear damage definition finds a significantly lower failure load. This failure load agrees very well with the experimental result, but shows a too ductile post-failure behaviour which has not been observed in any experiments on headed studs and is not expected for a concrete cone failure. The reason why the bilinear damage definition finds the failure earlier than the other analyses is probably that the stress–plastic displacement curve obtained is steeper right after the tensile strength is reached than that of the other damage definitions. This indicates a faster propagation of the cracks after the first crack initiates, since the failure load according to Eligehausen et al. (1989) is not reached until 40 % of the cone is developed, a faster crack propagation leads to an earlier failure. The same plastic displacement curve might also explain the more ductile post-failure behaviour as the curve flattens out significantly after the bilinear break point, which leads to slower loss of the stress transfer ability across the crack as the crack opens.

A typical crack pattern from the ABAQUS analyses is shown in Fig. 5.16. Note that the analysis only consists of the quarter model, as described above, which has been mirrored in the post processor to show half the test setup.

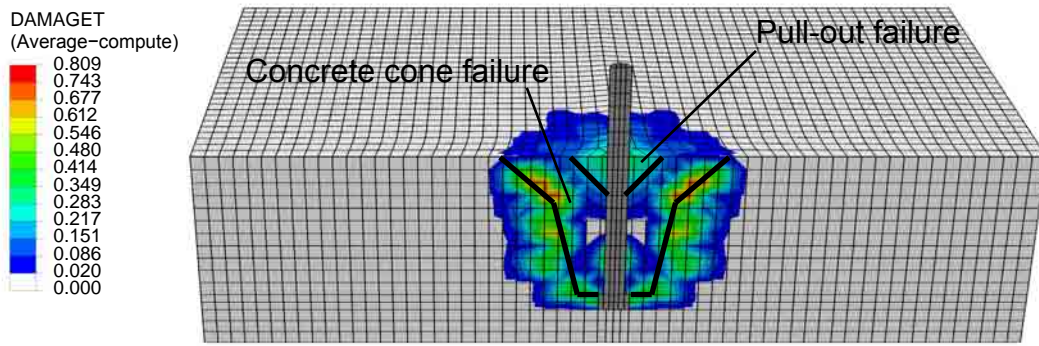


Figure 5.16: Illustration of the concrete cone after the failure load is reached through the tensile damage parameter in ABAQUS. Max damage = 0.95.

The crack pattern in Fig. 5.16 clearly shows that the failure occurs due to a concrete break-out body. Although, the angle of the break-out body is steeper than the typical concrete cone break-out body shown in experiments. This may be an indication that the failure occurs due to a combination of pull-out and cone failure, as indicated by the calculations from SIS-CEN/TS 1992-4 (2009) given in Tab. 5.4.

In Fig. 5.17, the blue area above the bolt head is subjected to a state of triaxial compressive stress; as indicated by the negative maximum principal stress. These high compressive stresses in combination with the tensile damage close to anchor at the top surface of the slab also clearly indicates the presence of a pull-out behaviour.

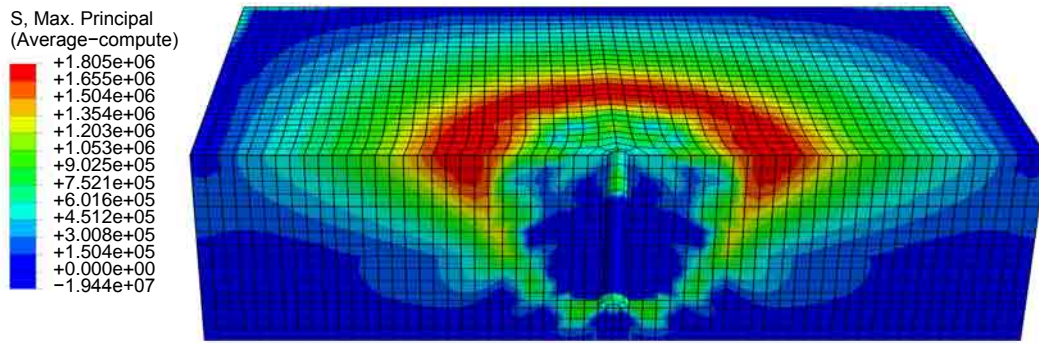


Figure 5.17: Maximum principal stresses after the failure load is reached from the ABAQUS model.

The analyses from the concrete damaged plasticity model shows that the material model is able to describe the behaviour of a headed stud with sufficient accuracy. The parametric studies showed that a dilation angle of 5°–20° is appropriate when analysing headed studs. For a coarse mesh, a dilation angle of 5° agrees best with the experimental failure load, but such a small dilation angle may give unstable results and showed a deviating post-failure behaviour. Therefore, a dilation angle of 10° is considered to show sufficiently good agreement with the experimental result and will

be used for analyses of the headed stud anchor plates in section 6.3. The analysis with a dilation angle of 10° also converged towards the experimental failure load, as the mesh was refined. As to the tensile damage parameter, best agreement with the experimental failure load was achieved with the bilinear definition of the damage parameter, for the coarse mesh. But it also showed a to ductile and unrealistic post-failure behaviour. The other definitions of the damage parameter showed almost identical failure loads and it was shown in the mesh refinement study that a linear definition with max damage 0.95 converged towards the experimentally obtained failure load. Either one of these could be used, but since good results have been obtained with max damage 0.95 and that 5 % residual stiffness is reasonable due to for example aggregate interlocking, the linear function with max damage 0.95 will be used in all subsequent analyses in this thesis.

5.3 Expansion anchor

The intention with this verification example is to verify the material model to be used for expansion anchors, and also study how to model the interaction between the anchor and the concrete. This will be accomplished through a comparison with test results of an expansions anchor subjected to a pure tensile load. The result from the calculations in this example will later be used for all analyses of the expansion anchor plates in section 6.4.

The test results used for comparison were presented by Rodriguez et al. (2001). This study was included in a research project aimed to determine the difference in static and seismic loading of different type of anchors. In the project, four different tasks were defined which resulted in that a total of 595 tests were carried out. All tested anchors were selected on the basis of their frequency of use in nuclear power facilities in the US. Some of the tested parameters were different concrete strengths, loading rates and presence of cracks in the concrete member. For anchors in uncracked concrete, the typical test specimen was a block of concrete 1.00 m wide, 0.60 m deep and 2.20 m long. Reinforcement was placed in the middle of the block to enable test of anchors on both the top and bottom surface.

As mentioned above, different type of anchors were tested during the project; one of the tested anchors was a M20 sleeve-type expansion anchor. The effective embedment depth of the anchor was 102 mm while the expansion sleeve was about 62.5 mm long. Nothing is mentioned about the steel quality, therefore the ultimate steel strength has been assumed to $f_{uk} = 800$ MPa and the yield strength to $f_{yk} = 640$ MPa. Since the failure is governed by the concrete properties, the steel failure is of minor interest and should not affect the result. The concrete had a compressive strength of 32.4 MPa which corresponds to a concrete of quality C30/37. All specimens were not tested until 28 days after casting, hence the material properties defined in EC 2 (2004) may be used, see Tab. 5.5.

Table 5.5: Material properties of a C30/37 concrete.

Density	ρ	2400	kg/m ³
Elastic modulus	E	33	GPa
Poisson's ratio	ν	0.2	-
Compressive strength	f_c	32.4	MPa
Tensile strength	f_t	2.9	MPa
Fracture energy	G_f	100	Nm/m ²

5.3.1 Finite element model

The analyses are displacement controlled and made in ABAQUS/Explicit where the load has been applied as a forced displacement. Since the analyses are quasi-static, a velocity of 0.02 m/s was applied in order to avoid dynamic effects.

In ABAQUS, the concrete damage plasticity material model has been used to describe the behaviour of concrete. However, all included parameters are not easy to define and require further investigation. The analyses made in section 5.1 showed that a bilinear softening behaviour agreed very well with the experiments. Hence, the tension softening behaviour in these analyses has been modelled as bilinear. The compressive behaviour has been defined as a tabular function, according to the stress-strain relation for non-linear structural analysis given in section 3.1.5 of EC 2 (2004). In principle, the used compressive curve resembles the one shown in Fig. 5.10. This function assumes that the compressive behaviour is linear elastic up to 40 % of the compressive strength. The tension damage parameter is also rather difficult to define, but according to the parametric studies performed in section 5.2 a linear definition gave sufficient accuracy. Therefore, the damage parameter will be defined as linear with a maximum damage of 0.95. The dilation angle is dependent of several parameters concerning the structure and the load case. Hence, an appropriate dilation angle will be determined through a parametric study. All other material properties have been chosen in compliance with Tab. 5.5.

The test setup has been modelled in 3D. However, only a quarter of the structure has been modelled in order to reduce the computational time. This means that two symmetry planes have to be used to solve the whole model. Boundary conditions are applied on the two remaining sides, where all degrees of freedom are constrained. This differs from the test setup but should not affect the response of the structure since the large thickness of the concrete member reduces the bending. The depth of the hole, in which the bolt is mounted, has been modelled a bit deeper than the length of the bolt. This has been done to avoid the underlying concrete to be damaged unrealistically. The reinforcement, placed in the middle of the concrete block below the anchors, has not been modelled because it will not affect the stress distribution in the concrete cone. The interaction between the expansion anchor and the concrete consists of two different formulations. Along the length of the expansion sleeve the interaction is modelled as a tied constraint; this means that no slip will occur between the sleeve and the concrete. The concrete cone failure show

limited amount of slip; therefore, the simplification with a tied constraint should not substantially affect the results. The compressive forces originating from the expansion of the sleeve will be neglected due to this simplification. The compressive forces tend to reduce the angle of the concrete cone with a higher bearing capacity as a result. However, this can be compensated through the definition of the dilation angle. The interaction between the rest of the bolt and the concrete is considered to be hard in normal direction and frictionless in tangential direction.

To be able to follow the crack propagation in the concrete member, the global element size has been chosen rather small. In the concrete member, the element size is approximately 10 mm while the elements in the bolt are slightly smaller to better describe the circular shape. The elements are 8 node linear brick elements with reduced integration, called C3D8R in ABAQUS, in both the bolt and the concrete block. The used mesh is depicted in Fig. 5.18.

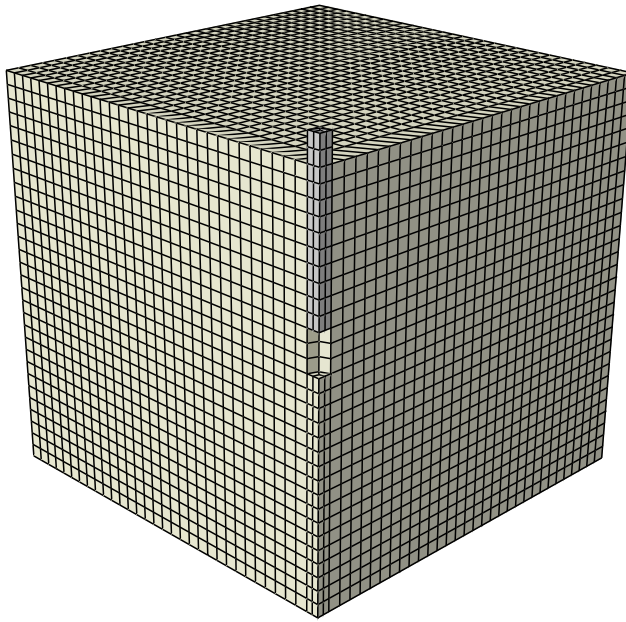


Figure 5.18: Mesh used for the analysis in ABAQUS.

5.3.2 Results

The experimental result is presented in Tab. 5.6, together with the characteristic resistance calculated according to SIS-CEN/TS 1992-4 (2009). The same material properties are used in the hand-calculations as in the finite element analyses.

Table 5.6: Failure loads from the experiment and hand-calculations.

	Cone failure [kN]	Pull-out failure [kN]	Steel failure [kN]
Experiment	108	—	—
CEN/TS	63.3	—	251.2

The characteristic pull-out failure load for expansion anchors can not be determined with any equation; instead, the characteristic resistance must be evaluated through experiments. Since no product descriptions of the anchors are available the resistance is omitted in Tab. 5.6. As can be seen, the decisive failure mode is concrete cone failure with a characteristic resistance of 68.3 kN. However, according to the test results the resistance is 108 kN, which is almost 70 % larger. This shows that the design codes are very conservative for post-installed non-headed fasteners; the reason is probably that there are many insecurities regarding the installation procedures. Furthermore, it can be seen that the steel failure load is considerably larger compared to the other failure loads and the experimental results; which indicates that this is not the decisive failure mode.

The parametric study of the dilation angle is depicted in Fig. 5.19, together with the hand-calculated concrete cone failure load and the experimental result.

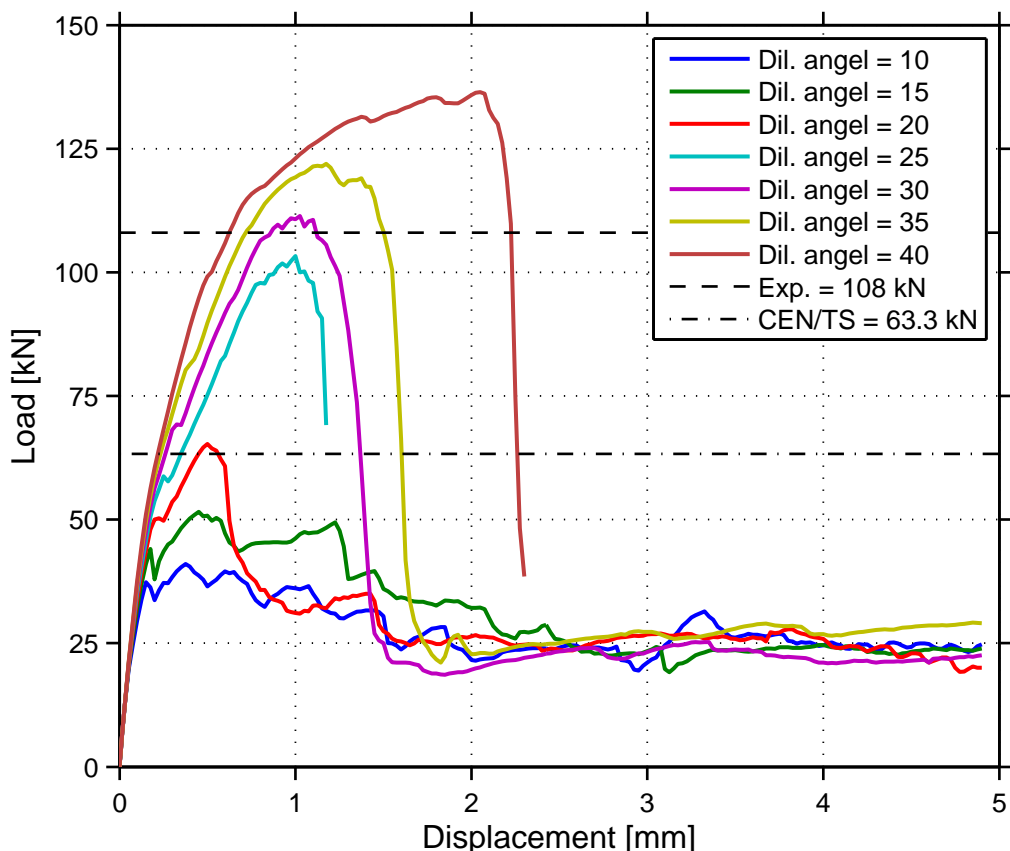


Figure 5.19: Parametric study of the dilation angle.

As can be seen, a dilation angle of 30° has the best agreement with the experimental result. The dilation angle has a vast effect on the failure load, since the angle of the concrete cone failure surface is reduced with larger dilation angles. This can clearly be seen in Fig. 5.19, where a dilation angle of 10° results in a failure load of 38 kN while a dilation angle of 40° approximately gives 138 kN. Further, the major

difference between a dilation angle of 20° and 25° is probably also explained due to a change in failure mode. Where a lower dilation angle exhibits more of a pull-out failure, which can be seen in Fig. 5.20a). For dilation angles above 25° , the failure is a more pronounced concrete cone failure mode, see Fig. 5.20b). The concrete blocks in Fig. 5.20 are shown in a symmetry plane and cut in the bottom. These results show that it is important to calibrate the material model to experimental results.

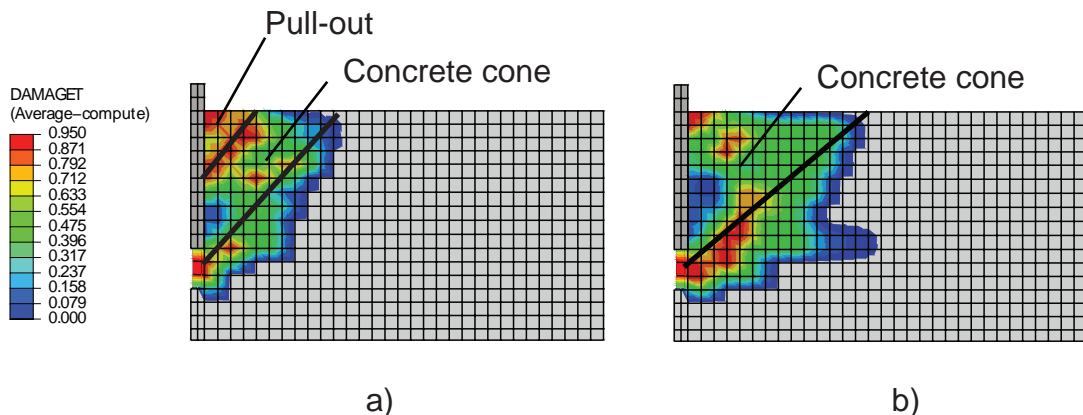


Figure 5.20: Comparison of two concrete cone surfaces with a dilation angle of a) 10° and b) 30° .

A comparison of the load-displacement curves from the experiment and the finite element analysis, with a 30° dilation angle, is depicted in Fig. 5.21.

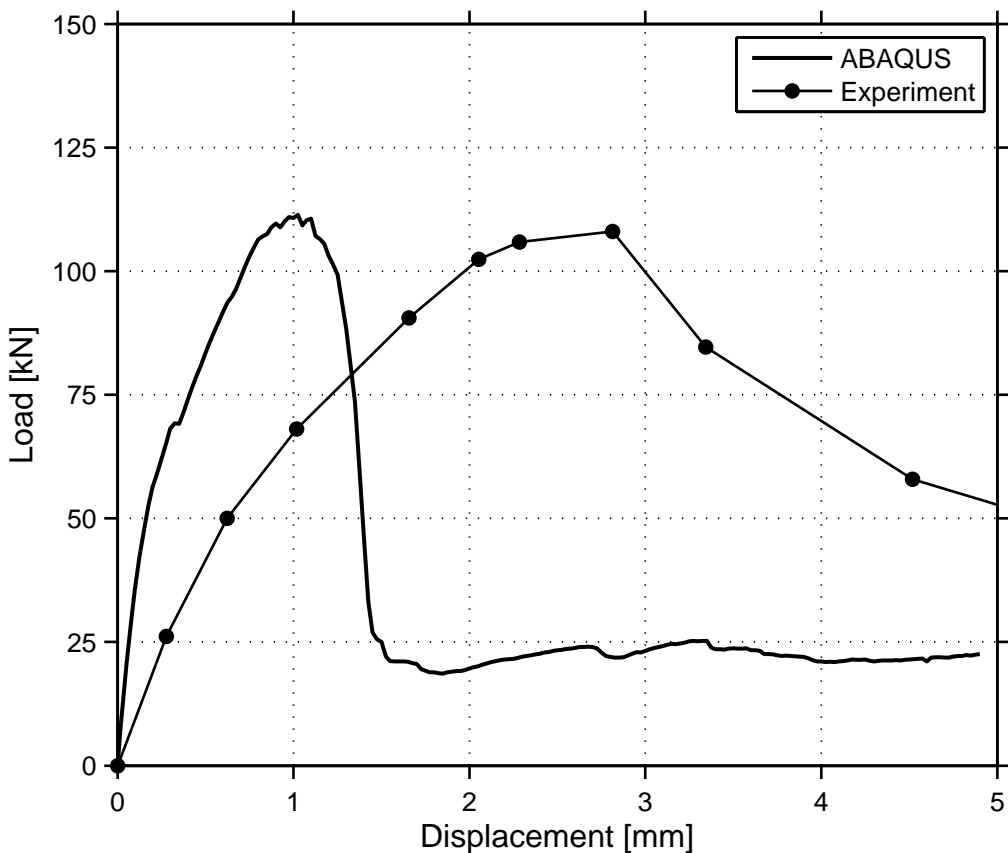


Figure 5.21: A comparison between the finite element analysis and the experiments.

The experimental result shows a more ductile behaviour than the finite element analysis. As mentioned above, the interaction between the concrete and the anchor is modelled with a tied constraint in the numerical analysis; which means that slipping of the anchor in the hole is neglected. However, in the experiments these slipping effects are not omitted, therefore the behaviour becomes more ductile. Further, there are mainly two types of slipping occurring when a sleeve-type expansion anchor is subjected to a tensile load. Partly the frictional slip between the expansion sleeve and the concrete and partly when the expansion cone is pulled through the sleeve. Both types of slipping result in a more ductile behaviour, which can clearly be seen in the comparison of the two load-displacement curves.

A dilation angle of 30° will be used for all analyses in section 6.4, since this value coincides best with the experimental result. The interaction between the expansion sleeve and the concrete will be modelled with the tied constraint since the primary purpose is to obtain the failure load. A more exact model of the expansion anchor, with the pull-through behaviour of the expansion cone, will not be covered in this thesis since the objective is to observe the concrete behaviour.

@Seismicisolation

Chapter 6

Analysis of anchor plates at Forsmark nuclear facility

In this chapter a selection of anchor plates subjected to different load cases will be analysed. There are mainly two purposes with these analyses, where the first is to control if non-linear finite element analyses may be applied to the analysis of anchor plates. And secondly to examine how the finite element method corresponds with calculations according to SIS-CEN/TS 1992-4 (2009) and evaluate whether any overcapacity is present. Most of the performed analyses are static but a few dynamic analyses have also been made and is presented herein.

The result from the static analyses are used to develop failure envelopes for several load cases, which are presented in section 6.3.4 and 6.4.4. The intention of the failure envelopes is to be a support in the design process of anchor plates. However, the failure envelopes presented in this thesis are mainly meant to show the concept and perhaps not for practical use.

6.1 Anchor plates at Forsmark nuclear facility

There are mainly two type of anchor plates used at Forsmark nuclear facility; cast-in-place anchor plates installed during the construction and post-installed anchor plates installed during both the construction phase and after the facility was put into service. A number of standard cast-in-place anchor plates were developed and used during the construction phase to simplify the design work. These can be divided into four main categories, used for different load and support cases. Two of them are mainly intended as pinned supports for beams, and only differ in their geometry where one of them is larger then the other and can be used to support a line load. These two categories of plates are anchored to the concrete through 250 mm long reinforcement bars which are welded to the steel plate. A typical anchor plate used as a pinned support can bee seen in Fig. 6.1a). This type of anchor plate will not be treated further in this thesis. The two other categories of cast-in-place anchor plates are intended for significantly higher loads then the previously mentioned. On these,

the beams are welded to the steel plate, i.e. a fixed support condition is assumed. The main purpose of these two categories of anchor plates is to support the piping of the process system in the facility. One of them is a specially designed anchor plate intended for extreme loads, such as the failure of a pipe and is only placed inside the containment vessel. To assure a ductile failure, this type of plate has a very large embedment depth so that steel failure is governing, therefore this type of anchor plate is not of interest in this thesis. The other category, called an M-type anchor is a smaller plate with shallower embedment depth and is therefore of more interest. It is anchored to the concrete through headed studs welded to the steel plate with an embedment depth of 225-270 mm. A typical M-type anchor plate can be seen Fig. 6.1b). The M-type anchor plates will be examined further in section 6.3.

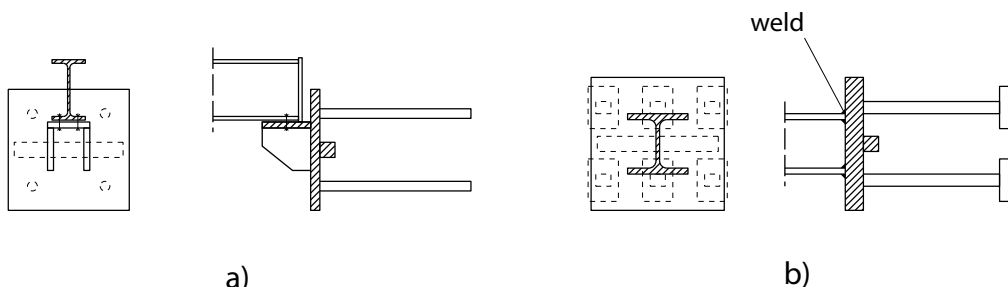


Figure 6.1: Example of standard type anchor plate used as a) pinned support and b) fixed support. Reproduction from (Kallersjö & Trepp AB, 1977)

Due to construction deviations and changes to the piping system during the construction phase many of the cast-in-place anchor plates where improperly placed and did not fit properly to the piping system. In some cases, modifications could be made to the anchor plate so it could be used. If this was not possible, a new anchor plate had to be installed; although this was preferably avoided during the construction phase. Many new systems have been installed to the power facilities since they were put into service, and as a consequence many new anchor plates have also been installed. The post-installed anchor plates at Forsmark normally consists of a steel plate with a size in the range 300x300 to 500x500 mm² and a varying thickness of 15 to 30 mm. Different types of post-installed anchors have been used to anchor the steel plates to the concrete. Chemical anchors are normally used for pinned supports while some type of expansion anchors, either sleeve-type or bolt-type, are normally used for fixed supports.

The anchor plates using sleeve-type expansion anchors will be examined further in section 6.4. Further, a few examples of both cast-in-place and post-installed anchor plates are given in appendix B.1.

6.2 General aspects of the finite element models

The finite element models of the M-type anchor plates and the expansion anchor plates are similar concerning some aspects. These equalities will be presented in this section while some special aspects of the individual models will be given in relevant sections below.

All the analyses are expected to show discontinuities which result in convergence problems. Therefore, all analyses are solved with a quasi-static approach using the explicit solver included in ABAQUS. The quasi-static load is applied as a forced displacement with a low velocity to minimise the dynamic effects that would otherwise arise. Regarding analyses where moments are applied, the same approach for applying the moment is used but with a forced rotation instead. As mentioned above, the structures are attached to the steel plates through steel beams of different size and types. In all analyses, a HEB100 beam has been assumed to be attached to the steel plate. However, only the perimeter of the connecting beam has been modelled on the steel plates to reduce the complexity of the analyses, i.e. a load area of $100 \times 100 \text{ mm}^2$. This means that the applied loads correspond to the reaction forces of the beam, since they have been applied in the center of the load area and are equally distributed over it.

The concrete have been modelled with the concrete damaged plasticity material model, included in ABAQUS. However, the verification examples showed that the dilation angle cannot be defined identical for cast-in-place and post-installed anchors. As previously mentioned in section 5.2, the low value of the dilation angle might be explained by young concrete used in the verification example. By using this dilation angle for the headed studs the results will always be conservative; therefore, a dilation angle of 10° will be used for the headed studs. Hence, the analyses are performed with all parameters equal, except for the dilation angle. This means that the damage parameters are defined linear while the tension softening behavior is defined bilinear, which correspond to the results of the verification examples. The compressive behaviour has been defined as a tabular function, according to the stress-strain relation for non-linear structural analysis given in section 3.1.5 of EC 2 (2004). In principle, the used compressive curve resembles the one shown in Fig. 5.10. This function assumes that the compressive behaviour is linear elastic up to 40 % of the compressive strength.

Symmetry has not been used on the geometry, since all studied load cases do not permit such an assumption. Therefore, all concrete slabs have been modelled with boundary conditions on all four sides. Since the anchor plates are installed in walls, which are substantially larger than the concrete slabs used in the analyses, all degrees of freedom have been constrained. No reinforcement has been included in the analyses, mainly because the emphasis in this thesis is on the concrete behaviour. Furthermore, reinforcement does not significantly affect the resistance of a fastener, given that the provided reinforcement is not of stirrup-type. This probably means that a post-installed anchor plate are not substantially influenced by the presence of reinforcement. For cast-in-place anchor plates the reinforcement design differs

depending on where the anchor plate is installed; hence, it is hard to define a typical design. Because of this and the aforementioned, reinforcement has been omitted in all analyses. The elements used are 8 node linear brick elements with reduced integration, called C3D8R in ABAQUS. The reduced integration means that only one integration point is used in each element.

6.3 M-type anchor plate

As previously mentioned, the M-type anchor plates are one of the standard type of cast-in-place anchor plates used during the construction of Forsmark nuclear facility. They are intended for high load values and rigid beam connections, i.e. they are designed to resist moment loads. Several different M-type plates with different sizes, number of anchors and embedment depths have been used; for the analyses in this section a plate called M3 has been chosen. It is one of the smallest M-type plates used, with a size of 240x240 mm² and is anchored to the concrete through six headed studs welded to the steel plate. Further, it has the smallest embedment depth of the M-type plates, which makes it suitable for analyses of concrete failure modes. The purpose of these analyses is partly to show that the finite element method can be used to analyse anchor plates with headed studs, the small size of the M3 plate is therefore convenient as it keeps the model at a reasonable size while it still represents the given category of plates. The dimensions of the M3 anchor plate can be seen in Fig. 6.2. As a comparison, the largest M-plate is 420x420 mm² and is anchored to the concrete through ten headed studs (Kallersjö & Trepp AB, 1977).

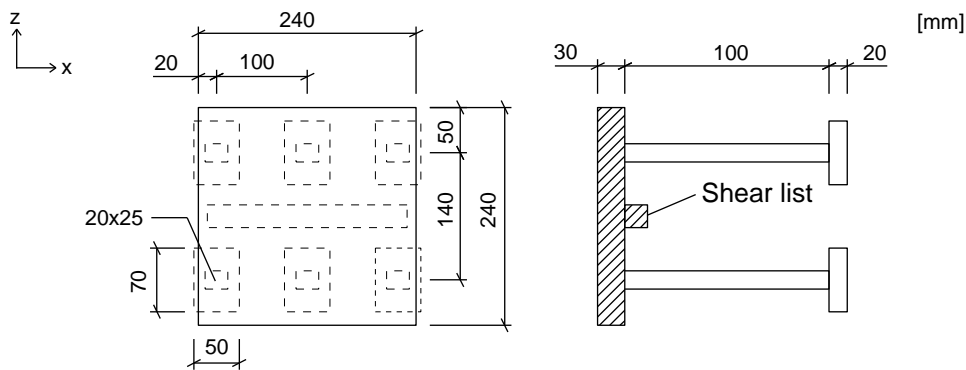


Figure 6.2: Dimensions of the M3 anchor plate. Reproduction from (Kallersjö & Trepp AB, 1977).

It is also stated in Kallersjö & Trepp AB (1977), that a plate has to be placed in a concrete member with a minimum thickness of 300 mm and that maximum a HEB140 may be attached to it. Both the plate and the studs are made of a steel quality called SS1412, which has a yield strength $f_{yk} = 270$ MPa and an ultimate strength $f_{uk} = 430$ MPa. Further, the steel is assumed to have an elastic modulus $E = 200$ GPa and a Poisson's ratio $\nu = 0.3$. The concrete in which the plate is cast has to, at minimum, be of a quality called K250, which in today's terms would

correspond to a C20/25 concrete. The characteristic material properties of a C20/25 concrete taken from EC 2 (2004) are presented in Tab. 6.1. No definition of fracture energy is given in EC 2 (2004), the value presented in Tab. 6.1 is instead taken from MC 90 (1993), which can be found in Malm (2006). The chosen fracture energy corresponds to a concrete with an aggregate size of 8 mm, which is a conservative assumption of the aggregate size since the fracture energy increases with increasing aggregate size.

Table 6.1: Material properties of a C20/25 concrete.

Density	ρ	2400	kg/m ³
Elastic modulus	E	30	GPa
Poisson's ratio	ν	0.2	-
Compressive strength	f_{ck}	20	MPa
Tensile strength	f_{tk}	1.5	MPa
Fracture energy	G_f	50	Nm/m ²

6.3.1 Design calculations

During the construction phase, when the cast-in-place anchor plates were designed, design methods such as the CC-method used today were not yet developed. Instead, from the available knowledge, a general guideline was developed by Kallersjö & Trepp AB (1972) built on the design codes available at the time, such as B-7 (1968). Most of the controls that were made was related to the interaction with the attached beam and the steel plate itself, but contact pressure on the concrete and cone failure was also examined. The cone failure was treated as a punching shear failure, where the concrete cone was idealised as a cylinder. The diameter correspond to half the diameter of a cone with an angle of 45° and a height equal to the embedment depth of the anchor. The failure load due to cone failure was then calculated as the total shear resistance of the surface area of the cylinder. Cone failure was only considered for a pure tensile load. Shear forces, were assumed to only be transferred to the concrete through the steel plate and the shear list, which can be seen in Fig. 6.2. However, it was shown that shear capacity of the beam connected to the steel plate was limiting for the smaller plates.

Calculations according to SIS-CEN/TS 1992-4 (2009) have been made for the load cases of pure tensile loading and pure moment loading in both directions. The results from these are presented in Tab. 6.2 together with the old design values from Kallersjö & Trepp AB (1977). The values presented in Tab. 6.2 are characteristic values, i.e. no partial coefficients nor safety factors have been used. To be able to compare the two, the design values from Kallersjö & Trepp AB (1977) have been increased with a factor 1.8 to translate them into characteristic values. The design procedures from TS are presented in more detail in section 4.1 and in the example given in appendix A.2, which describes the design of an anchor plate subjected to a moment about the z-axis. In the design calculations according to TS, no considerations have been taken to possible failure in the steel plate itself due to for

example bending.

Table 6.2: Design loads of the M3 anchor plate.

Load case	Tensile load [kN]	M_x [kNm]	M_z [kNm]
Old design values	252	28.8	16.2
According to TS	314	39.9	41.7

6.3.2 Finite element model

The general aspects of the finite element models are described in section 6.2, in this section some specific aspects used in the analysis of the M3 anchor plate will be given. The geometry of the anchor plate is shown in Fig. 6.2, although the shear list has been omitted since mainly tensile loads are considered in the analyses. The geometry of the concrete slab has been chosen so that the expected concrete cone does not reach the perimeter of the slab, while the thickness is chosen as the minimum wall thickness specified in Kallersjö & Trepp AB (1977). A slab with the dimensions 1500x1500x300 mm³ is therefore used, the slab together with the anchor plate can be seen in Fig. 6.3. In reality the top surfaces of the concrete slab and the anchor plate coincide, i.e. the anchor plate is cast in the concrete. This has been neglected in the finite element model, mainly due to simplifications in the mesh generation. It should be noted that this is a conservative assumption, since the embedment depth is decreased. In both the concrete slab and the anchor plate an approximate element size of 12.5 mm is used, the mesh is shown in Fig. 6.3.

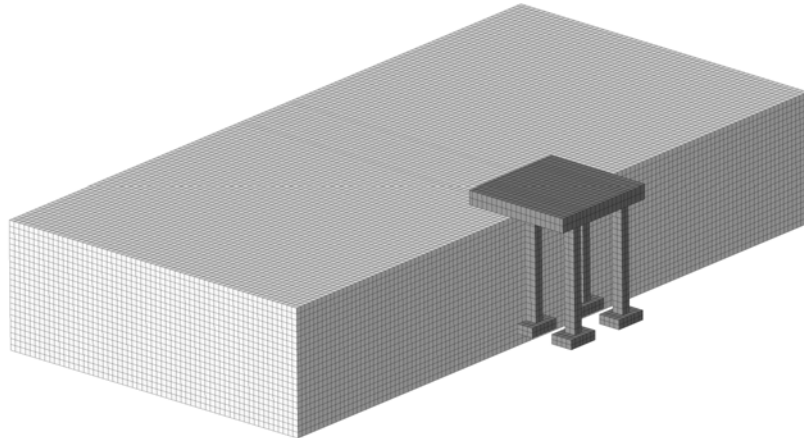


Figure 6.3: The finite element model of the M3 anchor plate and concrete slab.

As in the verification example in section 5.2 of a single headed stud, the interaction between the anchors and the concrete has been defined as hard in the normal direction and as frictionless in the tangential direction. Since the steel in both the plate and the anchors have a rather low yield strength, which might be reached for some load cases, the strain hardening has been included in the finite element analysis. In

ABAQUS, the relationship between the plastic stress and plastic strain has to be given in terms of true stress and true strain, instead of the usual engineering values. The engineering stress and strain can be transformed into the true stress and strain values according to Eq. 6.1.

$$\sigma_{true} = \sigma_{eng}(1 + \varepsilon_{eng}) \quad (6.1a)$$

$$\varepsilon_{true} = \ln(1 + \varepsilon_{eng}) \quad (6.1b)$$

where,

- σ_{true} is the true stress
- ε_{true} is the true strain
- σ_{eng} is the engineering stress
- ε_{eng} is the engineering strain

The stress-strain relationship of the steel material used in the analyses is given in Tab. 6.3, where the engineering values corresponds to a steel quality of SS1412 as previously mentioned. Further, a linear strain hardening has been assumed.

Table 6.3: Stress-strain relationship of the steel used in the analyses, given both in engineering values and true values.

σ_{eng} [MPa]	ε_{eng} [%]	σ_{true} [MPa]	ε_{true} [%]
0	0	0	0
270	1.35	270	1.35
430	20.3	487	20.1

As mentioned in section 6.2, the concrete damaged plasticity model has been used, where the general material properties are taken from Tab. 6.1. The only input parameter that is specific for the analyses of the M3 anchor plate is the dilation angle, which is chosen as 10° in accordance with the findings from the verification example in section 5.2.

6.3.3 Static analysis

The majority of the analyses made on the M3 anchor plate are performed for static load cases. Many different load combinations of the three basic loads: tensile load, moment about the x-axis and moment about the z-axis, have been analysed. A selection of the analyses are presented in detail in this section, while the results from all load combinations are given in section 6.3.4 where they are used to develop failure envelopes. The three basic load cases are first presented followed by two load combinations; a tensile load in combination with a moment and a combination of moment about both the axes.

The results from the load case with a pure tensile load is shown in Fig. 6.4 in comparison with the corresponding design loads previously presented in section 6.3.1.

It should be observed that most of the load curves presented in this section have been smoothed to better represent a static event, since small dynamic effects are often shown right after the failure is reached due to the nature of the quasi-static method used.

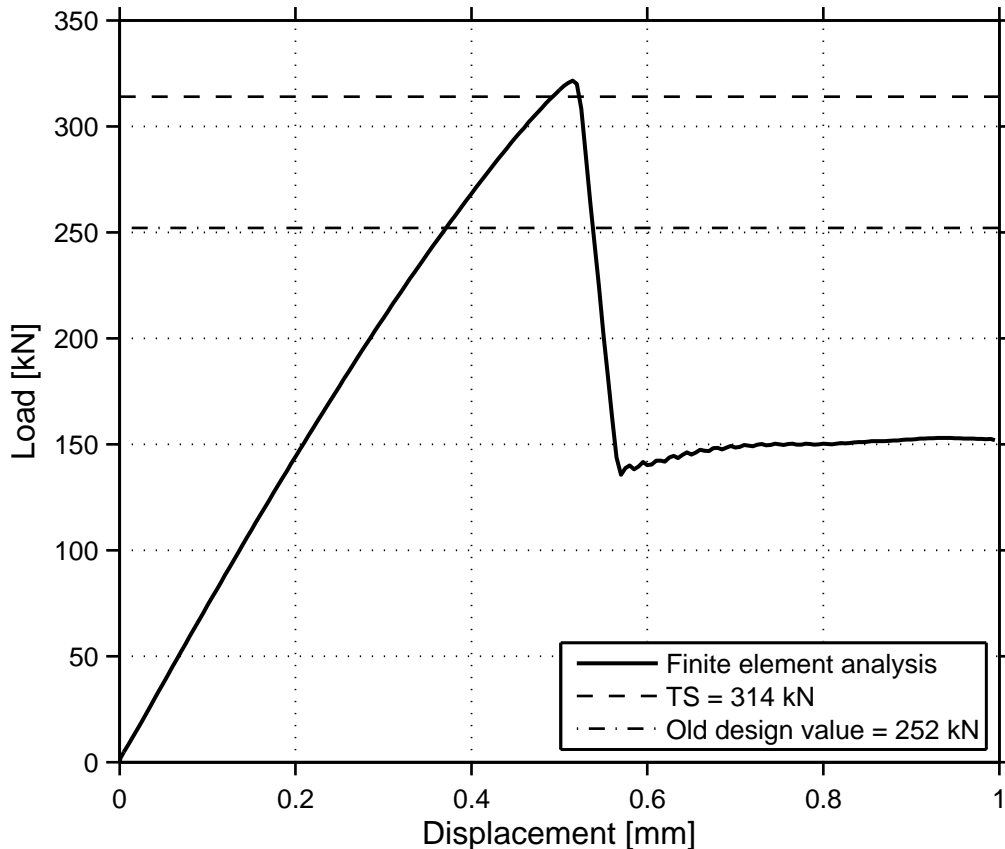


Figure 6.4: Load-displacement curve of the M3 plate subjected to a tensile load.

For the pure tensile load case, the finite element analysis and the design load calculated according to TS shows very good agreement. The finite element analysis, with a failure load of 325 kN, only overestimates the load from TS with 3.5 % while the old design value is overestimated with 29 %. Hence, the old design values must be regarded as very conservative for this load case, both in comparison with the numerical analysis and with the new design codes.

A typical crack pattern from the finite element analysis is depicted in Fig. 6.5, where it can be seen that a pure concrete cone failure mode is governing. The break out body has an angle of approximately 40° , which corresponds well with the assumptions made in the design codes and with the experimental observations. Some minor surface cracks can also be observed, which probably occurs due to bending of the concrete slab and should not affect the failure mode. Further, some radial cracks starting from the anchor heads can be observed, which in some sense coincide with the concrete cone but probably initiates at an earlier stage.

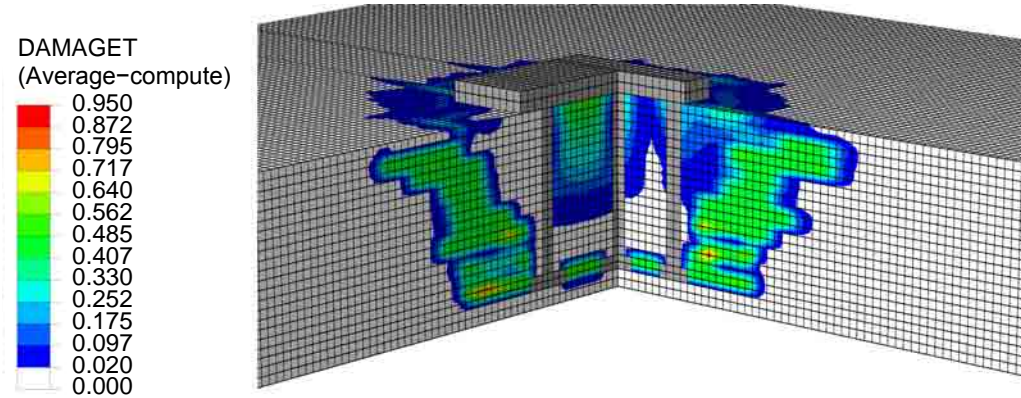


Figure 6.5: Crack pattern of the failure cone from a tensile pull-out load, illustrated through the induced tensile damage.

The load cases of pure moment about the x-axis and z-axis respectively are presented in Fig. 6.6 together with their respective design loads, which were presented earlier in section 6.3.1. In the analysis of the moment about the z-axis, mass scaling have been utilised so that the point of failure was possible to observe. Without the use of mass scaling the analysis terminated prematurely due to wave speed problems, checks have been made to ensure that the mass scaling does not affect the overall response significantly.

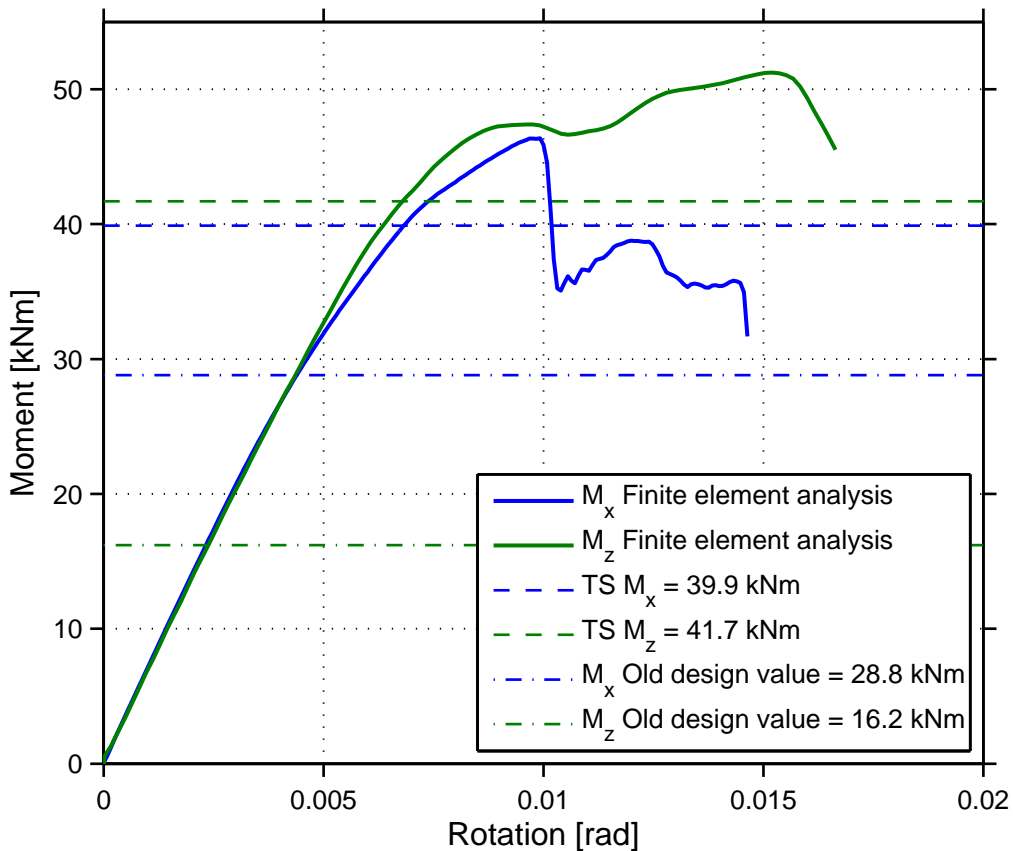


Figure 6.6: Moment-rotation curve of the M3 plate subjected to moments in two orthogonal directions.

It can be seen that the analysis of both load cases shows an overcapacity when compared to the design loads. For M_x , an ultimate failure is reached for 46.4 kNm, which is 16 % more than the design load according to TS and 60 % more than the old design value. For M_z it's clear when the ultimate failure occurs, but for M_x its not clear when the ultimate failure occurs, but for M_z the load curves flattens out significantly as the load reaches 45 kNm and above. First a peak is reached for 47.3 kNm, here the most heavily loaded anchors starts to fail and a small drop in the load curve is exhibited. But at this point the steel in these anchors starts to yield, this in conjunction with the emerging concrete failure leads to load being transferred to the middle anchors and more load may be applied. The ultimate failure then occurs at 51.2 kNm where a complete concrete failure occurs, it should also be noted that some parts of the steel plate, especially around the load application point, has reached the yield limit of the steel. At this point an overcapacity of 23 % is received when compared to TS while the old design value is overestimated with 220 %. A possible explanation to the vast difference might be the fact that the limiting failure mode in the old design calculations was another one. Probably, failure in the steel plate or the attached beams were governing.

The crack patterns after failure for both load cases are shown in Fig. 6.7.

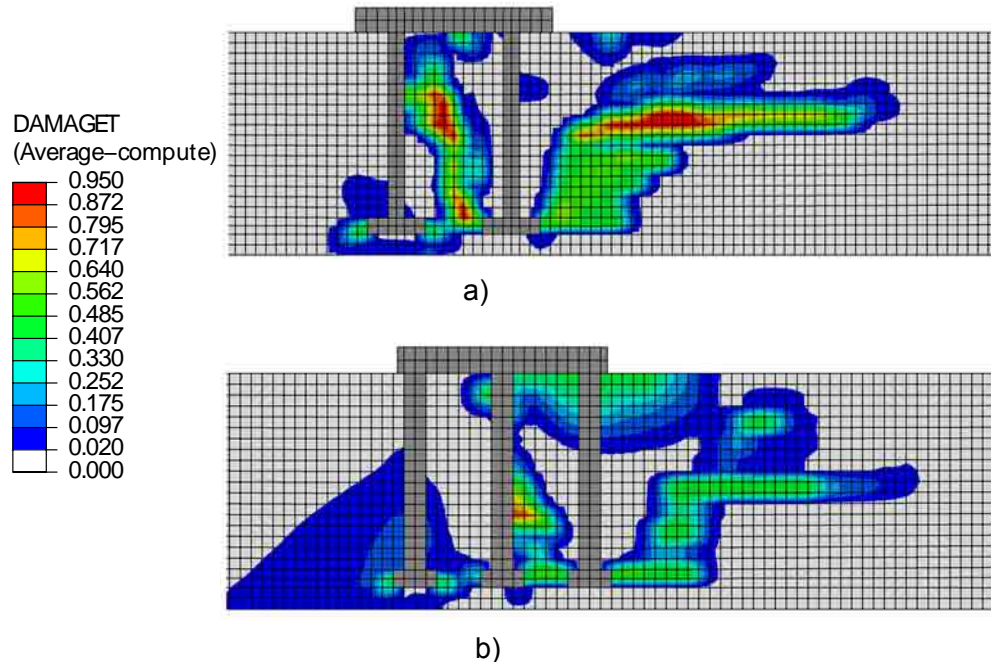


Figure 6.7: Crack pattern of the failure cone illustrated through the induced tensile damage for pure moment loads a) M_x and b) M_z .

From Fig. 6.7a), the crack pattern obtained from the plate failing due to a moment M_x can be seen. A cone is mainly developed behind the anchor plate while its development is prohibited in the opposite direction by the compressive stresses developed in the concrete. The diagonal crack between the back and front row of anchors is developed before the cone failure occurs. It originates from the difference in lateral movement between the two rows of anchors, resulting in large shear forces and eventually a crack. The crack pattern clearly resembles that of a pry-out failure but mainly occurs due to tensile forces in the anchors. The crack pattern in Fig. 6.7b) is obtained when the plate fails due to a moment M_z . The principles of the crack pattern is similar to the crack pattern in Fig. 6.7a), although some differences are present. Since a middle row of anchors is introduced, which is mainly subjected to tensile forces, the appearance of the diagonal shear crack described above changes. Instead of going between two rows of anchors it actually coincides with the middle row, as the cross-section of the concrete slab is weaker there, and only grows diagonally close to the top and bottom of the slab. In the figure it can clearly be seen how the concrete in the vicinity of the anchors subjected to compression is damaged, this is probably due to an imminent punching failure. This phenomena starts at the same time as the concrete cone failure in the back row of anchors. Some of the tensile load is at that time transferred to the middle row of anchors, i.e. the lever arm decreases and the resultant compressive force increases. The same type of bending induced surface cracks and radial cracks around the anchor heads described for the tensile load case, can also be observed in both of the moment load cases.

In Fig. 6.8, it can be seen how the load that is applied to the steel plate is distributed

into the individual anchors. The figure describes the distribution received from the numerical analyses of the three basic load cases described above.

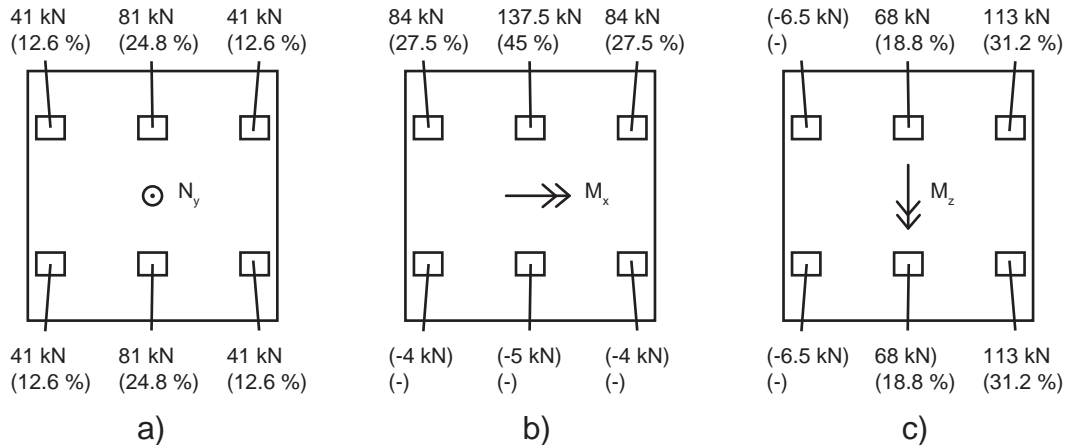


Figure 6.8: Distribution of loads on the individual anchors from the finite element analyses for a) tensile load b) moment about the x-axis and c) moment about the z-axis.

For the tensile load case in Fig. 6.8a), it can be observed that the two middle anchors are subjected to approximately twice the load than the rest of the anchors. This is due to the inclusion of plate bending in the finite element analysis. The design calculations on the other hand assumes a rigid plate, hence, all the anchors are assumed to resist the same amount of load. The same effect can be observed in Fig. 6.8b) where a moment M_x is applied, although a slightly smaller percentage is concentrated to the middle anchor. The majority of the compressive forces is handled by the contact pressure between the steel plate and the concrete, whereas the forces in the anchors on the compressive side only account for a small amount of the total compressive load. This is in good agreement with the hand-calculations where the compressive forces in the anchors are neglected. In Fig. 6.8c), where a moment M_z is applied to the steel plate, the majority of the load is handled by the two edge anchors in the tensile zone. The same pattern is obtained in the linear elastic analysis made in the hand-calculations, where even more of the load is concentrated to the two edge anchors, see appendix A.2. In the linear elastic analysis each of the two edge anchors resist 43.5 % of the total load. The difference is partly due to the inclusion of plate bending, and partly that the load is redistributed to the middle anchors before an ultimate failure occurs, as previously mentioned.

As previously mentioned, a significant redistribution of the load occurs between the anchors for the load case with a pure moment about the z-axis, see Fig. 6.6. To further investigate this, the distribution of the loads acting on the individual anchors is given in Fig. 6.9. Since the load distribution is symmetric about the x-axis, see Fig. 6.8, the anchors are divided into three groups; left anchors, middle anchors and right anchors. The loads are normalised against the total current tensile load for each step of the deformation, since compressive forces in anchors are generally omitted in design codes.

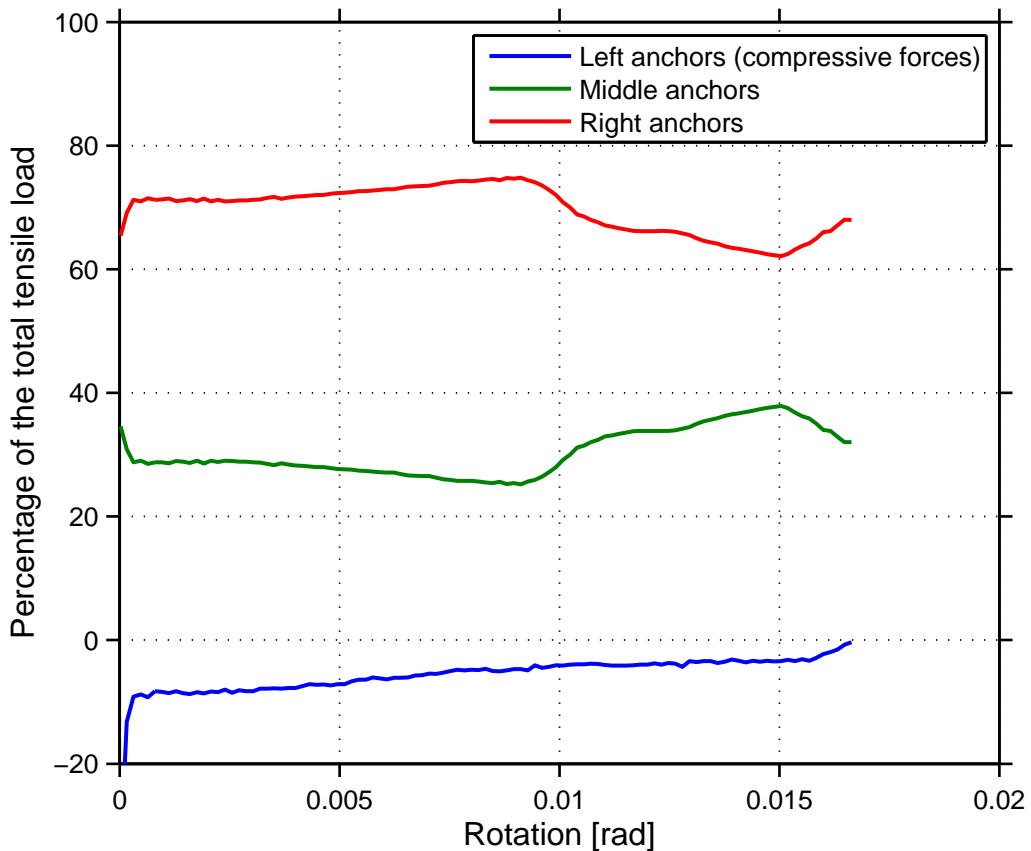


Figure 6.9: Changes in the distribution of loads during the load step, for the M3 anchor plate subjected to a moment about the z-axis.

Note that the left anchors are subjected to compressive forces, hence, the total percentage of the load on the anchor plate is not equal to 100 %. As seen in the figure, the load starts to redistribute after a approximate rotation of 0.009 rad, which coincides with the first peak observed in the load-deformation cure in Fig. 6.6. The load is redistributed from the right anchors to the middle anchors, as further deformation is applied to the anchor plate. The compressive forces in the anchors are small in comparison to the tensile forces during the whole load step. This confirms the assumption that the compressive forces in anchors can be omitted for design calculations.

A load case of a combined tensile load and moment M_x is presented in Fig. 6.10.

The applied deformations in the presented load case have been chosen equal to the respective pure load case, so that a load case of 50 % tensile load and 50 % moment load is obtained. To be able to compare when failure occurs for both the tensile load and the moment they are presented against the percentage of the given load step instead of their respective deformation.

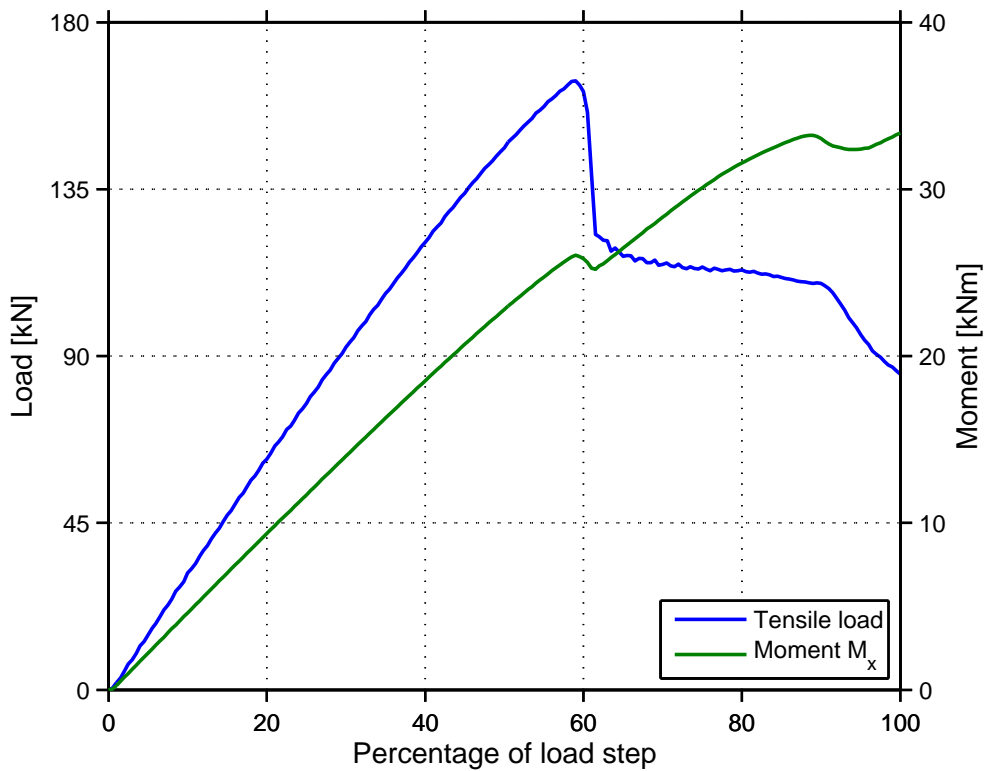


Figure 6.10: Load curves for a combined load case with a tensile load and moment about the x-axis.

As seen in the figure, failure occurs after approximately 60 % of the load step and is primarily due to the tensile load. In fact the moment load increases after this failure, but a global failure is considered to have occurred since the tensile load drops significantly. A maximum tensile load of 196 kN is reached, which is 60 % of the load reached for the pure tensile load. At the point of tensile failure, a moment load of 30.3 kNm is attained, which is also about 60 % of the pure M_x load case. This should be seen as an indication that a non-linear interaction is present between the two loads as the total amount of load exceeds 100 %.

The resulting crack pattern of the above presented load case is depicted in Fig. 6.11.

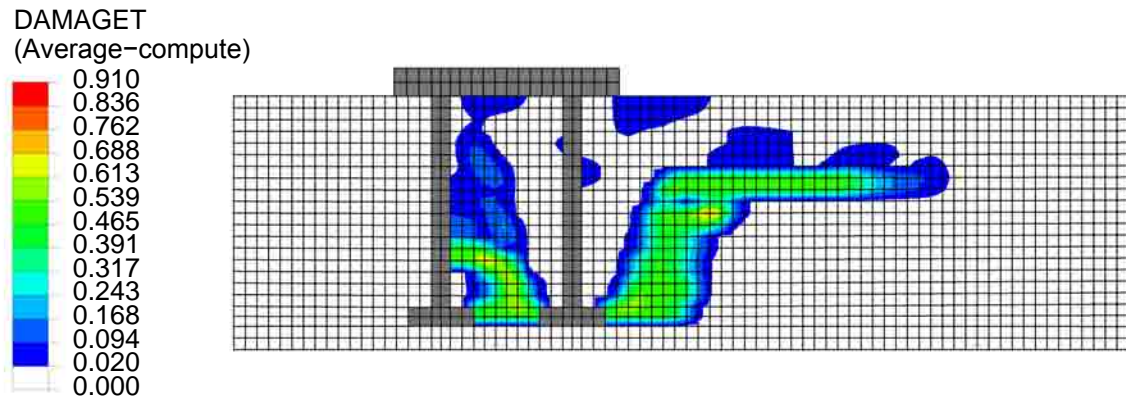


Figure 6.11: Crack pattern of the failure cone illustrated through the induced tensile damage for a combined tensile and moment M_x load.

The crack pattern clearly resembles that of the pure M_x load case from Fig. 6.7a). The main difference is in the diagonal crack between the two anchor rows which is much flatter for the combined load case. The reason is probably that the lateral movement between the anchors rows is less pronounced since both anchors are translated upwards by the tensile load. The diagonal crack intersects the front anchor row at about two thirds of the anchor depth, thereafter the crack grows parallel to the anchor in the vertical direction as the cross section of the concrete slab is weakest in the plane of the anchor row. As for the previously presented load cases, including a moment load, the failure cone resembles the expected break-out body of a pry-out failure but occurs due to tensile forces in the anchors. The reason to this is that the back row of anchors are resisting most of the tensile load; hence, the concrete cone originates from them. When the crack meets the compressive pressure due to the moment load and the weakened cross section of the front anchor row, the crack finds an easier way to propagate instead of the typical diagonal crack of a concrete cone. Further, the radial cracks originating from the anchor heads observed in the previous load cases are also present in this load case.

The next, and last load case presented in this section is a combination of moments in perpendicular directions, i.e. M_x and M_z . As for the other combined load case the two moments are applied so that a 50/50 load case is obtained. The results are presented in Fig. 6.12.

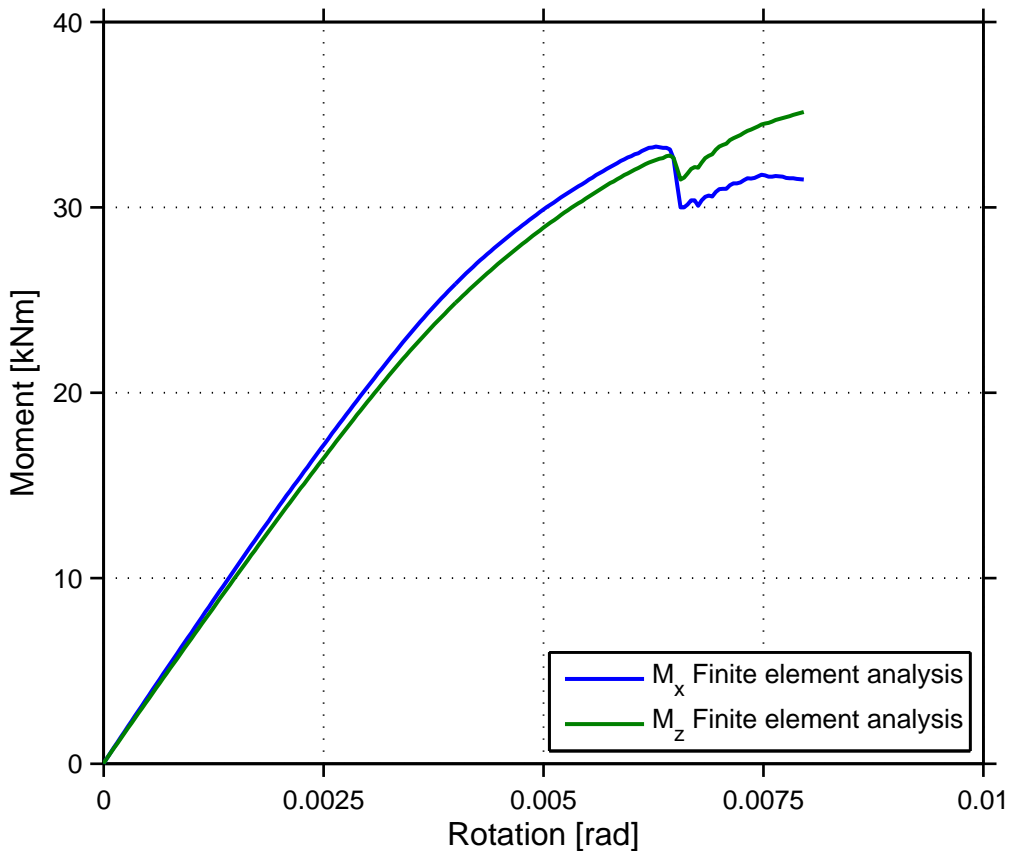


Figure 6.12: Load curves for a load case with equal rotations applied about both the x-axis and z-axis.

A failure clearly occurs at the same time for both loads, although further load may be applied to M_z after the failure. The reason is probably the redistribution of loads from the edge anchors to the middle row of anchors, as for the pure M_z load case. Despite this, the mentioned failure should be considered as the global failure of the anchor plate since M_x reaches its peak load there. The peak load of M_x is 33.3 kNm which is 72 % of the pure M_x load case. The local peak load of the M_z load curve at the same time is 32.8 kNm which is 64 % of the pure M_z load case. As for the previous load case this indicates a non-linear interaction between the two loads.

The break-out body obtained from the analysis of the given load case can be seen in Fig. 6.13. It is clear that the concrete cone has a diagonal shape limited by the expected compressive zone over the diagonal of the anchor plate. Further, the cone originates from the two anchors subjected to the highest tensile loads, i.e. the ones farthest away from the limit between the tensile and compressive zone of the anchor plate. Otherwise, the same surface cracks that have been observed due to bending are also present for this load case.

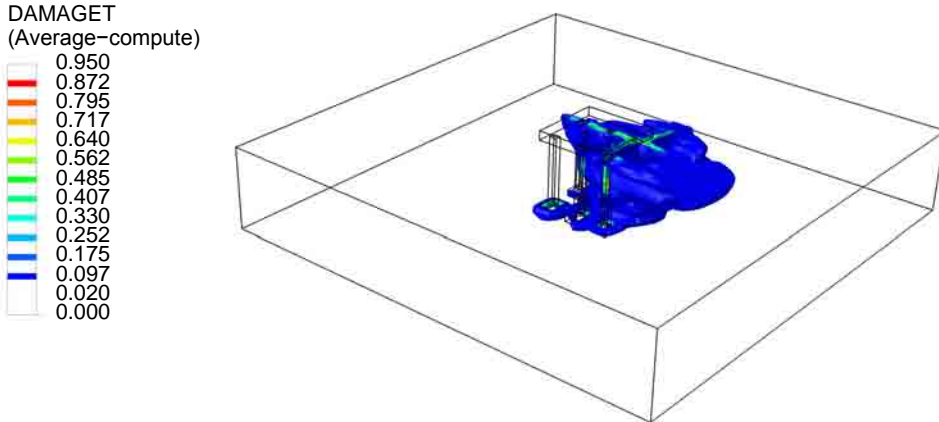


Figure 6.13: Crack pattern of the failure cone illustrated through the induced tensile damage for a combined moment M_x and moment M_z load.

The distribution of loads between the different anchors can be seen in Fig. 6.14 for the two above presented load combinations. In the combined tensile and moment M_x load case in Fig. 6.14a), the same effects as for the pure load cases in Fig. 6.8 can be observed; concentration of load to the middle anchor due to plate bending and to the back row of anchors due to the moment load. The effect of adding a tensile load to the moment load case is that less compressive forces are transferred to the front row of anchors and it can be observed in the figure that the edge anchors in the front row actually are subjected to tensile forces. However, compressive forces are still transferred between the plate and the concrete to account for the force couple that emerge due to the moment load. In Fig. 6.14b), which describes the load case of combined moments it can be seen that the majority of the tensile load is resisted by two of the anchors; in agreement with the break-out body from Fig. 6.13. Further, it can be seen that the limit between the tensile and the compressive zone of the anchor plate is diagonal, since only two of the anchors in the front row are subjected to compressive forces. Actually, the majority of the contact pressure between the anchor plate and the concrete is concentrated around the front corner anchor, that is subjected to compressive forces.

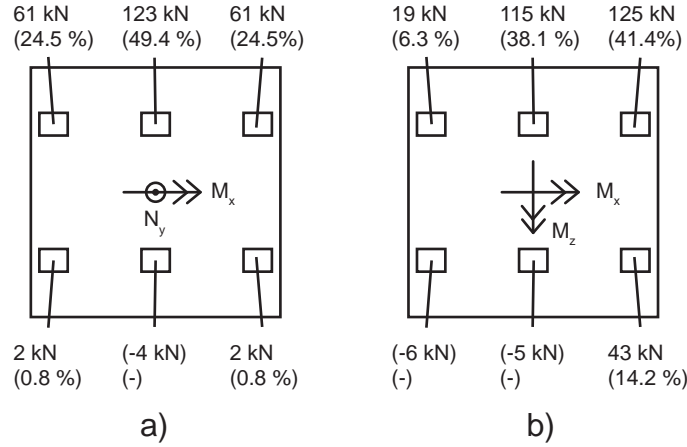


Figure 6.14: Distribution of loads on the individual anchors for a) combined tensile and moment load and b) combined moments.

The fracture energy is not a material property used in the design calculations and it has been shown that it can have a significant effect on the failure load, see section 2.2.1. Therefore, a parametric study has been made on how the fracture energy affect the failure load for a pure tensile load case. The results from the parametric study is shown in Fig. 6.15. The previous analyses have been made with a fracture energy $G_f = 50 \text{ Nm/m}^2$, which correspond to a aggregate size of 8 mm. This is a rather small aggregate size which is not commonly used, and must be considered as conservative. Normally used aggregate has a size of approximately 32 mm, which for the given concrete quality corresponds to a $G_f = 80 \text{ Nm/m}^2$. As an even higher value, a $G_f = 110 \text{ Nm/m}^2$ has also been analysed.

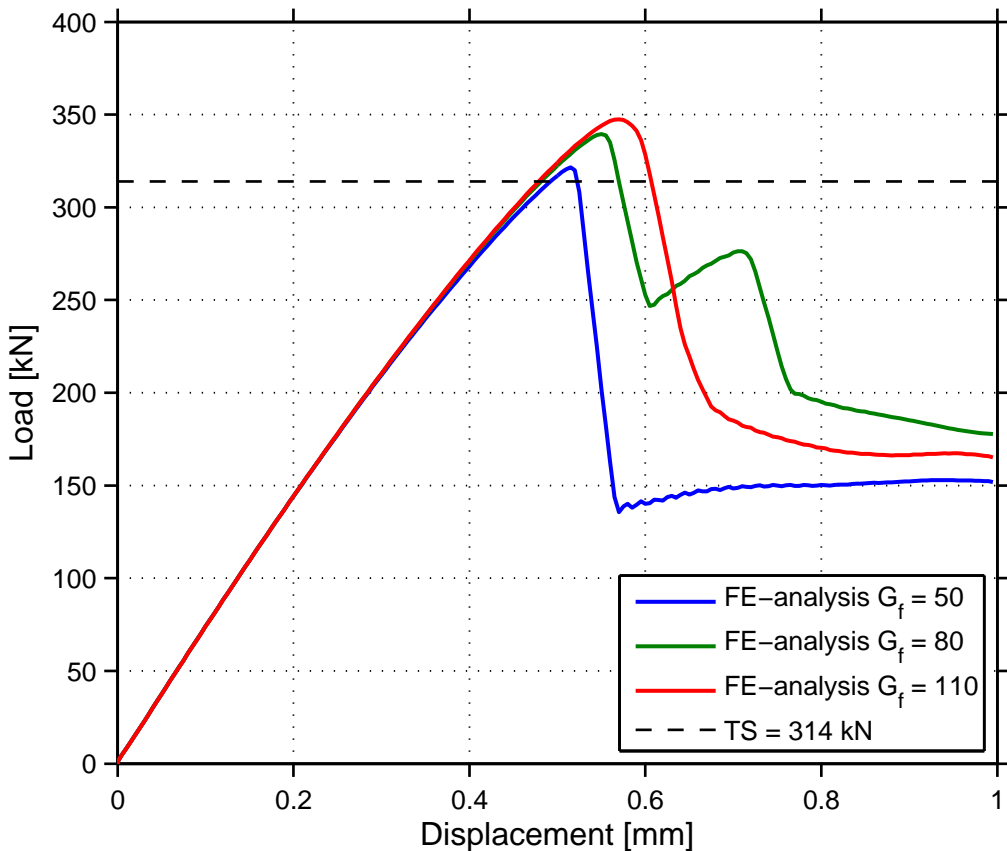


Figure 6.15: Parametric study on how the failure load for a pure tensile load case depends on the fracture energy.

The results show an increase in failure load of 4.5 % and 7 % for an increase of fracture energy with 60 % and 120 %, respectively. The numerical study by Ozbolt (1995) presented in section 2.2.1, showed for the same amount of increase of fracture energy, an increase of the failure load with over 20 %. The difference between the two might be explained by the deeper embedment depth used by Ozbolt (1995). Despite this, the parametric study indicates that the failure loads presented throughout this thesis are conservative.

6.3.4 Failure envelopes

Only a few of the static analyses made were presented in section 6.3.3. In this section results from all of the analyses are used to develop failure envelopes for different load combinations. As presented in the previous section, combinations of the three basic loads: tensile load, moment about the x-axis and moment about the z-axis have been considered and used for the development of failure envelopes. The failure envelopes are curve fitted to the finite element analysis results with a second degree polynomial function and normalised to the maximum values of the pure load cases. The first failure envelope is presented in Fig. 6.16 and describes

the interaction between a tensile load and a moment M_x . A linear interaction curve is also presented in the figure for comparison.

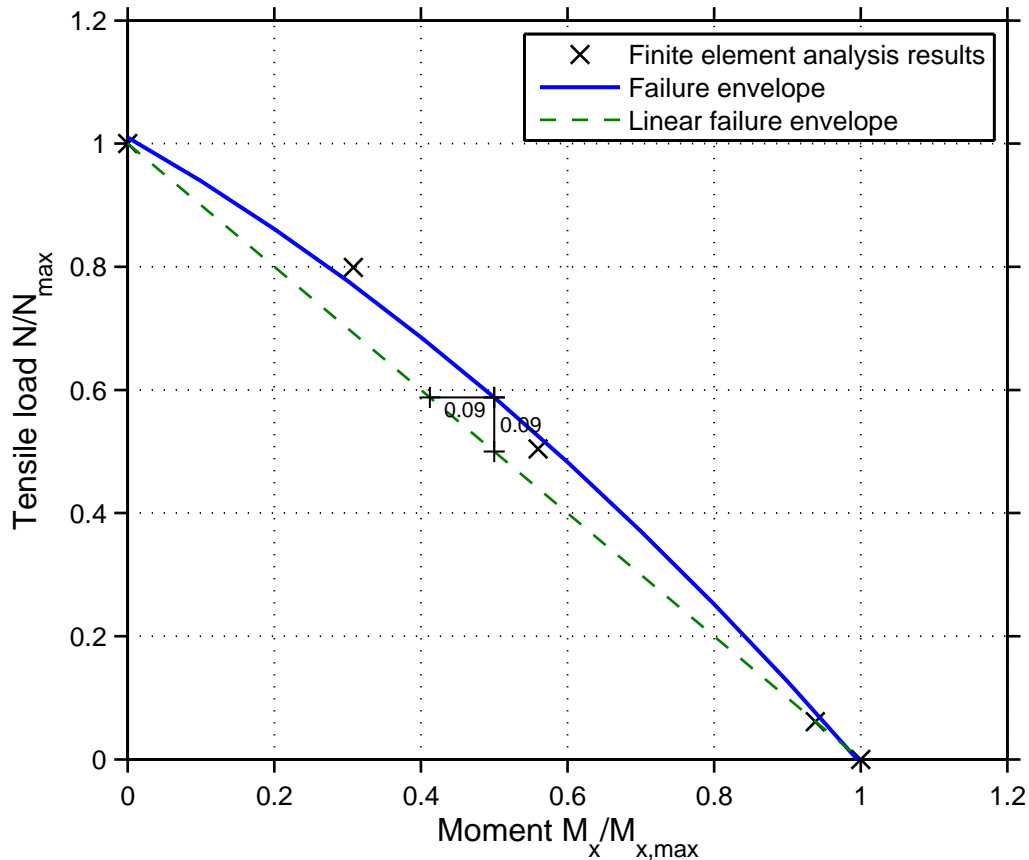


Figure 6.16: Normalised failure envelope for a tensile load and moment about the x-axis for the M3 anchor plate.

As seen in the figure, at most 9 percentage points are gained when comparing the second order failure envelope to its linear counterpart. Most overcapacity is gained when the tensile load is dominant, whereas if the moment is dominant the second order failure envelope and the linear function almost coincide.

The second failure envelope describes the interaction between a tensile load and a moment M_z and is depicted in Fig. 6.17.

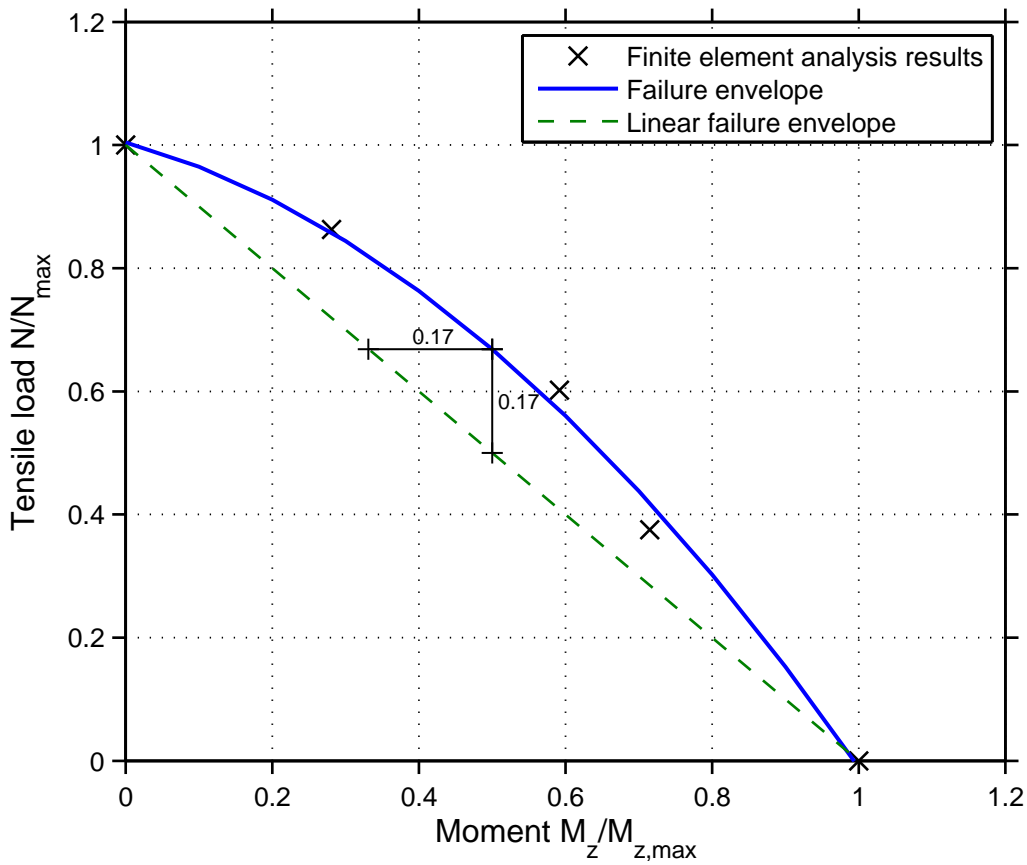


Figure 6.17: Normalised failure envelope for a tensile load and moment about the z-axis for the M3 anchor plate.

The second order failure envelope for this load combination gives a quite large increase in capacity when compared to a linear interaction assumption, at most 17 percentage points. As for the previously presented failure envelope, most overcapacity is gained when the tensile load is dominant.

The third and last failure envelope developed for the M3 anchor plate describes the interaction between the two moments M_x and M_z and can be seen in Fig. 6.18.

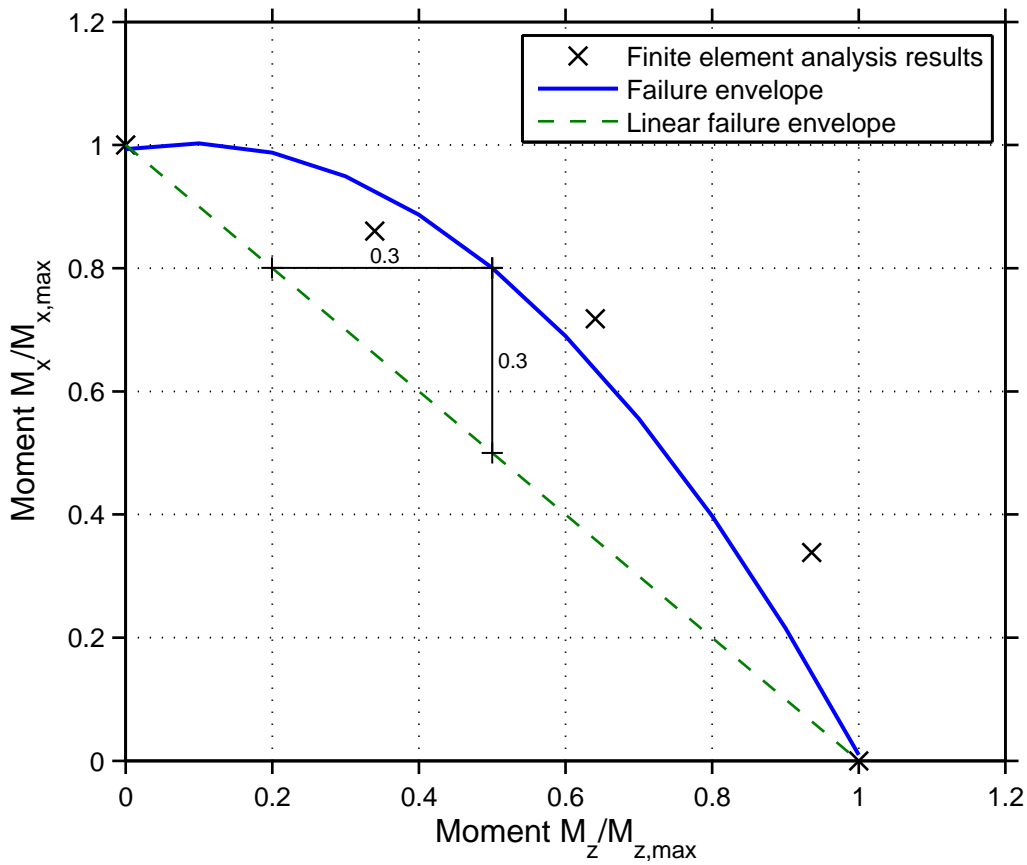


Figure 6.18: Normalised failure envelope for a moment about the x-axis and moment about the z-axis for the M3 anchor plate.

This failure envelope shows that a load combination of a moment load in two directions, i.e. a skew bending of the plate, must be considered as a beneficial load case. At most 30 percentage points are gained in comparison to the linear failure envelope. Further, it can be observed that a high proportion of M_x results in the highest overcapacity when compared to the linear function.

6.3.5 Dynamic analysis

To show that the method of finite element analysis is able to take dynamic effects associated with failure of anchor plates into account, one of the load cases presented in section 6.3.3 are analysed with the inclusion of dynamics. These dynamic effects might include events such as earthquakes, pipe failure and pressure peaks in the piping system. The chosen load case is the pure tensile load, since it is the simplest load case. In reality, a dynamic event probably consists of a combination of all different type of loads, including shear loads and torque which are not covered in this thesis. But for convenience, the load case has, as mentioned, been reduced to only consist of a tensile load. This simplification is motivated by the fact that

the purpose of this analysis only is to show that dynamic analysis of the problem category is possible.

An event describing pressure peak due to the closure of a non-return valve in the piping system is chosen for the analysis. The normalized amplitude of the event is given in Fig. 6.19, in both the time and frequency domain. For earthquakes, only frequencies under 50 Hz are considered in the design of nuclear facilities in Sweden, according to VBB consulting Ltd (1992). This should also apply to the chosen event, for which the frequency associated with the highest amplitude is 27.3 Hz. Although, frequencies up to approximately 400 Hz are included in the event, most of these probably do not affect the response of the structure. The amplitude is multiplied with the failure load obtained in the corresponding static analysis of the tensile load case, 325 kN, to investigate whether a dynamic load is more or less beneficial than a static load. As can be seen in the figure, the chosen event is largely of compressive nature and only contains small peaks with tensile loads. This together with the fact that the maximum tensile peak only has an amplitude of 0.6 would suggest a more beneficial load case than the static load.

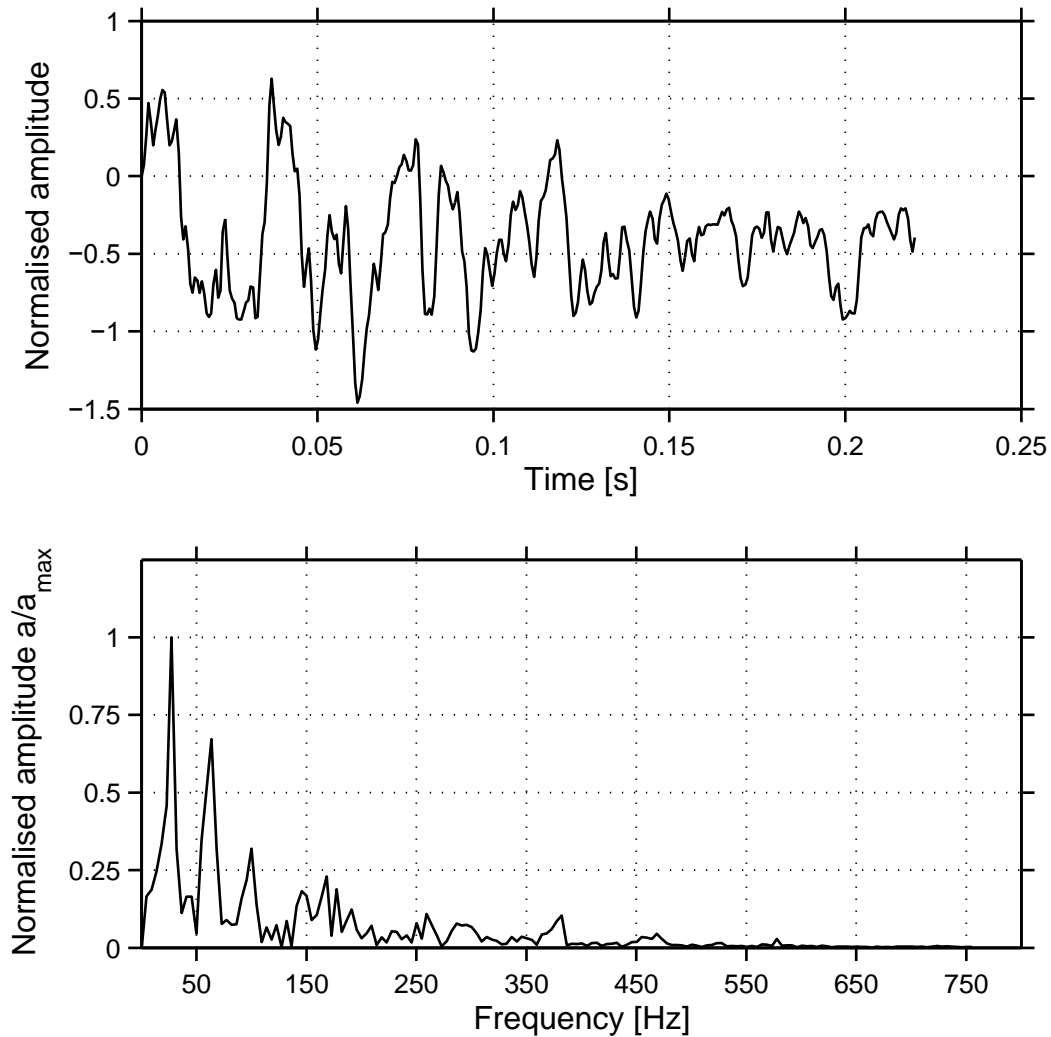


Figure 6.19: Normalised amplitude of an event describing the closure of a non-return valve in a piping system.

Since high compressive forces are present, the concrete slab have been constrained against lateral movement in the bottom surface to avoid a punch through failure, because that is of no interest. Basically, this means that the concrete slab is considered to have an infinite thickness and no bending of the slab will occur.

The crack pattern in the concrete slab after the event is depicted in Fig. 6.20.

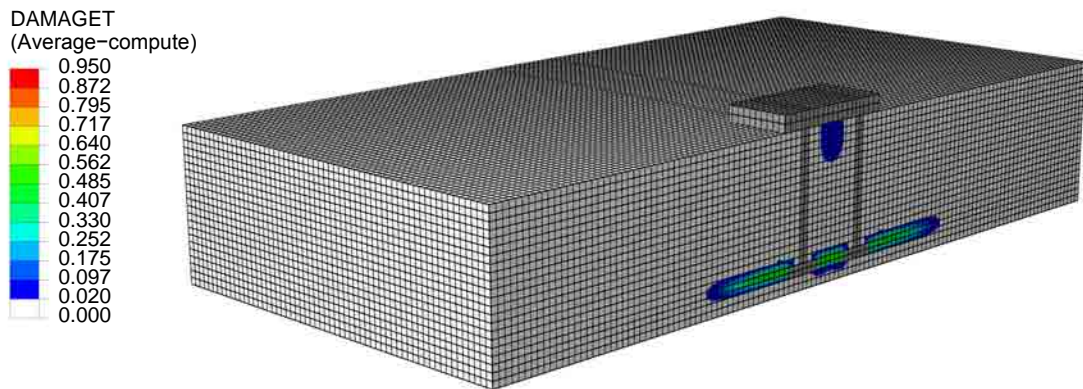


Figure 6.20: Crack pattern after the dynamic event, illustrated through the induced tensile damage.

As can be seen in the figure, the only cracks that occur during the event are radial cracks that originate from the anchor heads and some minor damage close to the top surface of the slab. The radial cracks are expected since the plate moves both upwards and downwards due to the nature of the load, resulting in large strains around the anchor heads. This suggest that no failure have occurred and that the assumption that this dynamic event is more beneficial then the static load is correct. Looking at the distribution of the maximum principal stress in Fig. 6.21, the diagonal stress band originating from the steel plate is an indication that a punch through failure might had occurred if the slab would have been thinner. No clear indication of a concrete cone failure can be observed other than the concentration of stress at the top of the slab which might also be related to the large compressive forces.

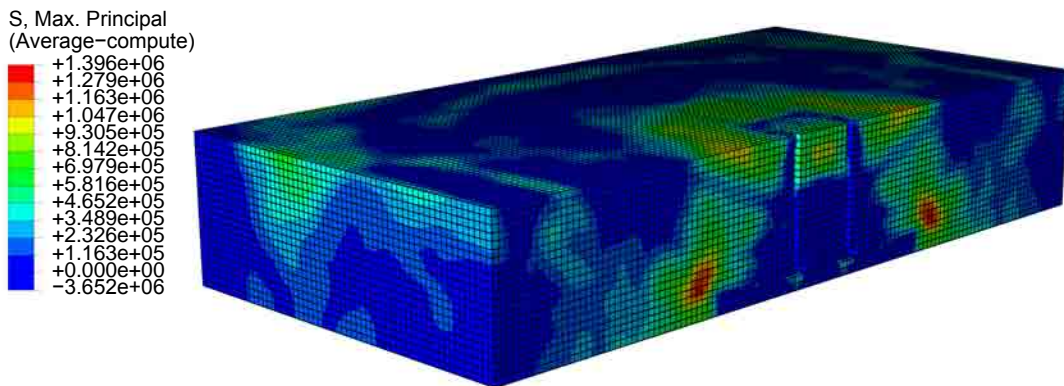


Figure 6.21: Maximum principal stress distribution in the concrete slab.

6.4 Expansion anchor plates

The main purpose of these analyses is to determine whether there is any overcapacity of the resistance in comparison to the resistance calculated with the design codes. Furthermore, the aim is to study whether the non-linear finite element models are able to describe the concrete behaviour of an expansion anchor plate, subjected to tensile load, moments and a combination of these. The result from the analyses with combined loads, will after this be used to construct failure envelopes with the intention to simplify the design procedures for load combinations not covered in the design codes.

There is a range of post-installed expansion anchor plate types at Forsmark nuclear facility. Three different anchor plates have been analysed, which together represent a majority of the post-installed plates. All the analysed anchor plates are quadratic and 20 mm thick with one expansion anchor in each corner, i.e. a total of four expansion anchors. The dimensions of the three plates can be seen in Fig. 6.22. From now on, the three anchor plates are referred to as the 300x300, 400x400 and 500x500 anchor plate, respectively. The steel quality of the plates is rather hard to determine, since the documentation is limited.

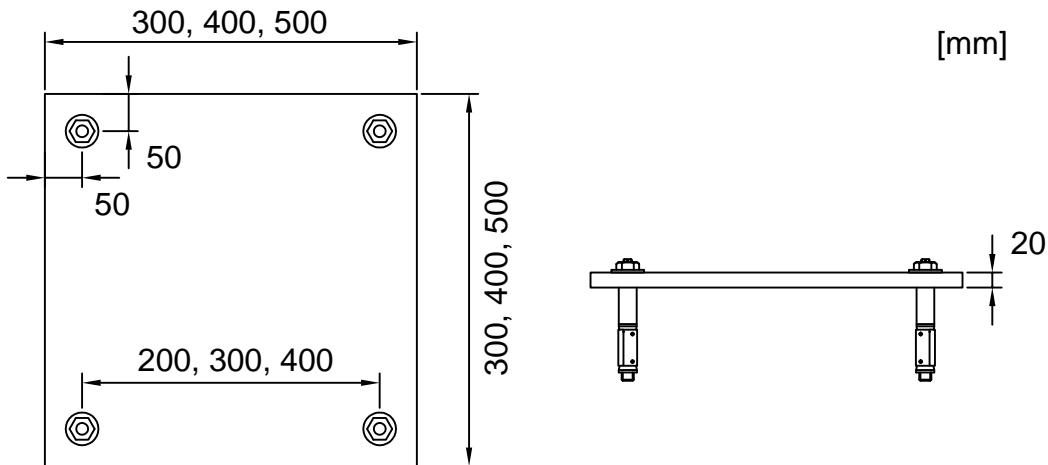


Figure 6.22: The dimensions of the three analysed expansion anchor plates.

The expansion anchors have a threaded diameter of 16 mm and use a expansion sleeve to develop the interlock between the anchor and the concrete. They are manufactured by Simpson Strong-tie and called *Liebig Safety bolt type B* in the product description. The bolt is depicted in Fig. 6.23 while the relevant dimensions of the bolt are given in Tab. 6.4 (Simpson strong-tie, 2009). The steel quality may vary between the expansion anchors since they have been designed and installed during a long period of time. A steel quality of 8.8 has been assumed, which correspond to the present standard quality. This quality correspond to a yield strength $f_{yk} = 640$ MPa and an ultimate strength $f_{uk} = 800$ MPa, while the elastic modulus $E = 200$ GPa and Poisson's ratio $\nu = 0.3$.



Figure 6.23: The Liebig safety bolt type B (Simpson strong-tie, 2009).

Table 6.4: A selection of bolt dimensions (Simpson strong-tie, 2009).

Threaded diameter	16	mm
Drill hole depth	125	mm
Effective embedment depth	100	mm
Expansion sleeve length	50	mm

The concrete used for the analyses is of quality C20/25, which corresponds to the specified minimum quality K250 in Kallersjö & Trepp AB (1972). The characteristic material properties according to EC 2 (2004) for a C20/25 concrete are presented in Tab. 6.1.

6.4.1 Design calculations

Expansion anchor plates have been designed both during the construction phase and afterward. However, the old design procedures differ from those presented in TS, which are based on the CC-method. Guidelines for the design of anchor plates with expansion anchors were developed by Kallersjö & Trepp AB (1972) and consists of five steps. In the first and second step, the designer shall calculate the tensile load on each fastener according to linear elastic theory; equations for this are specified in the directions for both tensile and shear loads. The directions also specify the allowable tensile loads for fasteners produced by different manufacturers and dimensions. These specifications are used in the third step, where the calculated tensile load on each fastener is verified so that they are smaller than the specified allowable load. In the fourth step, the required thickness of the steel plate is calculated, as well as the allowable load area. In the fifth and last step, one fastener in the group is considered to be inactive. New tensile loads for the active fasteners are calculated, which shall not be more than 100 % larger than the old tensile loads.

The design procedures according to SIS-CEN/TS 1992-4 (2009) are presented in chapter 4. The resistance calculated according to these procedures for the three anchor plates analysed, subjected to tensile loads and moments, are given in Tab. 6.5. All calculations have been made without partial coefficients and safety factors, i.e. the characteristic resistance of the anchor plates have been determined. The design procedure is analogous to the example presented in appendix A.2, where a M3-anchor plate has been designed to a moment load.

Table 6.5: Characteristic resistance of the three anchor plates presented according to TS.

Plate type	Tensile load [kN]	Moment[kNm]
300x300	140	19.3
400x400	202	28.4
500x500	202	33.3

Note that only one characteristic moment capacity is given for each anchor plate since they are symmetrical, i.e. the capacity is equal in the directions perpendicular to the edges of an anchor plate.

6.4.2 Finite element model

The general aspects mentioned in section 6.2 have been applied to the analyses made herein. Beyond these aspects, the finite element models are defined in accordance to the results from the verification example of the sleeve-type expansion anchor in section 5.3.

The expansion anchor plates have been placed in the center of the concrete slabs in all analyses. In theory, the concrete cone failure surface has an angle of 35° relative to the horizontal plane. Hence, the concrete cone has a diameter of approximately 140 mm on the top surface, since the effective embedment depth is 100 mm. To avoid that the concrete cone reaches outside the concrete slab, the width has been chosen as three times the embedment depth. Since the dimensions of the concrete walls have a vast variation, the depth of the concrete slabs have been modelled with the minimum concrete thickness specified in Simpson strong-tie (2009) for a M16 anchor. The concrete slab dimensions for each expansion anchor plate are presented in Tab. 6.6.

Table 6.6: Concrete slab dimensions.

Plate type	Area [mm ²]	Thickness [mm]
300x300	800x800	200
400x400	900x900	200
500X500	1000x1000	200

The concrete slabs and steel plates have an approximate element size of 15 mm. The expansion anchor elements are defined smaller, to be able to describe the circular shape of the anchors more accurately. The mesh of a 400x400 anchor plate and its concrete slab is depicted in Fig. 6.24.

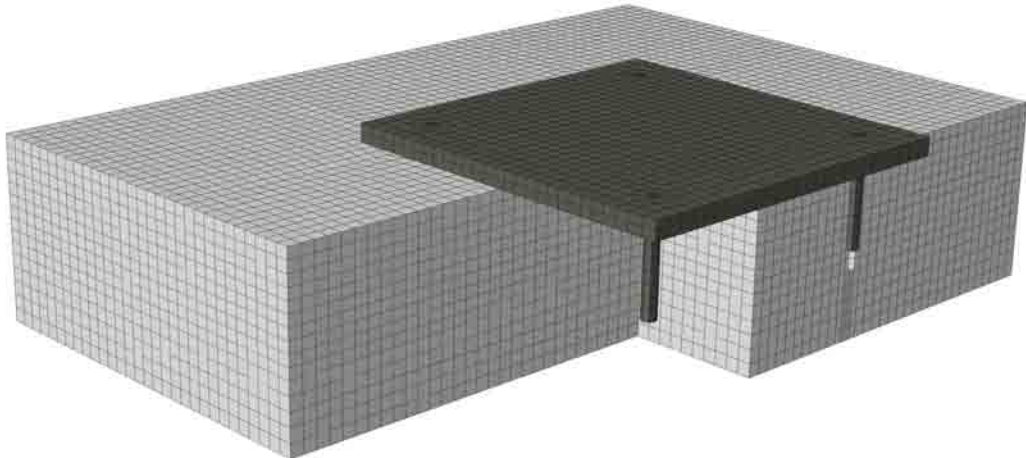


Figure 6.24: Mesh of a 400x400 expansion anchor plate.

As mentioned in section 6.2, the concrete damage plasticity material model have been utilised to describe the behaviour of concrete. The dilation angle differs depending on the structure analysed; the results from the verification example in section 5.3 showed that a dilation angle of 30° was appropriate for sleeve-type expansion anchors. A concrete of quality C20/25 has been used, where all the material properties are given in Tab. 6.1. The steel plates have been modelled as linear elastic with the elastic modulus $E = 200$ GPa and Poisson's ratio $\nu = 0.3$. The anchors are modelled with the same linear elastic behaviour up to their yield strength $f_{yk} = 640$ MPa. When the yield strength is reached, a linear plastic behaviour with no strain hardening is assumed. The interaction between the concrete and the expansion anchors have been modelled in accordance to the results from the verification example in section 5.3. This means that a tie constraint has been used along the length of the expansion sleeve, while the remaining parts are modelled with hard contact in the normal direction and frictionless contact in the tangential direction.

6.4.3 Static analysis

This section will include a selection of the results from the performed static analyses as well as a detailed discussion about these results. The selection consists of the two basic load cases where the anchor plates are subjected to a tensile load and a moment, respectively. Also, two load combinations for each of the three anchor plates are presented, where the first consist of a tensile load and a moment and the second of two moments acting in perpendicular direction to each other. In section 6.4.4, failure envelopes will be developed based on all the load cases analysed.

In Fig. 6.25, the load-displacement curves, for the load case with a tensile load, are depicted together with the resistance calculated according to TS in section 6.4.1.

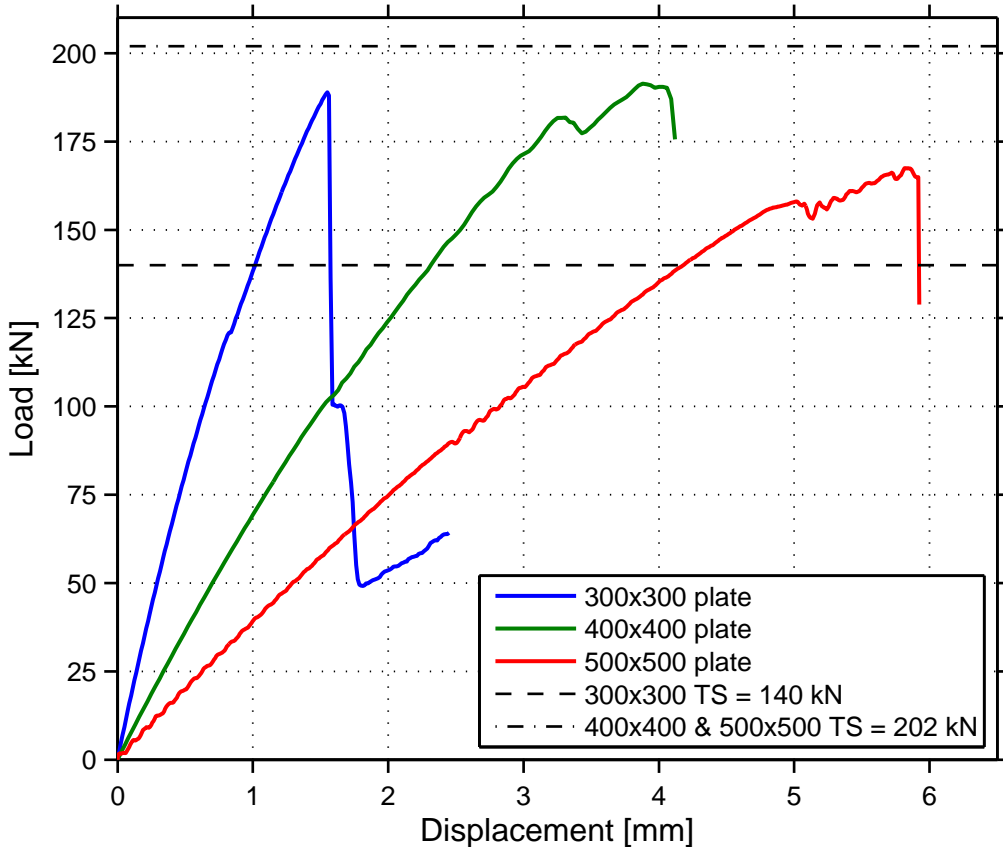


Figure 6.25: Load-displacement curves for the three anchor plates subjected to a tensile load together with the resistance according to TS.

As can be seen in the load-displacement curves, the resistance of the 300x300 anchor plate is approximately 190 kN according to the finite element result while TS result is 140 kN. This means that an overcapacity of 34 % is present. However, for the 400x400 and 500x500 anchor plate the resistance from the finite element analyses are smaller than TS results. While TS calculations give a failure load 202 kN for both anchor plates, since the concrete cones do not intersect, the finite element analyses result in a capacity of 192 kN and 168 kN, respectively. The cause to these results is probably the large bending deformation that the steel plates are subjected to during loading. For the 300x300 anchor plate, the deformation is not as severe. The reason is that the area of the steel plate in comparison to the load area is smaller than for the two larger plates. Due to the large deformations of the steel plate, the expansion anchors also deform. This induces relatively large shear forces in the anchors; for the 400x400 anchor plate, approximately 13 kN on each anchor. Hence, the expansion anchors are subjected to a load case with a combined tensile and shear load. According to Simpson strong-tie (2009) the shear load capacity is 101 kN, which gives that the induced shear forces in one anchor is 13 % of the shear load capacity. If this value is used in Eq. 4.13 with the tensile load capacity, 50.4 kN according to Simpson strong-tie (2009), the resulting tensile resistance is 195 kN which only differs 1.5 % from the finite element analysis. The same reasoning also

applies to the 500x500 anchor plate, but with even larger shear forces.

Two additional analyses were performed in order to prove this theory, where the load area was extended to include the whole steel plate area of the 400x400 anchor plate and one analysis where the load area of the HEB100 was considered as rigid, also for the 400x400 anchor plate. For the first analysis, this means that the tensile load becomes evenly distributed over the area, and that the steel plate is not subjected to any bending. However in the second analysis, the steel plate will be subjected to bending but not in the same extent as for the standard analyses with a non-rigid load area. The result from these two analyses can be seen in Fig. 6.26, together with the resistance from the calculations according to TS and the standard analysis of the 400x400 anchor plate.

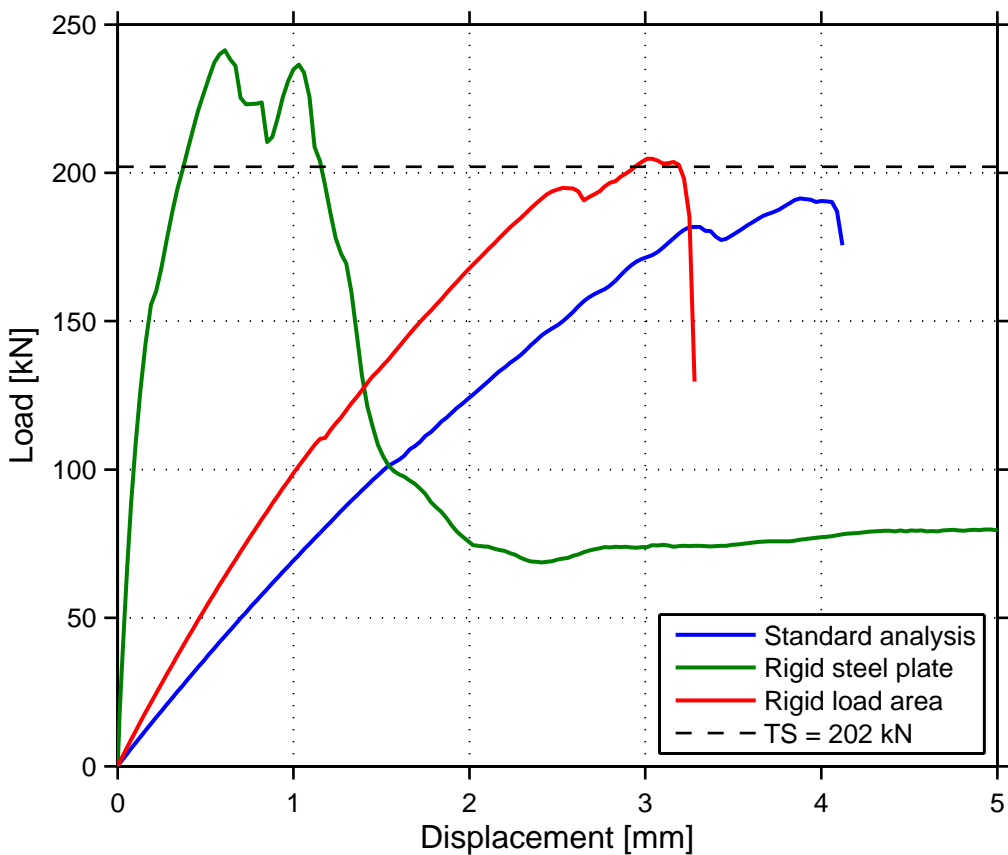


Figure 6.26: Load-displacement curves for the 400x400 anchor plate modelled with three different interactions together with the resistance according to TS.

The resulting resistance becomes 241 kN for the analysis with the load distributed over the whole steel plate area, which implies an overcapacity of 19 %. This assumption corresponds best with the theory of the design procedure. The analysis with a rigid load area shows a resistance of 205 kN, i.e. an overcapacity of 1.5 %. These results show that severe bending of the steel plate and the expansion anchors have significant disadvantages regarding the tensile resistance. As mentioned above, the

anchor plate with a rigid load area will deform but not as much as the anchor plate with a non-rigid load area. This explains why the resulting resistance is larger for the rigid load area analysis in comparison to the analysis with a non-rigid load area. A comparison of the deformation of the three anchor plates with a non-rigid load area is shown in Fig. 6.27, together with the deformation of the 400x400 anchor plate with a rigid load area. All deformations in Fig. 6.27 are presented for the peak load of each load case.

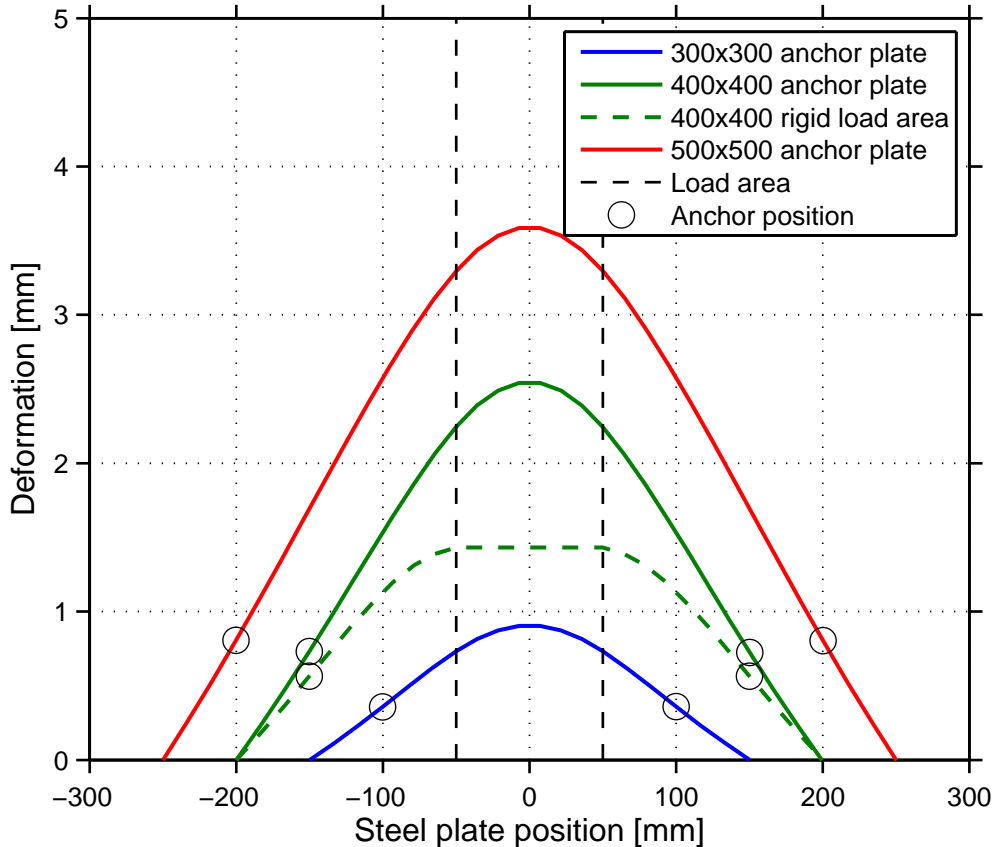


Figure 6.27: Deformation of the three anchor plates and the 400x400 anchor plate with a rigid load area along the center line of respective anchor plate. The coordinate 0 on the x-axis represent the midpoint of the steel plates.

As can be seen, the deformation of the 400x400 and 500x500 anchor plates are considerably larger than for the 300x300 anchor plate. Further, it can be seen that the inclination of the steel plate in the vicinity of the expansion anchors is much steeper for the two larger anchor plates. This means that these anchors are subjected to more bending, which generate larger shear forces. The anchor plate with a rigid load area do not deform as much. This results in a lower inclination in the vicinity of the expansion anchors, which yields a larger resistance due to smaller shear forces. The real behaviour of the interaction between the anchor plate and the connecting beam, is probably a combination of the rigid and the non-rigid load area

behaviour. However, by choosing to model the interaction as non-rigid the results will be conservative.

The load distribution between the four anchors in the three anchor plates subjected to a tensile load are shown in Fig. 6.28.

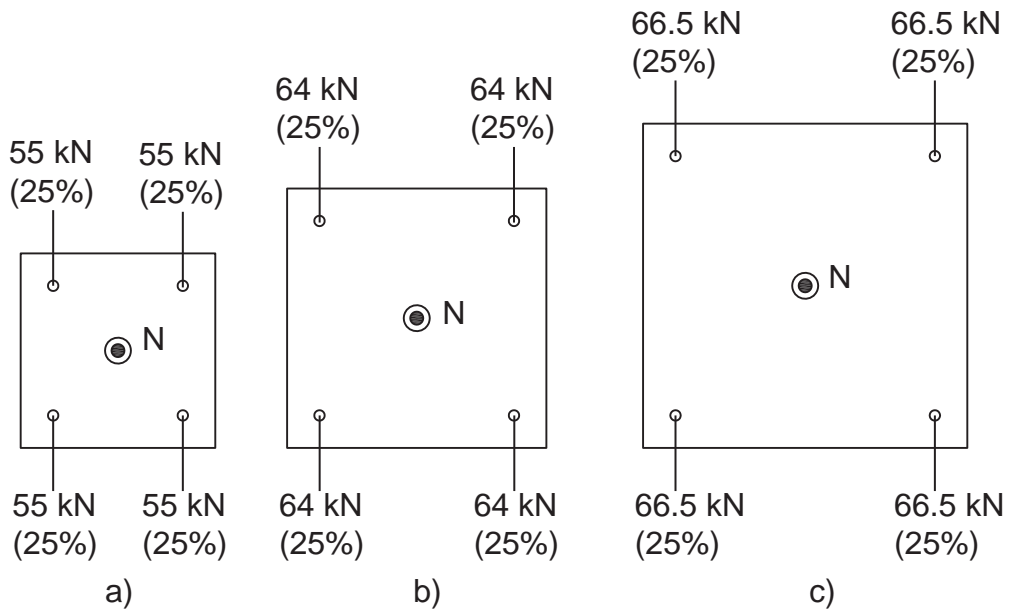


Figure 6.28: Tensile load distribution between the four anchors.

The load is evenly distributed between the four bolts for all three anchor plates. However, the load on each expansion anchor for the 300x300 anchor plate is considerably smaller than for the other two anchor plates. The reason is that the concrete cones from the four anchors intersect with each other for the 300x300 anchor plate, while they do not intersect for the two larger anchor plates. This can be seen in Fig. 6.29, where a comparison is made between the concrete cones of the 300x300 and 500x500 anchor plate.

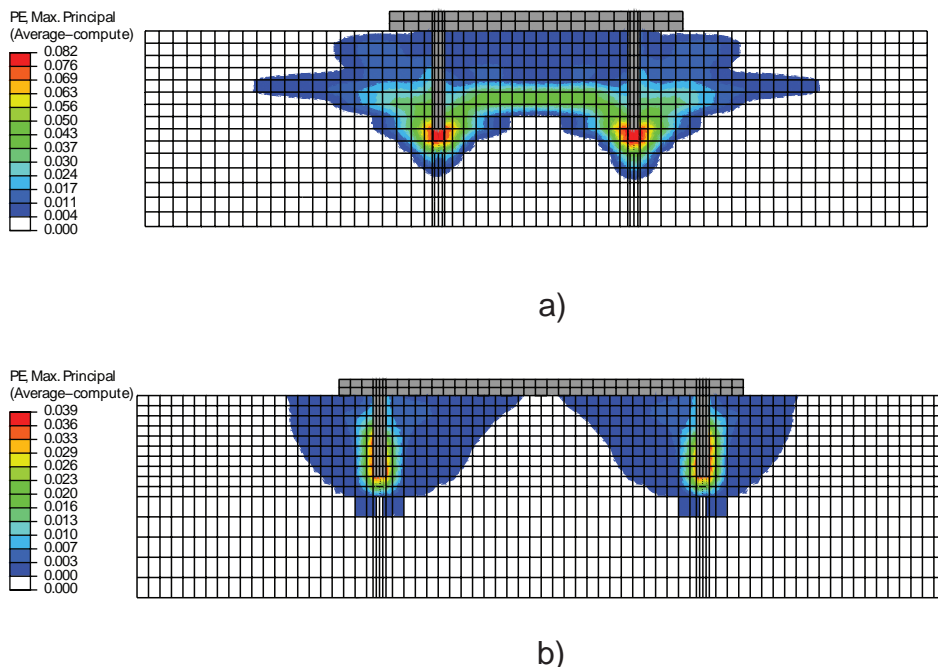


Figure 6.29: Concrete cone comparison, a) 300x300 anchor plate and b) 500x500 anchor plate. Illustrated by the maximum principal plastic strains.

It can clearly be observed that the concrete cones intersect with each other for the 300x300 anchor plate, while the concrete cones are more independent for the 500x500 anchor plate. Furthermore, the concrete cone surfaces have an angle of approximately 40°, which corresponds well with the empirical derived assumption of 35° in TS.

In Fig. 6.30, the moment-rotation curves of the three analysed anchor plates, subjected to a moment, are depicted together with the calculated resistance according to TS.

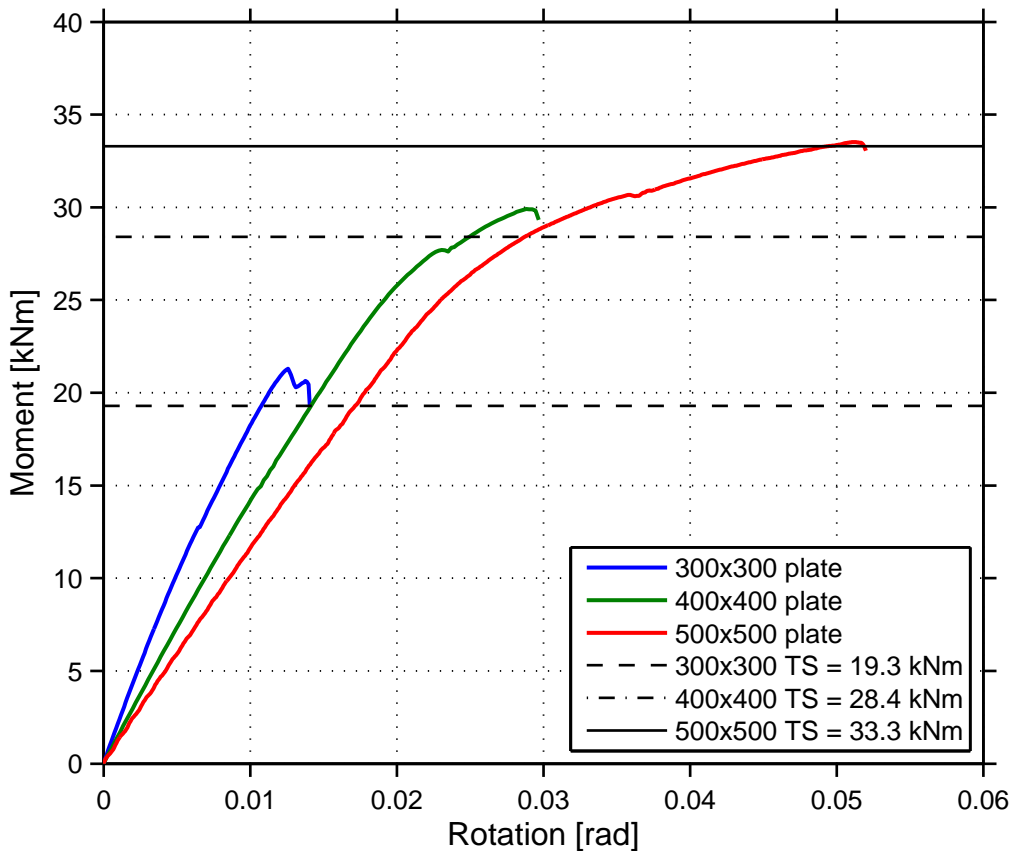


Figure 6.30: Moment-rotation curves for the three anchor plates subjected to a moment together with the resistance according to TS.

The finite element results show very good agreement with the analytical calculations according to TS. However, some overcapacity is present for all three anchor plates, where the 300x300 anchor plate shows 10 %, the 400x400 anchor plate 5 % and the 500x500 anchor plate 0.6 % overcapacity. The reason to this decreasing overcapacity is again the difference in deformation of the steel plate. While the 300x300 anchor plate is moderately deformed, the two larger plates deform to a greater extent. This induces shear forces which clearly reduce the amount of overcapacity, in accordance to the reasoning for the tensile analyses. When a moment is applied to the anchor plates, two of the expansion anchors are subjected to tensile forces while the other two are in compression, this can be seen in Fig. 6.31. Hence, the two expansion anchors loaded in tension will fail due to concrete cone failure. Since the concrete cones intersect for the 300x300 anchor plate, the resistance is smaller than for the two larger plates. In addition, the resistance of the 400x400 anchor plate is smaller than that of the 500x500 anchor plate; although the concrete cones do not intersect for any of them. Instead, the difference is due to the length of the lever arm; as the 500x500 anchor plate has a longer lever arm, the moment resistance becomes larger.

The distribution of the tensile loads between the expansion anchors due to the applied moment is shown in Fig. 6.31.

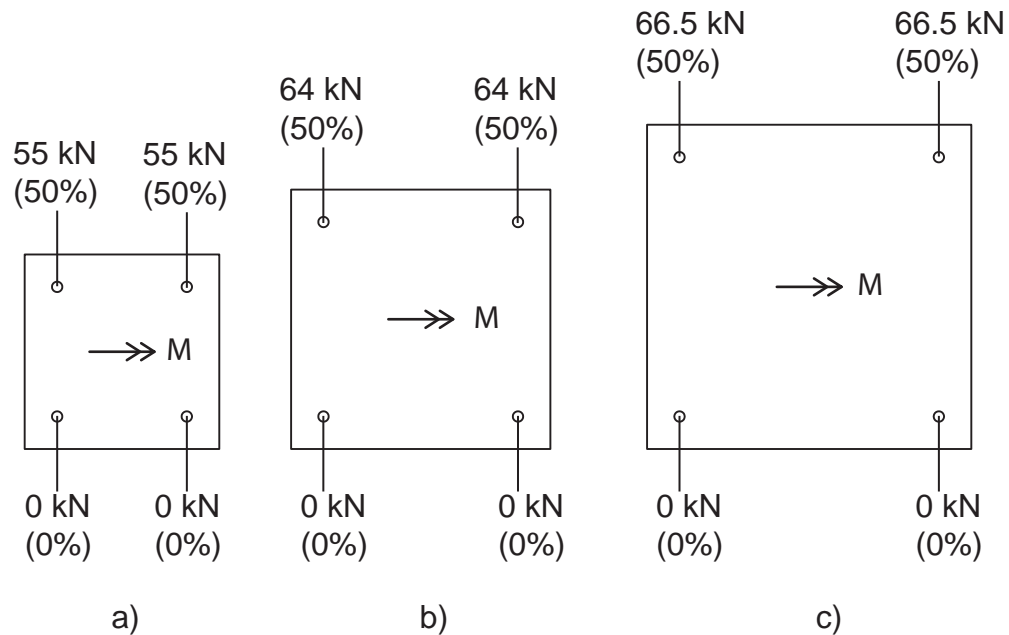


Figure 6.31: Load distribution between the four anchors due to moment load.

As mentioned above, two of the expansion anchors becomes loaded in tension because of the applied moment while the other two are subjected to compressive loads. In TS, the distribution is stated to be calculated according to linear elastic theory. The steel plate is considered as a concrete beam section where the expansion anchors are equal to the reinforcement. However, for the 400x400 and 500x500 anchor plate, this method yields a different distribution than the finite element analyses. Instead of two expansion anchors in tension, all four are subjected to tensile loads in the linear elastic analysis. Fortunately, the two anchors nearest the compressive side of the steel plate are only subjected to 1.6 % and 2.4 % of the total tensile load, acting on the 400x400 and 500x500 anchor plates, respectively. Hence, the difference is rather small and do not have a vast affect on the calculated resistance.

The concrete cone failure surface for the 500x500 anchor plate subjected to a moment is depicted in Fig. 6.32. The concrete cones for the two smaller anchor plates are similar, with the difference that the concrete cones intersect for the 300x300 anchor plate. It is also shown that the concrete cones are only developed on the side where tensile forces are present due to the applied moment, in accordance to the load distribution in Fig. 6.31.

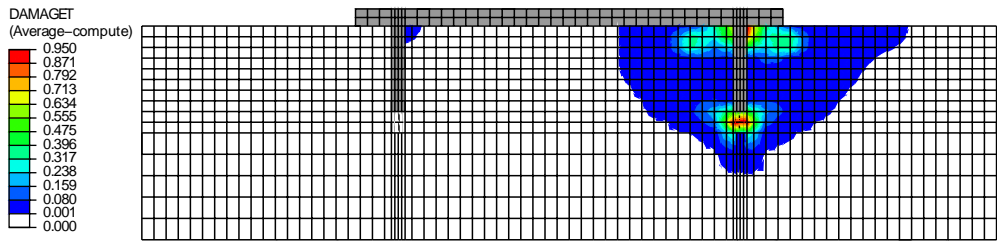


Figure 6.32: Concrete cone failure surface for the 500x500 anchor plate subjected to a moment.

A series of load combinations have been analysed in order to be able to construct failure envelopes in section 6.4.4. However, only a selection is presented in this section since the results from the analyses are similar. A analysis with a combined tensile load and moment is shown in Fig. 6.33 for the 300x300 anchor plate. The loads are applied as a forced displacement and rotation, where the velocity have been reduced to 50 % of the velocity used in the analyses with only one of the loads. To be able to compare when failure occurs, the tensile load and the moment are plotted against the percentage of the load step instead of their respective deformation.

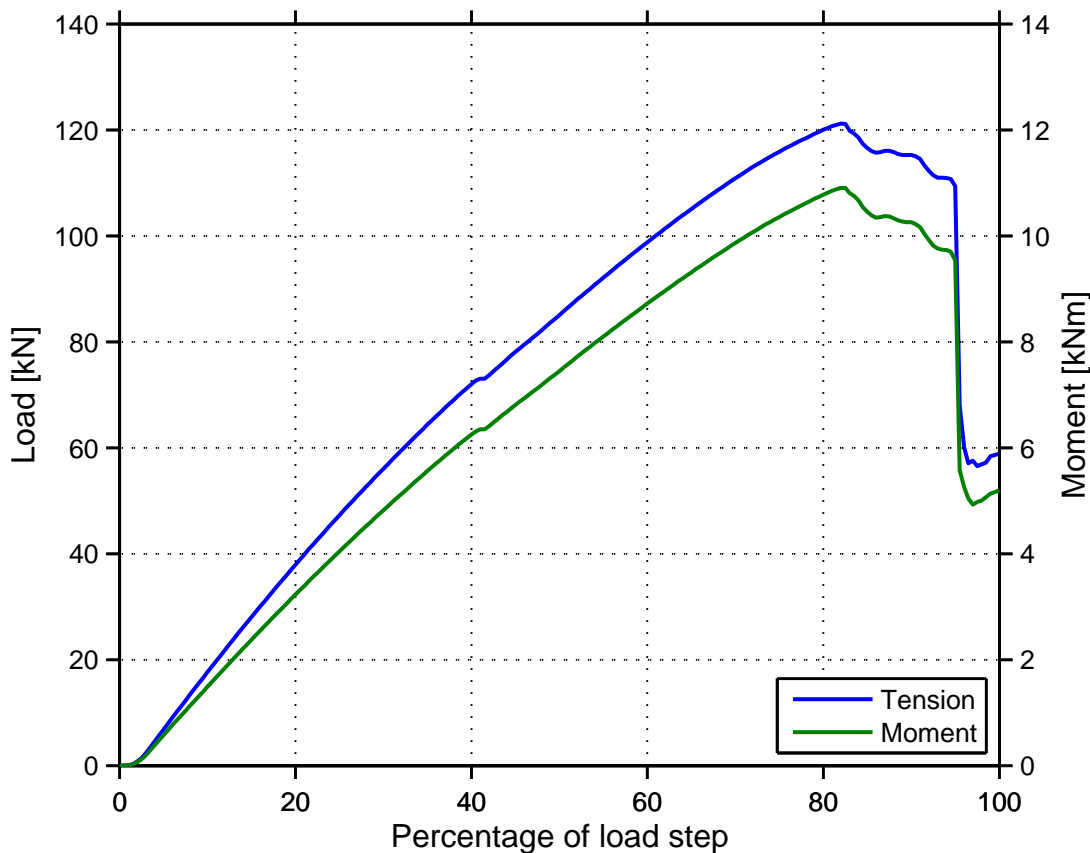


Figure 6.33: Load and moment curves for a load case with combined tensile load and moment.

Ultimate failure occurs after approximately 80 % of the load step, where both the tensile load and moment drops rapidly. The maximum tensile load reached in the analysis is 121 kN, which corresponds to 64 % of the tensile resistance. The analysis results also show that the maximum moment is 11 kNm, which is 52 % of the moment resistance of the 300x300 anchor plate subjected to a single moment. If a linear interaction is assumed between the tensile load and moment, the sum of the percentage shall not exceed 100 %. However, this is not the case for the analysed combination since the sum exceeds 100 %, i.e. the interaction is non-linear. This also means that a combined load case is more beneficial and that an overcapacity is present.

The second combined load case that will be presented is a combination of two moments acting, in perpendicular directions on the 300x300 anchor plate. The moments acting on the anchor plate are 75 % and 25 % of the maximum moment, as defined in the analysis anchor plate is subjected to only one moment, see Fig. 6.30. The results from the analysis are shown in Fig. 6.34, where the moments are plotted against the percentage of the load step.

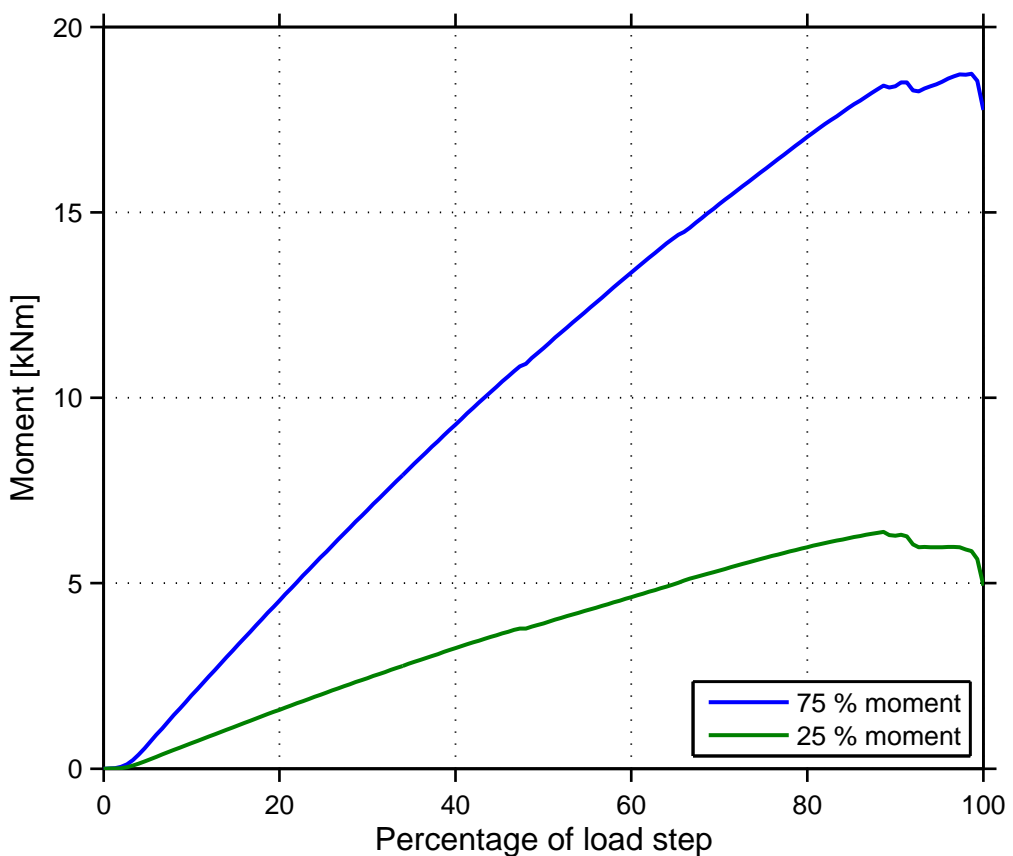


Figure 6.34: Moment curves for a load case with two moments acting in perpendicular direction.

As can be seen, the failure occurs at the same time for both the applied moments. The moment resistance in the direction with the larger moment is 18.7 kNm, which is 88 % of the maximum moment in the analysis presented in Fig. 6.30. In the other direction, the moment resistance is 6.4 kNm, which is 30 % of the maximum moment. This means that the interaction between the two applied moments is non-linear, and that an overcapacity is present for this type of load combination.

The tensile load distribution between the expansion anchors in the 300x300 anchor plate due to the two presented load combinations are depicted in Fig. 6.35.

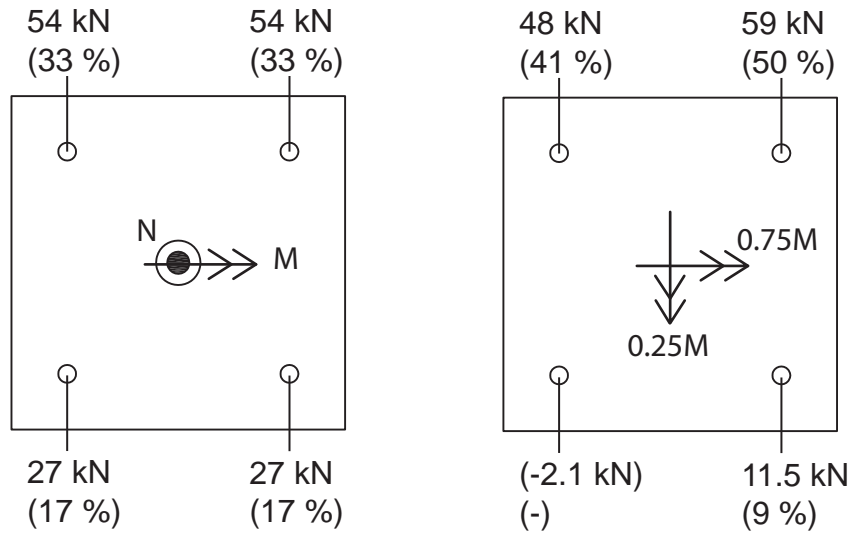


Figure 6.35: Tensile load distribution between the expansion anchors due to the two presented load combinations.

For the first load combination with a tensile load and a moment, all four expansion anchors are subjected to tensile loads. The two expansion anchors on the side of positive moment are subjected to larger tensile loads than the other two, which could be expected. The reason to the smaller tensile loads, is that the applied moment give compressive forces on that side. For the second load combination, three of the expansion anchors are subjected to tensile loads, while one is under compression. The two expansion anchors on the side where the larger moment is positive, are subjected to the largest tensile loads. While the smallest tensile appears on the expansion anchor where the smaller moment is positive. The compressed expansion anchor is placed where both the applied moments are negative.

6.4.4 Failure envelopes

All results from the static analyses were not presented in the previous section. However, all the results have been used to construct the failure envelopes presented in this section. Two different load combinations have been studied for the three anchor plates. The first load combination include a tensile load and a moment, and the second two moments acting in perpendicular direction. The failure envelopes are developed by first normalising the finite element results to the maximum resistance, obtained from the analyses where the anchor plates are subjected to just a tensile load or a moment. And secondly, by fitting these normalised values with a quadratic function through the method of least squares.

The failure envelopes for the three anchor plates from the first load combination, with a tensile load and a moment, are shown in Fig. 6.36, 6.37 and 6.38.

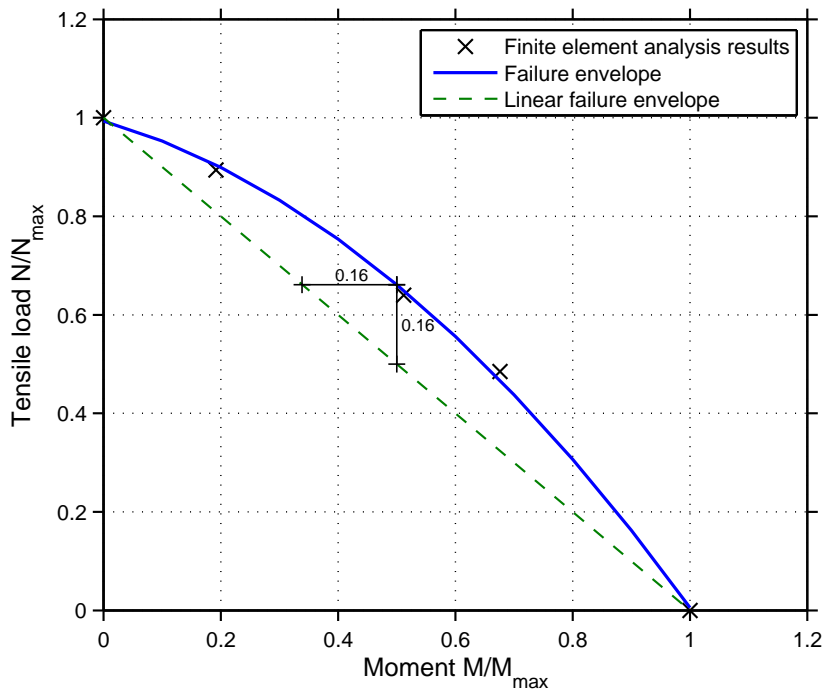


Figure 6.36: Failure envelope for the 300x300 anchor plate subjected to a combined tensile and moment load.

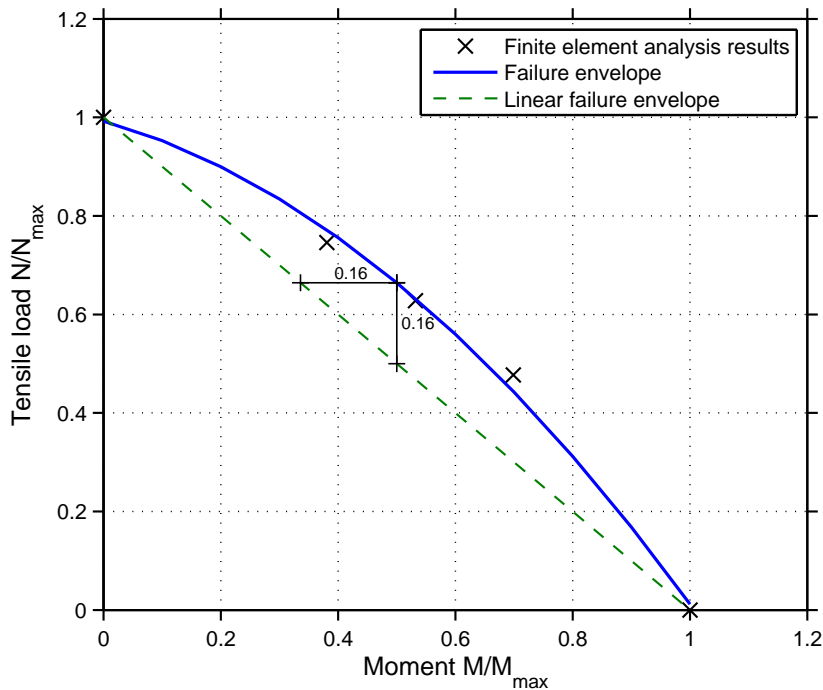


Figure 6.37: Failure envelope for the 400x400 anchor plate subjected to a combined tensile and moment load.

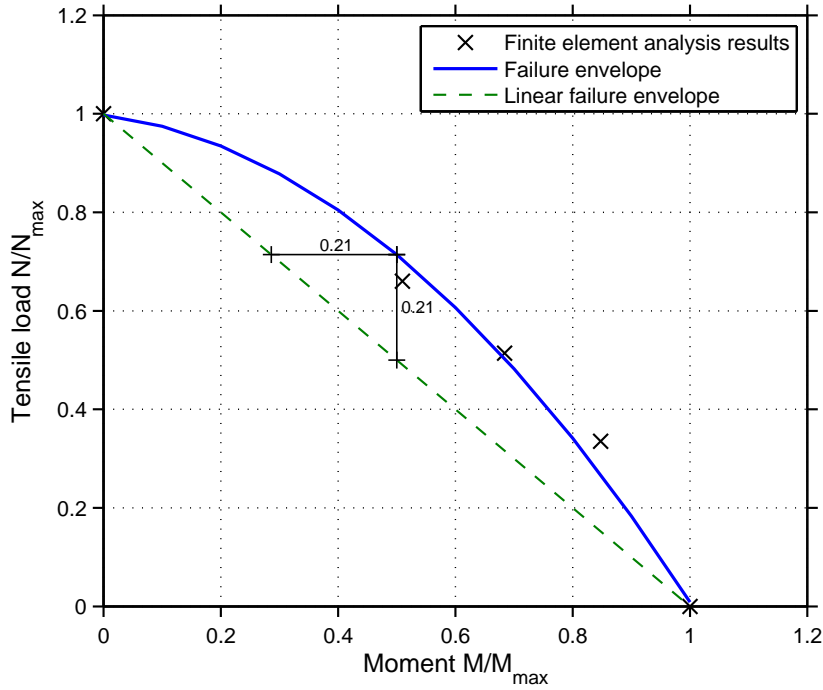


Figure 6.38: Failure envelope for the 500x500 anchor plate subjected to a combined tensile and moment load.

As seen, the combination of a tensile load and a moment result in some overcapacity in comparison to a linear failure envelope. What also can be observed, is that the overcapacity increase slightly for the larger anchor plates. However as shown in section 6.4.3, the maximum resistance for the pure load cases with only a tensile load is reduced for the larger anchor plates. This means that the actual resistance might be smaller for the larger anchor plates, while the relative overcapacity in comparison to the normalised values is larger.

The analyses of the second load combination, with two moments acting in perpendicular directions, for the three anchor plates have resulted in the failure envelopes shown in Fig. 6.39, 6.40 and 6.41.

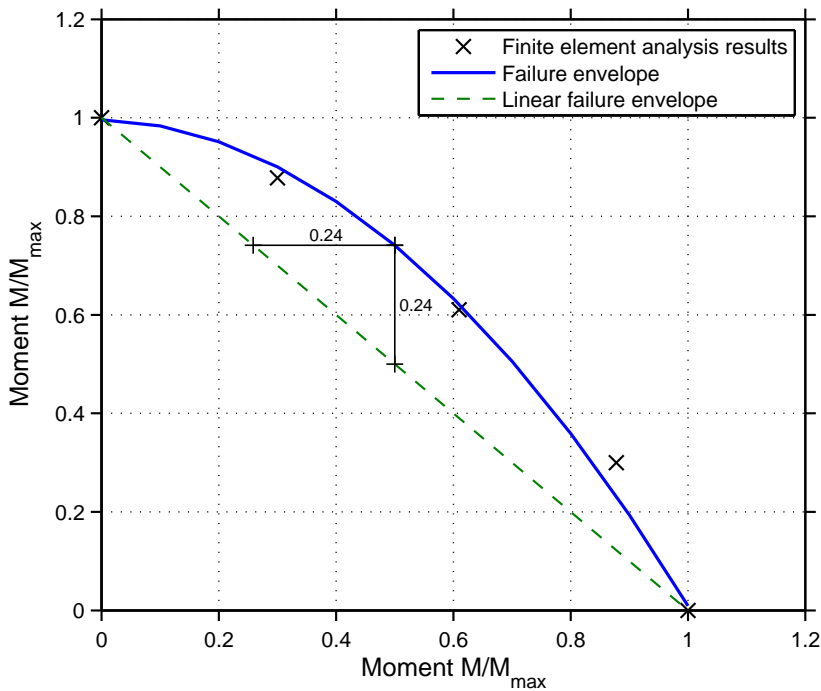


Figure 6.39: Failure envelope for the 300x300 anchor plate subjected to two moments acting in perpendicular directions.

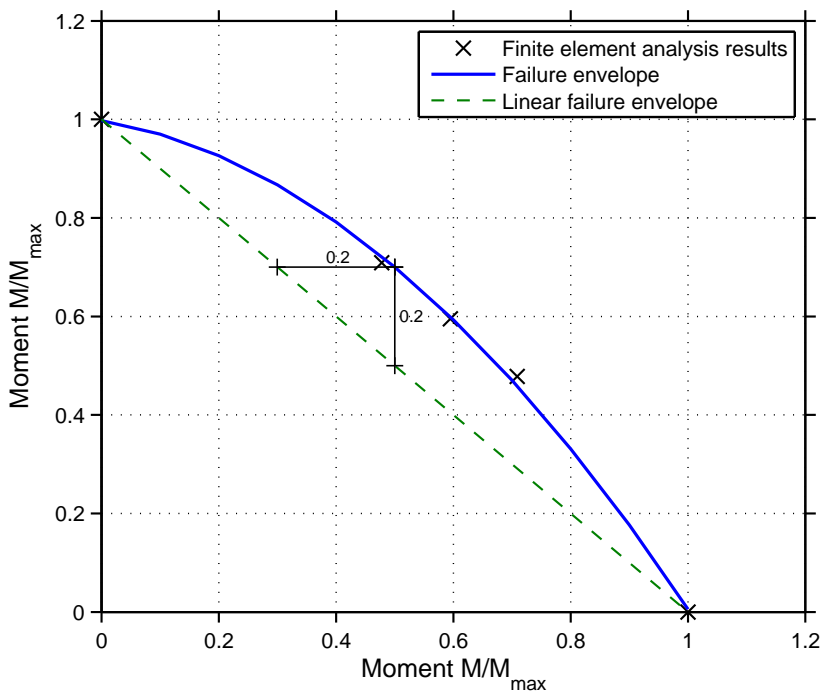


Figure 6.40: Failure envelope for the 400x400 anchor plate subjected to two moments acting in perpendicular directions.

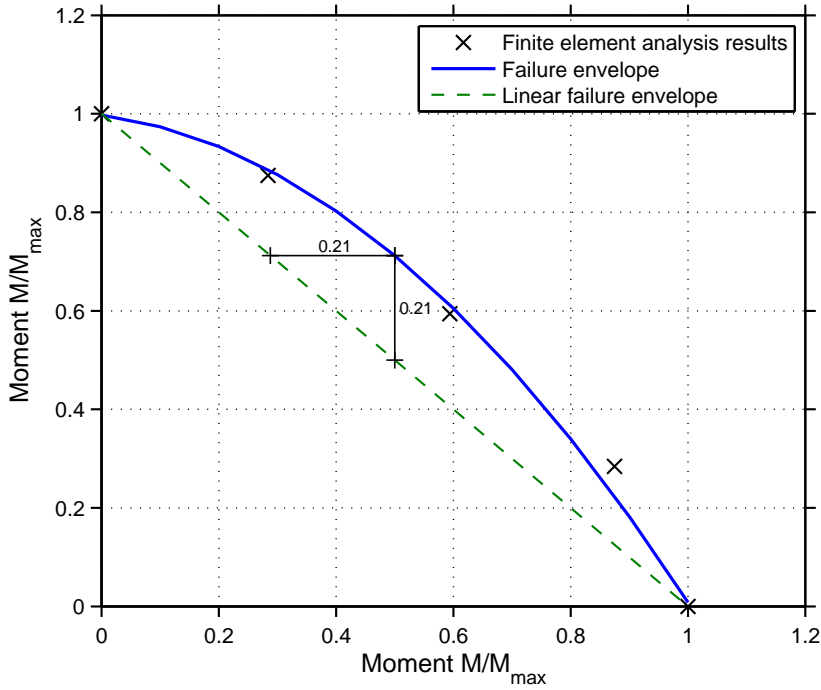


Figure 6.41: Failure envelope for the 500x500 anchor plate subjected to two moments acting in perpendicular directions.

The failure envelopes show that an overcapacity is present, in comparison to the linear interaction, for the combination of two moments acting in perpendicular directions to each other. Hence, this combined load case is more beneficial than when only one moment is applied. For the 300x300 anchor plate, the overcapacity is slightly larger than for the two larger anchor plates. The reason is probably, as mentioned before, that the anchor plates deform to a greater extent for the two larger anchor plates.

To be able to consider a combination of three different loads, a 2-dimensional failure envelope is not enough. Instead, a 3-dimensional surface has to be considered, where each axis represent one of the three loads. As for the normal failure envelopes, the failure loads are normalised and fitted to a surface by a quadratic function. A failure surface for the 300x300 anchor plate subjected to two moments acting in perpendicular directions and a tensile load is depicted in Fig. 6.42. Note that the failure surface should be regarded as conceptual, since there is a unique failure surface for every anchor plate. A failure surface is hard to use in practice, the purpose of this failure surface is just to show the concept.

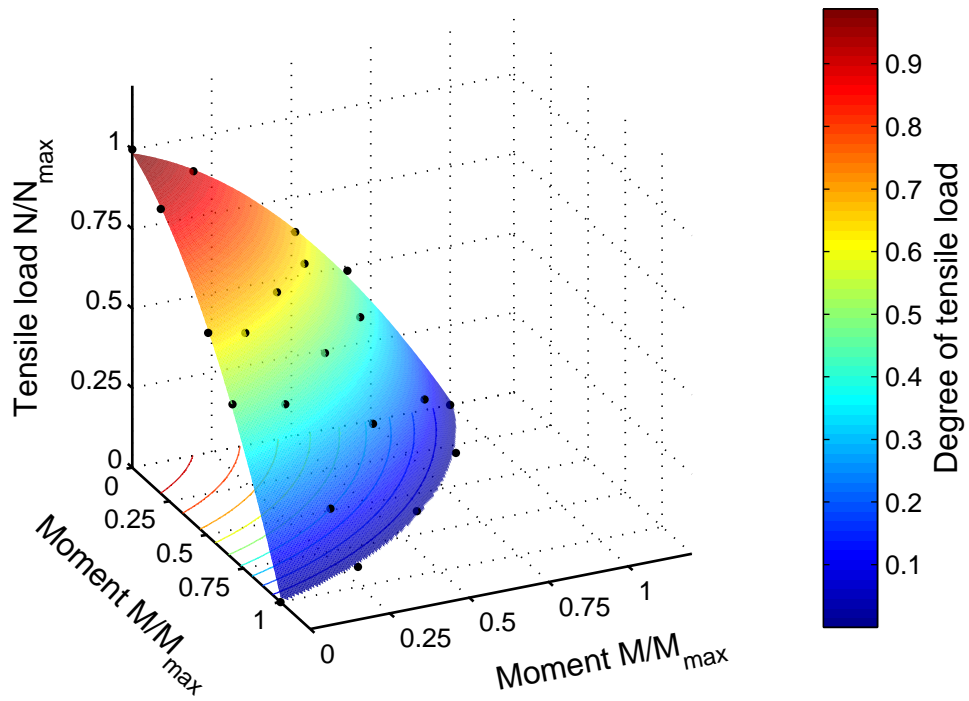


Figure 6.42: Failure surface for the 300x300 anchor plate subjected to two moments and a tensile load.

As mentioned above, a failure surface is hard to use in practice. A more convenient way of using a failure surface is to project the values belonging to one of the axis to the plane formed by the other two axes. This creates a contour plot, which can be used in a equivalent manner to the failure envelopes. A contour plot created from the failure surface in Fig. 6.42 is shown in Fig. 6.43. The axis of the contour plot shows the normalised moments while the level curves represent the normalised tensile load.

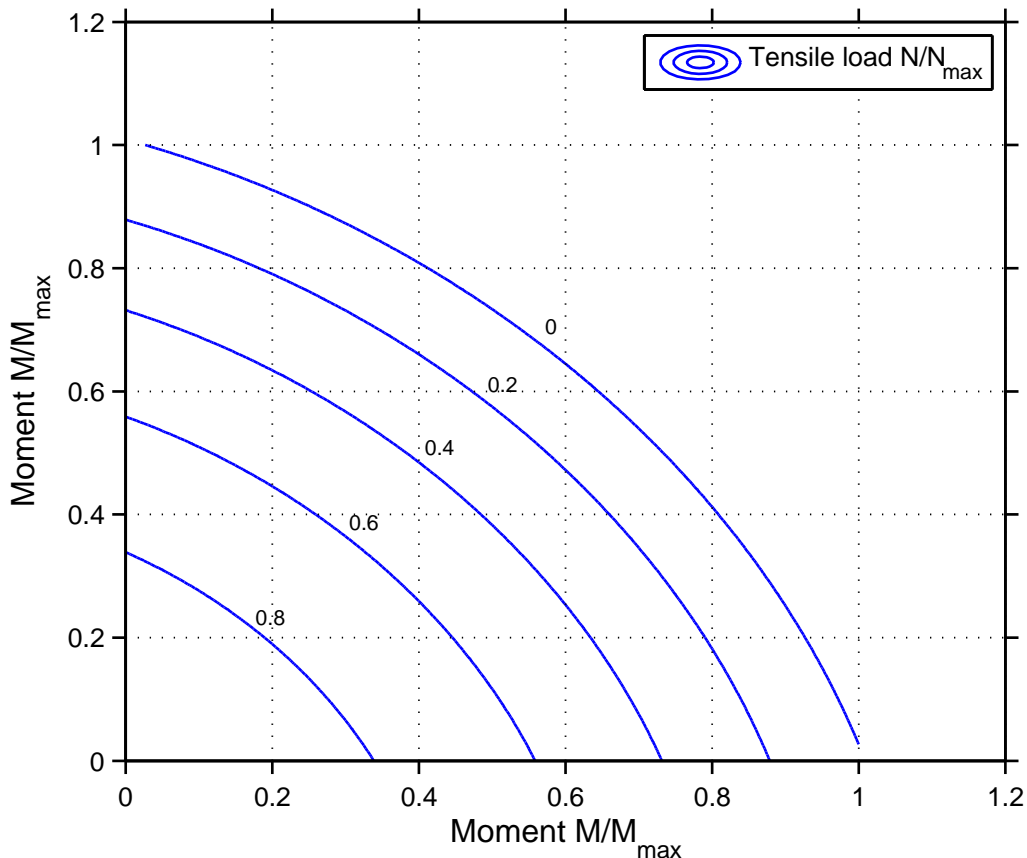


Figure 6.43: Failure contour plot for the 300x300 anchor plate subjected to two moments and a tensile load.

6.4.5 Dynamic analysis

As mentioned in section 6.3.5, the intention with this analysis is to show that it is possible to analyse dynamic loads with the finite element method. The analysed load case is equivalent to the one specified in section 6.3.5 and is depicted in Fig. 6.19. The dynamic load case is only studied for the 300x300 anchor plate. The normalised amplitude is multiplied with the failure load from the analysis of the 300x300 anchor plate subjected to a tensile load, which is approximately 190 kN. The bottom of the concrete slab is constrained in lateral direction to avoid a punch through failure.

The crack pattern obtained from the dynamic analysis is depicted in Fig. 6.44.

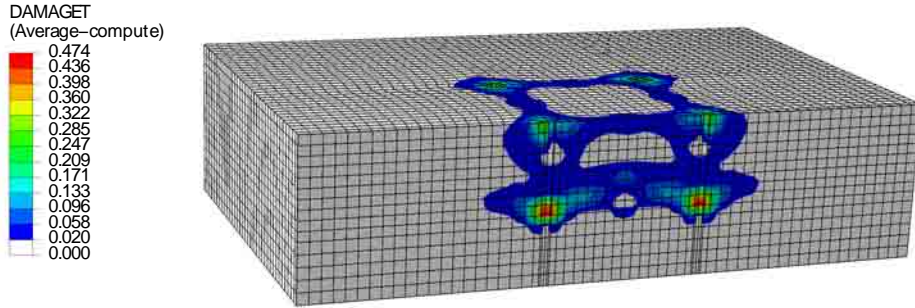


Figure 6.44: Cracks after the dynamic load, illustrated by the tensile damage parameter.

The cracks that appear are mainly concentrated to the top and bottom of the expansion anchors. In the bottom, the cracks propagate in radial direction from the expansion anchors. But an indication of concrete cones may also be observed in the vicinity of the expansion anchors. As the concrete cones are not fully developed, a failure has not occurred which implies that a dynamic load is more beneficial than a static load. The radial cracks are expected since the expansion anchors move upwards and downwards during the applied dynamic amplitude. The surface cracks probably appears due to the bending of the expansion anchors in diagonal direction, which induce tensile stresses between the expansion anchors. If the concrete slab had not been constrained in lateral direction a punch through failure may have occurred, as indicated by the maximum principal stress distribution in Fig. 6.45.

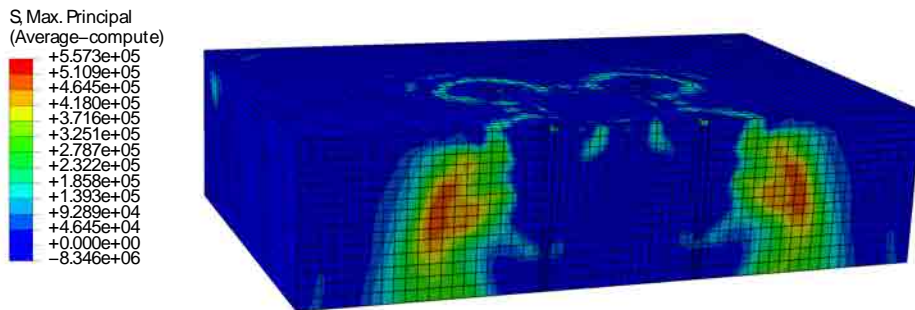


Figure 6.45: Maximum principal stress distribution in the concrete slab.

@Seismicisolation

Chapter 7

Conclusions

In the following chapter, the results presented in this thesis are summarised and commented. The main objective has been to estimate the load capacity of anchor plates in comparison to design calculations. As well as to examine whether the finite element method is applicable to this type of structures. The analyses are primarily static and have been made for many different load combinations, to examine how these effect the structural behaviour of the anchor plates.

7.1 Considerations regarding finite element analysis of anchorage to concrete

The analysis results presented in chapter 5 and 6 show that the finite element method is able to analyse the concrete failure modes associated with anchorage to concrete. Further, the analyses show that the finite element method can describe the crack propagation associated with closely placed anchors, i.e. anchor plates. For example, when the individual concrete cone of each anchor intersects and instead forms one large break-out body. However, there are some limitations regarding the chosen type of material model, which are based on the smeared crack approach. In the definition of the tensile behaviour, a residual stiffness is left after a crack is fully opened; normally 1 % of the tensile strength. This means that the concrete cone will never be completely separated from the concrete slab, resulting in a residual resistance of the anchor. Often, the cracks propagate very fast and unstable, which sometimes may result in that the break-out cone does not reach the top surface of the concrete slab, for an example see Fig. 6.7. This phenomenon results in a further increase of the residual resistance, i.e. the residual resistance is probably irrelevant.

The main issues found when analysing anchorage to concrete is how to model the interaction between the connecting structure and the steel plate, as well as the interaction between the anchor and the concrete. In this thesis, no connecting beam has been modelled. Instead, the load on the anchor plates have been applied as reaction forces from the connecting beam. Since most beams have different stiffness in their different cross-sectional directions, the used method is a simplification of

the real behaviour. However, this should only affect the resistance of the beam itself and not the concrete failure, which is the emphasis in this thesis. The interaction between the anchors and the concrete differs depending on the anchor type used. For the analyses of headed studs, the interaction in the tangential direction was modelled as frictionless, while no penetration of the two was allowed in the normal direction. This must be considered as a conservative simplification, since a small part of the load should be transferred due to cohesion and frictional forces in reality, which probably increases the resistance. The interaction properties of the expansion anchors are more complex than for the headed studs. In this thesis, a simplified approach have been used, which is composed of rigid links between the expansion sleeve and the concrete. The rest of the anchor is considered to be frictionless. This approach severely underestimate the deformation of the anchor as slip is not allowed, which results in a too stiff behaviour, see Fig. 5.21. This approach could be accepted since the emphasis in this thesis, as previously mentioned, is to determine the load associated with concrete failure. If more information and data were available on the analysed expansion anchors, a more accurate interaction model could be devised. As an example, the pressure developed on the concrete from the expansion sleeve could be included in the numerical model. This in combination with an accurate description of the frictional coefficient in the tangential direction fitted to experimental data, would probably yield a softer and more accurate response. Another alternative is to use spring elements between the expansion sleeve and the concrete, with a non-linear definition of the stiffness in the tangential direction. With a non-linear definition, it is also possible to account for the pull-through behaviour of the expansion cone inside the sleeve. However, these two modelling approaches require experimental data on each anchor type analysed. An additional aspect that may affect the results is the connection between the steel plate and the anchors, especially for post-installed anchor plates. In the analyses made, a rigid connection was assumed, whereas the behaviour is probably more elastic in reality. The reduced integration elements used in the analyses do not describe bending very accurate. Since it was shown in the results that bending of the steel plates had a significant effect on the failure load another element type might have been preferable for the steel plates.

Another issue that is related to the unstable crack growth described above, is the problem with excessive distortion of elements due to a too high wave speed in the material. As a consequence, the analysis is aborted; sometimes before the peak load is reached. This is a problem that is associated with the dynamic explicit solvers and can be overcome either by reducing the velocity of the applied deformation, or by using a technique called mass scaling. The mass scaling technique is often included in commercial finite element softwares, but it should only be used with care since it may affect the result. In this thesis, mass scaling have only been used when the analyses aborted before failure was reached and if the option with a reduced velocity did not help. When it was used, the new results were compared to the ones without mass scaling so that they did not deviate significantly.

7.2 Capacity assessment of anchor plates

In most cases, the finite element analyses presented in chapter 6 yield higher failure loads than the design calculations, with the same material properties used. Although, some of the analyses show lower failure loads than the design calculations, especially some of the larger expansion anchor plates. However, as mentioned above, many conservative simplifications were made in the construction of the finite element models. This along with the chosen characteristic material properties of the C20/25 concrete given in EC 2 (2004), result in failure loads that are conservative in comparison to the reality. The characteristic values are a low estimation of the real material strengths; to better describe the real material properties the mean values from EC 2 (2004) should be used. As an example the mean value of the compressive strength is 40 % higher than the characteristic value for the used C20/25 concrete. As previously discussed in section 6.3.3, the chosen fracture energy correspond to an aggregate size of 8 mm. In reality, the concrete used during the construction of the nuclear facilities at Forsmark probably consists of an aggregate with a size exceeding 32 mm. An aggregate size of 32 mm instead of 8 mm would according to MC 90 (1993) result in a 60 % increase of the fracture energy. The numerical study by Ozbolt (1995), presented in Fig. 2.7, would in this case result in an increase of the failure load with about 30 %. Though, the parametric study of the fracture energy for the M3 anchor plate in section 6.3.3 only showed an increase of less than 10 %. The reason for this difference is probably the deeper embedment depth used by Ozbolt (1995). Beyond this, the concrete at Forsmark is a slowly hardening C20/25 concrete, which probably means that the concrete today has gained in strength. According to Ljungkrantz et al. (1994), the compressive strength of an ordinary portland cement increases with 60 % during the first seven years. Thus, a reasonable assumption is that the concrete would measure up to at least a concrete of quality C35/45, based on the mean values of the compressive strength. Since the cement is slowly hardening, a quality of C50/60 is perhaps more probable.

It should be noted that the results presented throughout this thesis cannot be used as design values, unless reduced according to a relevant design code, for example DRB:2001 (2002). Since the failure envelopes are presented with normalised values, these could theoretically be used for design purposes. Further, it should also be noted that all failure loads are determined with the assumption that the failure occurs in the concrete. For some load cases the failure may be located to the steel plate or the connecting beam.

7.2.1 Static analysis

All the analyses made on the M3 anchor plate in section 6.3 shows an overcapacity when compared to the design calculations. This especially applies to the moment capacity of the anchor plate. An interesting observation is that the moment capacity in the supposedly weak direction M_z exceeds that of the stiff direction M_x , for both the design calculations and the finite element results. A reasonable explanation to

this phenomenon is that the load is redistributed between the anchors as failures occur. This is the case for many of the other combined load cases as well. The load distribution obtained from the calculations according to SIS-CEN/TS 1992-4 (2009) do not allow any redistribution of the load since the steel plate is considered as rigid. The assumption of a rigid steel plate must be seen as conservative, since it concentrates even more load to the heavily loaded anchors in comparison to the finite element analyses. In the finite element analyses of the M3 anchor plate a dilation angle of 10° was used, which is rather small in comparison to what is normally used. As discussed in section 5.2, the reason for the low dilation angle is probably the young age of the concrete used in the experiments by Nilsson and Elfgren (2009). The dilation angle describes the shear resistance of the concrete, which increases as the concrete hardens. Hence, the dilation angle should also increase. Therefore, a dilation angle of 10° must be considered as a conservative value for an old concrete, as the one at Forsmark nuclear facility.

The larger expansion anchor plates did show failure loads lower than the resistance calculated according to SIS-CEN/TS 1992-4 (2009). The reason is the extensive bending of the steel plate as the load is applied, which induces shear forces on the expansion anchors. A smaller anchor plate has less pronounced bending and therefore agrees better with the design calculations, which assumes a rigid steel plate, and sometimes shows an overcapacity. Furthermore, as can be seen in Fig. 6.27, the definition of the load area significantly influences the bending of the steel plate and therefore the resistance, because of the induced shear forces. This means that if a more accurate description of the load area is made, i.e. a stiffer load area, even the larger anchor plates might show an overcapacity in comparison to the design code. Nevertheless, the moment capacity increases with the size of the steel plate, even though the disadvantageous shear forces are present for moment loads as well. This is due to the fact that the lever arm is increased for larger anchor plates, although the increase in failure load is not proportional to the increase of the lever arm.

As a concluding remark on the static analyses, it should once again be noted that the obtained failure loads are conservative due to the simplifications made and the conservative material properties used. It should also be pointed out that the analyses were made with an emphasis on design values. Therefore, the goal was not to capture the actual ultimate load that could be measured in experiments.

7.2.2 Failure envelopes

The developed failure envelopes are intended to be used as a design aid concept for structural engineers. As mentioned above, the values in the failure envelopes are normalised and may therefore be used for design, even though they are developed with characteristic values. To add even more safety margins, the curve fitting of the envelope could have been made so that none of the finite element results lies beneath the envelope.

A further development of the failure envelope is a failure surface, which can account for a combination of three different loads, an example is given in Fig. 6.42. The

failure surface itself is difficult to use in practice, but can be converted to a contour plot, as seen in Fig. 6.43. The contour plot can be an effective design aid used for complex load combinations. However, the development of failure surfaces through finite element analysis is very time consuming, since a lot of analyses have to be performed. The failure surface developed and presented in this thesis required results from 21 different load combinations, however due to the symmetry of the expansion anchor plate only 14 analyses had to be performed. With the computer resources available in this project, each analysis had a computational time of 2.5 hours; i.e a total commotional time of 35 hours. The total computational time needed for the development of a failure surface for an unsymmetrical anchor plate would increase vastly. As a comparison, the M3 anchor plate where each analysis takes about 4 hours, would require a total computational time of 84 hours.

7.2.3 Dynamic analysis

The performed dynamic analyses should be considered as a sort of benchmark rather than a regular analysis, since the emphasis was not on dynamics. The results showed that it is possible to analyse dynamic load cases, and that the analysed dynamic event was more beneficial than its corresponding static load case. This is especially interesting since the normal design procedure is to apply a dynamic amplification factor on the static load. Thus, the performed dynamic analyses show that the normal design procedures for dynamic loads are very conservative.

One of the issues with the analysis of dynamic load cases is the time span of the event when solving the problem with an explicit solver. The analysed dynamic event had a time period of 0.2 seconds, whereas for the quasi-static analyses a time period of 0.1-0.25 seconds were used. The computational time used by an explicit solver is proportional to the time period, why events such as an earthquake with a time period in excess of 20 seconds would be very time consuming to analyse. Therefore, earthquake analysis is normally performed with implicit integration.

7.3 Further research

When building the finite element models, the greatest uncertainty was found to be the description of the interaction between the anchors and the concrete, especially for complex anchors such as expansion anchors. Therefore, is it deemed necessary to further investigate different ways of modelling this interaction, as for example proposed in section 7.1. To obtain accurate descriptions it would probably be necessary to preform experimental validation of the models.

In the analyses of anchor plates, it was found that bending of the steel plate influenced the failure loads significantly. Since the design methods available do not account for any bending of the steel plates and assumes them to be rigid, some overestimation of the failure load for large anchor plates may be a consequence. It is therefore essential to investigate how to implement effects associated with plate

bending into the regular design procedures. This could for example be made by developing a new coefficient, such as those already given in Eq. 4.3, which accounts for the effect of large and slender steel plates.

Another development of the design methods would be the use of failure envelopes for complex load cases in a greater extent than today. Since no failure envelope can be developed which is valid for all type of anchor plates, it is difficult to give a general failure envelope in a design code. Instead, general guidelines on how to develop a failure envelope could be given, not necessarily through the use of finite element analysis. A general guideline would also enable that all kind of load cases could be covered, for example shear and torque loads which are not treated in this thesis. The most effective strategy is to use contour plots based on failure surfaces, since these can include a combination of three different loads.

During the literature study, no experiments on anchor plates were found. To better be able to validate the finite element models of anchor plates it is of great importance to perform such studies. These could for example include the influence of cracked concrete and different reinforcement, such as normal flexural reinforcement and specially designed stirrups. A good opportunity to perform such experiments, is in the decommissioned nuclear facility at Barsebäck. This would be very valuable for the nuclear industry, which has a lot anchor plates in their facilities. The experiments should further be complemented by the use of finite element analysis.

Bibliography

- ACI 349-6, 2007. Code requirements for nuclear safety-related concrete structures and commentary. American Concrete Institute, Michigan, USA.
- B-7, 1968. B-7 Bestämmelser för betongkonstruktioner—Allmänna konstruktionsbestämmelser. Statens Betongkomitté, Sweden.
- Bathe, K., 2009. ADINA User's Manual. Watertown, 8th Edition.
- BBK 04, 2004. Boverkets handbok om betongkonstruktioner, 3rd Edition. Boverket, Sweden.
- Björnström, J., Ekström, T., Hassanzadeh, M., 2006. Spruckna betongdammar - Översikt och beräkningsmetoder. Report 06:29, Elforsk.
- BKR 2010, 2011. Boverkets Konstruktionsregler, 13th Edition. Boverket, Sweden.
- Bower, A. F., 2009. Applied Mechanics of Solids, 1st Edition. CRC Press, New York.
- BSK 07, 2007. Boverkets handbok om stålkonstruktioner, 4th Edition. Boverket, Sweden.
- Cook, R. D., Malkus, D. S., Plesha, M. E., Witt, R. J., 2001. Concepts and Applications of Finite Element Analysis, 4th Edition. John Wiley & Sons Inc., University of Wisconsin-Madison.
- Cornelissen, H., Hordijk, D., Reinhardt, H., 1986. Experimental determination of crack softening characteristics of normal weight and lightweight concrete. Heron, Vol. 31, No. 2, Delft, The Netherlands.
- De Schutter, G., Taerwe, L., 1997. Fracture energy of concrete at early ages. Materials and Structures 30, 66–71.
- DRB:2001, 2002. Dimensioneringsregler för byggnade vid kärntekniska anläggningar. Barsebäck Kraft AB and OKG Aktiebolag and Scanscot Technology AB, Lund.
- EC 2, 2004. Eurocode 2: Design of concrete structures - Part 1-1: General rules and rules for buildings. EN 1992-1-1. European Committee for Standardization, Brussels.
- EKS 8, 2011. BFS 2011:10, Boverkets föreskrifter och allmänna råd om tillämpning av europeiska konstruktionsstandarder (eurokoder). Boverket, Sweden.

BIBLIOGRAPHY

- Elfgren, L., 1989. Fracture mechanics of concrete structures - From theory to applications, Report of the technical committee 90-FMA Fracture Mechanics to Concrete - Applications, RILEM Edition. Chapman and Hall Ltd, London.
- Elgehausen, R., Clausnitzer, W., 1983. Analytisches Modell zur Beschreibung des tragverhaltens von Befestigungselementen. Report no. 4/1-83/3, University of Stuttgart, Germany.
- Elgehausen, R., Mallée, R., F.Silva, J., 2006. Anchorage in Concrete Construction. Ernst and Sohn, Berlin.
- Elgehausen, R., Sawade, G., Elfgren, L., 1989. Anchorage to concrete (Chapter 13). RILEM REPORT: Fracture mechanics of concrete structures - From theory to applications (Edited by L. Elggren), 263–311.
- ETAG 001, 1997. Guideline for European technical approval of metal anchors for use in concrete. European Organisation for Technical Approvals, Brussels.
- Fuchs, W., Elgehausen, R., Breen, J. E., 1995. Concrete capacity design (CCD) Approach for fastening to concrete. ACI Structural Journal 92, 794–802.
- Hibbit, Karlsson, Sorensen, 2010. ABAQUS User's Manual. Pawtucket, 6th Edition.
- Kallersjö & Trepp AB, 1972. Typritningar, Beräkningar. Statens Vattenfallsverk, Sweden.
- Kallersjö & Trepp AB, 1977. Typritning på fästplåtar E-201–E-205 Formarks Kraftverkstation block 3. Statens Vattenfallsverk, Sweden.
- Lee, J., Fenves, G., 1998. Plastic-damage model for cyclic loading of concrete structures. Journal of engineering mechanics, ASCE Vol. 124, No. 8, 892–900.
- Ljungkrantz, C., Möller, G., Petersons, N., 1994. Betonghandbok - Material, 2nd Edition. AB Svensk Byggtjänst, Sweden.
- Lubliner, J., Oliver, J., Oller, S., Onate, E., 1989. A plastic-damage model for concrete. International journal of solids and structures Vol. 25, No. 3, 299–326.
- Malm, R., 2006. Shear cracks in concrete structures subjected to in-plane stresses. Lic. thesis, Royal Institute of Technology (KTH), Stockholm, Sweden.
- Malm, R., 2009. Predicting shear type crack initiation and growth in concrete with non-linear finite element method. Ph.D. thesis, Royal Institute of Technology (KTH), Stockholm, Sweden.
- MC 90, 1993. CEB-FIP Model Code 1990, 6th Edition. Thomas Telford, London.
- Ministry of the Environment Sweden, 2007. Sweden's fourth national report under the Convention on Nuclear Safety, Swedish implementation of the obligations of the Convention. Report no. ds 2007:30, Swedish Government, Sweden.

- Nilsson, M., Elfgren, L., 2009. Fastnenings (Anchor Bolts) in Concrete Structres – Effect of Surface Reinforcement on . Nordic Symposium on Nuclear Technology.
- Ozbolt, J., 1995. Massstabseffekt in Beton- und Stahlbeton- konstruktionen. Post-doctoral thesis, University of Stuttgarg, Germany.
- Petersson, P. E., 1981. Crack Growth and Development of Fracture Zones in Plain Concrete and Similar Materials. Report No. TVBM-1006, Division of Building Materials, University of Lund, Sweden.
- Rodriguez, M., Lotze, D., Gross, J., Zhang, Y.-G., Klinger, R., Graves, H., 2001. Dynamic behavior of tensile anchors to concrete. ACI Structural Journal 98, 511–524.
- Sawade, G., 1994. Ein energetisches Materialmodell zur Berechung des Tragverhal- tens von zugbeanspruchten Beton. Ph.D. thesis, University of Stuttgarg, Germany, Germany.
- Simpson strong-tie, 2009. Safety bolt - Twin-cone heavy duty bolt with cylindrical expansion for increased anchoring security. USA.
- SIS-CEN/TS 1992-4, 2009. Technical Specification - Design of Fastenings for use in Concrete - Part 4. European Committee for Standardization, Brussels.
- VBB consulting Ltd, 1992. Charcterization of seismic ground motions for porbabilistic safety analyses of nuclear facilities in Sweden - Summary Report. Ski technical report 92:3, Swedish Nuclear Power Inspectorate, Sweden.
- Wight, J. K., MacGregor, J. G., 2009. Reinforced Concrete Mechanics & Design, 5th Edition. Pearson Education Inc., New Jersey.

@Seismicisolation

Appendix A

Design codes

A.1 Further design procedures according to CEN/TS 1992-4:2010

Splitting failure The characteristic failure load due to splitting failure is normally lower than the characteristic concrete cone failure load. In TS, a number of situations are specified when no verification of splitting failure is required. If a verification is required, then Eq. (A.1) should be used to determine the characteristic failure load.

$$N_{Rk,sp} = N_{Rk}^0 \cdot \frac{A_{c,N}}{A_{c,N}^0} \cdot \Psi_{s,N} \cdot \Psi_{ec,N} \cdot \Psi_{re,N} \cdot \Psi_{h,sp} \quad [\text{N}] \quad (\text{A.1})$$

where,

N_{Rk}^0 is the minimum value of $N_{Rk,p}$ and $N_{Rk,c}^0$, which are found in section 4.1.4 and 4.1.2, respectively. [N]

$N_{Rk,c}^0$, $\Psi_{s,N}$, $\Psi_{ec,N}$ and $\Psi_{re,N}$ shall be calculated according to the directions for concrete cone failure but with $c_{cr,N}$ and $s_{cr,N}$ replaced by $c_{cr,sp}$ and $s_{cr,sp}$. The values of $c_{cr,sp}$ and $s_{cr,sp}$ have to be taken from the relevant product ETA or the CEN Product Standard. The tendency for splitting failure is dependent on the actual concrete member thickness h , where a deeper member results in a lower probability of splitting failure. The factor $\Psi_{h,sp}$ takes the depth of the actual concrete member into account.

$$\Psi_{h,sp} = \left(\frac{h}{h_{min}} \right)^{2/3} \leq \left(\frac{2 \cdot h_{ef}}{h_{min}} \right)^{2/3} \quad [-] \quad (\text{A.2})$$

where,

h is the actual concrete member thickness [mm]

h_{min} is the minimum concrete member thickness according to the relevant ETA or CEN Product Standard [mm]

Blow-out failure According to TS, a verification of blow-out failure is not required if the edge distance in all directions is greater than $c = 0.5 \cdot h_{ef}$. If this condition is not satisfied, then the characteristic resistance in case of blow-out failure must be determined according to Eq. (A.3). Note that this verifications is not required for post-installed anchors.

$$N_{Rk,cb} = N_{Rk,cb}^0 \cdot \Psi_{A,Nb} \cdot \Psi_{s,Nb} \cdot \Psi_{g,Nb} \cdot \Psi_{ec,Nb} \cdot \Psi_{ucr,Nb} \quad [\text{N}] \quad (\text{A.3})$$

$N_{Rk,cb}^0$ is the characteristic resistance of a single anchor, which is not influenced by any adjacent edges or other components connected to the structure. The resistance shall be calculated according to Eq. (A.4). All the coefficients in Eq. (A.3) and how to calculate them, are given in the following.

$$N_{Rk,cb}^0 = 8 \cdot c_1 \cdot \sqrt{A_h} \cdot \sqrt{f_{ck,cube}} \quad [\text{N}] \quad (\text{A.4})$$

where,

c_1 is the edge distance [mm]

A_h is the load bearing area of the fastener [m^2]

$f_{ck,cube}$ is the characteristic concrete cube strength [MPa]

The axial spacing and edge distance may disturb the stress distribution, and it should be taken into account by Eq. (A.5).

$$\Psi_{A,Nb} = \frac{A_{c,Nb}}{A_{c,Nb}^0} \quad [-] \quad (\text{A.5})$$

where,

$A_{c,Nb}^0$ is reference projected area ($4c_1^2$) [m^2]

$A_{c,Nb}$ is the actual projected area, see Fig.A.1 [m^2]

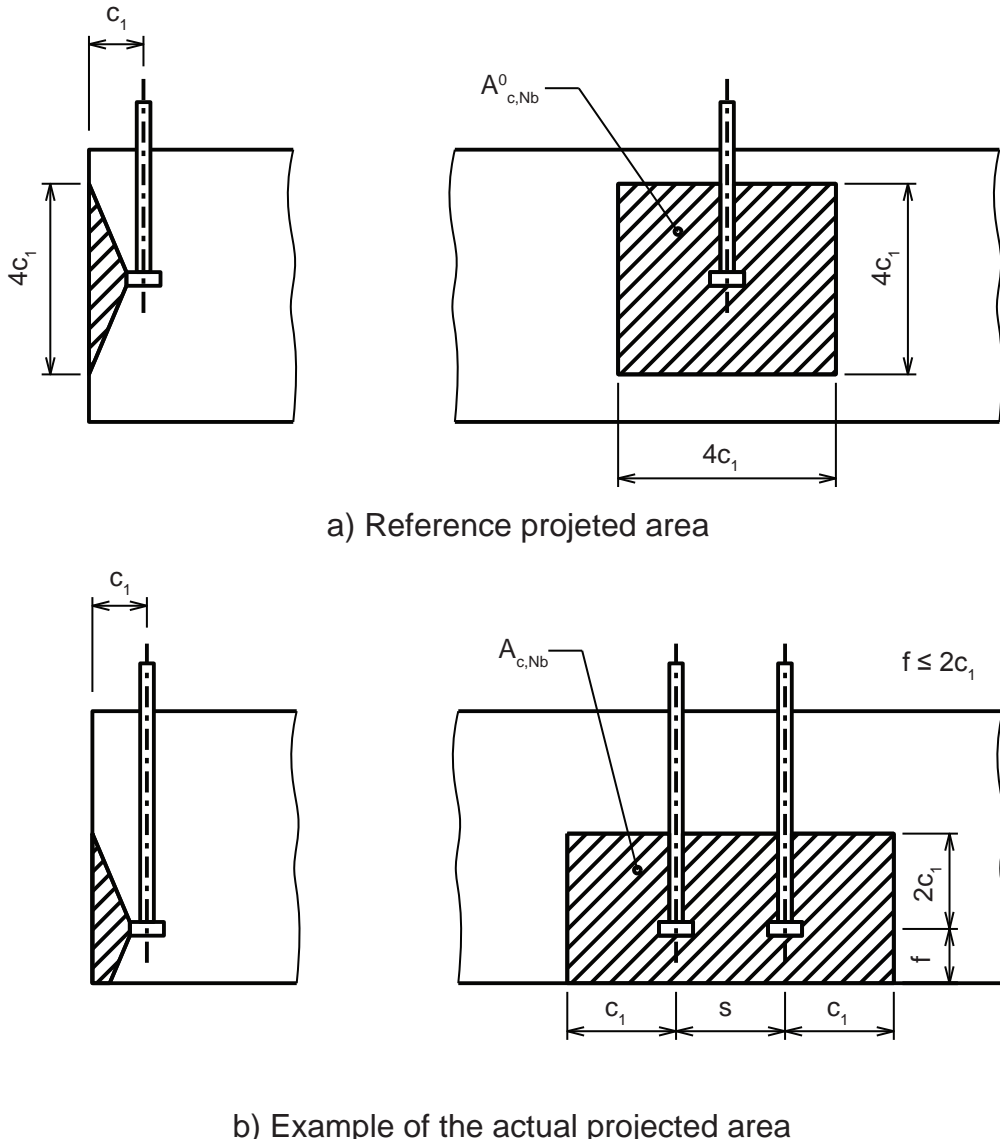


Figure A.1: Example of an actual projected break out area of a simple group of fasteners (SIS-CEN/TS 1992-4, 2009).

A corner of the concrete member may also disturb the stress distribution. This is taken into account by the factor $\Psi_{s,Nb}$ and it is obtained by Eq. (A.6).

$$\Psi_{s,Nb} = 0.7 + 0.3 \cdot \frac{c_2}{c_1} \leq 1 \quad [-] \quad (\text{A.6})$$

where,

c_2 is the smallest edge distance [mm]

In a group of fasteners, they will interact with each other and the effect is that the projected area of an individual fastener will overlap with the projected area of adjacent fasteners. This effect is taken into account by Eq. (A.7)

$$\Psi_{g,Nb} = \sqrt{n} + (1 - \sqrt{n}) \cdot \frac{s_1}{4c_1} \geq 1 \quad [-] \quad (\text{A.7})$$

where,

- n is the number of tensioned fasteners in a row parallel to the edge [-]
- s_1 is the distance between two fasteners parallel to the edge ($s_1 \leq 4c_1$) [mm]

A tensile load can act eccentric on a fastener or a group of fasteners. The effect of this eccentricity is obtained by Eq. (A.8).

$$\Psi_{ec,Nb} = \frac{1}{1 + 2 \cdot \frac{e_N}{s_{cr,N}}} \leq 1 \quad [-] \quad (\text{A.8})$$

where,

- e_N is the eccentricity of the tensile load [mm]

A fastener in uncracked concrete has a higher characteristic resistance than a fastener positioned in cracked concrete. The factor $\Psi_{ucr,N}$ takes this effect into account, and it is 1.0 for fasteners in cracked concrete and 1.4 for fasteners in uncracked concrete.

Steel failure with lever arm The characteristic resistance in case of steel failure of a fastener with lever arm, should be calculated according to Eq. (A.9).

$$V_{Rk,s} = \frac{\alpha_m \cdot M_{Rk,s}}{l} \quad [\text{N}] \quad (\text{A.9})$$

where,

- α_m is 1.0, if the fixture can rotate freely and 2.0 if the fixture is unable to rotate. For more information see CEN/TS 1992-4-1:2009, section 5.2.3.4. [-]

- l is the length of the fastener from the center of the fixture and $0.5 \cdot d$ into the concrete member. The parameter d is the diameter of the bolt or the threaded diameter. For more information see CEN/TS 1992-4-1:2009, section 5.2.3.4. [m]

- $M_{Rk,s}$ is the characteristic bending resistance of the fastener according to Eq. (A.10) given below. [Nm]

$$M_{Rk,s} = M_{Rk,s}^0 \cdot (1 - N_{Ed}/N_{Rd,s}) \quad [\text{Nm}] \quad (\text{A.10})$$

where,

- $M_{Rk,s}^0$ is given by Eq. (A.11), which can be found in ETAG 001 Annex C. [Nm]

- N_{Ed} is the tensile force acting on the fastener. [N]

- $N_{Rd,s}$ is $N_{Rk,s}/\gamma_{Ms}$, where $N_{Rk,s}$ is determined according to Eq. (4.1). [N]

$$M_{Rk,s}^0 = 1.2 \cdot W_{el} \cdot f_{uk} \quad [\text{N}] \quad (\text{A.11})$$

where,

- | | |
|----------|---|
| W_{el} | is the elastic bending resistance of the fastener [m ³] |
| f_{uk} | is the ultimate steel strength [Pa] |

Note that Eq. (A.11) is not valid for fasteners with a significant reduction of the sectional area along the length of the fastener. For these cases, $M_{Rk,s}^0$ must be determined according to the relevant ETA.

Concrete edge failure Single fasteners and groups of fasteners placed near and loaded towards an edge in a concrete member, may fail due to concrete edge failure. The fracture surface is semi-conical and develops in the radial direction from the fastener. The fracture surface developed by a group of fasteners will, if the distance between them is relatively small, be a common surface. Hence, one cannot utilise the full resistance of a single fastener in a group of fasteners. The characteristic resistance of a single fastener or a group of fasteners, due to concrete edge failure, shall be determined according to Eq. (A.12).

$$V_{R,kc} = V_{R,kc}^0 \cdot \Psi_{A,V} \cdot \Psi_{s,V} \cdot \Psi_{h,V} \cdot \Psi_{ec,V} \cdot \Psi_{a,V} \cdot \Psi_{re,V} \quad [\text{N}] \quad (\text{A.12})$$

All the parameters in Eq. (A.12) are given and explained below.

$V_{R,kc}^0$ is the characteristic resistance of a single fastener loaded in shear perpendicular to an edge, see Eq. (A.13).

$$V_{R,kc}^0 = k \cdot d_{nom}^\alpha \cdot l_f^\beta \cdot \sqrt{f_{ck,cube}} \cdot c_1^{1.5} \quad [\text{N}] \quad (\text{A.13})$$

where,

- | | |
|-----------|---|
| k | is 1.6 in cracked concrete and 2.4 in non-cracked concrete. [-] |
| d_{nom} | is the nominal diameter of the fastener ($\leq 60\text{mm}$), which may be found in the relevant ETA or product description. [mm] |
| l_f | is equal to h_{ef} if the diameter of the fastener is uniform. Otherwise, it may also be found in the relevant ETA or product description. [mm] |
| c_1 | is the edge distance in the direction of the shear load. [mm] |
| α | is $0.1 \cdot (l_f/c_1)^{0.5}$. [-] |
| β | is $0.1 \cdot (d_{nom}/c_1)^{0.2}$. [-] |

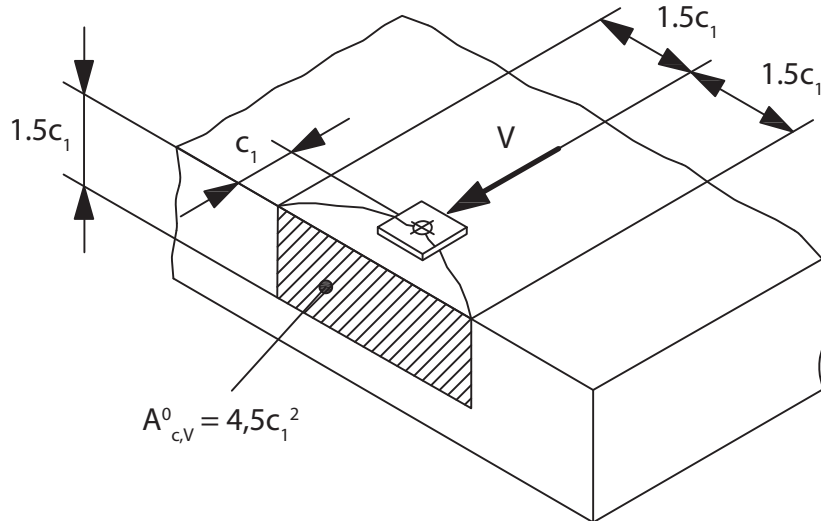
The ratio given in Eq. (A.14) take geometrical effects into account. One of great importance, is the spacing between the installed fasteners; a relatively small spacing can result in a reduced characteristic resistance. The effect of an increased edge distance and the concrete member thickness is also taken into account by Eq. (A.14).

$$\Psi_{A,V} = \frac{A_{c,V}}{A_{c,V}^0} \quad [\text{N}] \quad (\text{A.14})$$

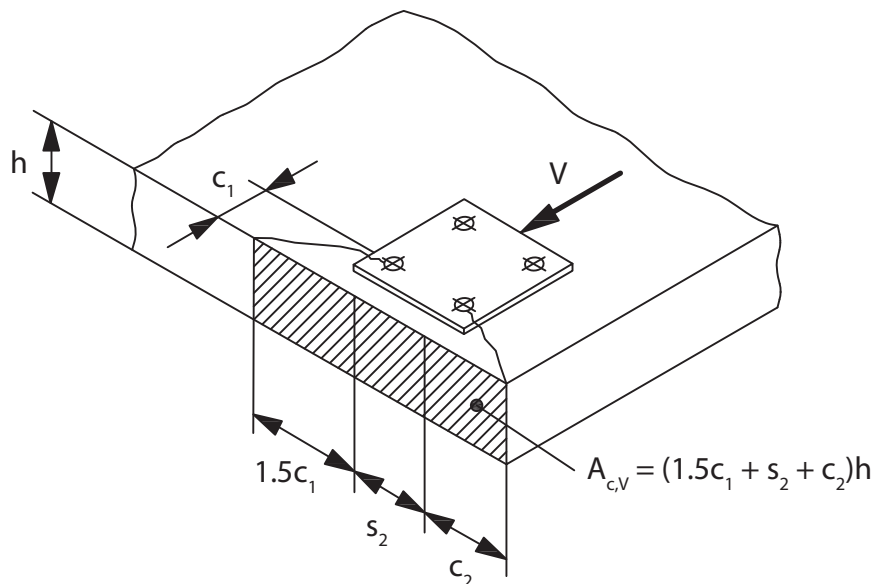
where,

$A_{c,V}$ is the actual projected area, see Fig. A.2 [m²]

$A_{c,V}^0$ is the reference projected area, $4.5 \cdot c_1^2$. See Fig. A.2 [m²]



a) Reference projected area



b) Example of the actual projected area in a thin concrete member

Figure A.2: Example of an actual projected break out area of a simple group of fasteners. Reproduction from (SIS-CEN/TS 1992-4, 2009).

The stress distribution in the concrete member, due to the concrete edge failure, may be disturbed by adjacent edges parallel to the shear load. The factor $\Psi_{s,V}$ takes this effect into account, and is given in Eq (A.15).

$$\Psi_{s,V} = 0.7 + 0.3 \cdot \frac{c_2}{1.5 \cdot c_1} \leq 1 \quad [N] \quad (A.15)$$

where,

- c_1 is the distance to an edge perpendicular to the shear load. [mm]
- c_2 is the shortest distance to an edge parallel to the shear load. [mm]

The ratio in Eq. (A.14) assumes that the concrete edge resistance decrease proportional to the member thickness. This assumption is valid for a concrete cone failure but not a concrete edge failure. Therefore, the factor $\Psi_{h,V}$, according to Eq. (A.16), is introduced.

$$\Psi_{h,V} = \left(\frac{1.5 \cdot c_1}{h} \right)^{0.5} \leq 1 \quad [N] \quad (A.16)$$

An eccentric load will also affect the characteristic resistance in case of concrete edge failure, because one or more fasteners will be subjected to a larger load than the others. The factors $\Psi_{h,V}$ account for these effects and is determined according to Eq. (A.17).

$$\Psi_{ec,V} = \frac{1}{1 + 2 \cdot e_v / (3 \cdot c_1)} \geq 1 \quad [N] \quad (A.17)$$

where,

- e_v is the eccentricity from the center of gravity to the resulting shear load. [mm]

Eq. (A.12) assumes that the shear load direction is perpendicular to an edge. This is of course not always the case, therefore, a factor $\Psi_{a,V}$, according to Eq. (A.18), is needed to take this into account.

$$\Psi_{a,V} = \sqrt{\frac{1}{(\cos \alpha_v)^2 + (0.4 \cdot \sin \alpha_v)^2}} \geq 1 \quad [N] \quad (A.18)$$

where,

- α_v is the angle between a line perpendicular to an edge and the shear load direction.

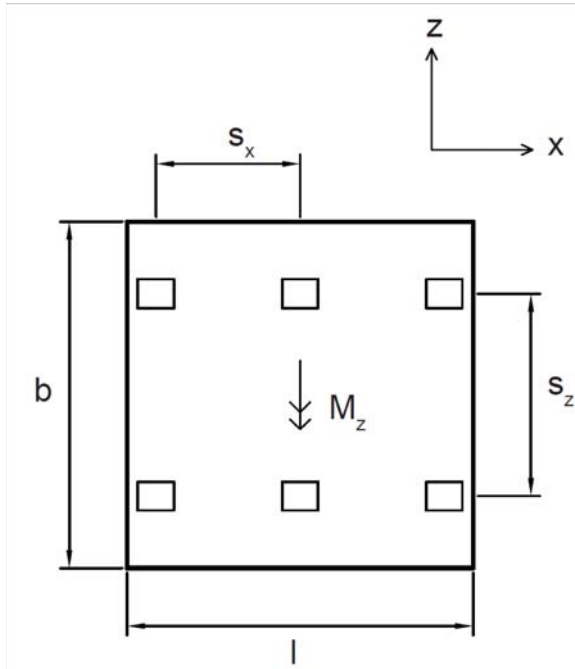
The fracture surface is dependent on whether the concrete member is cracked or not. Edge reinforcement will also influence the characteristic resistance due to concrete edge failure. The factor $\Psi_{re,V}$ is 1.0 for fasteners in cracked concrete and without reinforcement, 1.2 for fasteners in cracked concrete with straight reinforcement on the edge if the diameter ≥ 12 mm and 1.4 for fasteners in non-cracked concrete or in cracked concrete members with edge reinforcement and closely spaced stirrups. Note that the factor $\Psi_{re,V}$ only should be chosen > 1 if $h_{ef} \geq 2.5 \cdot a$, where a is the concrete cover of the reinforcement.

@Seismicisolation

A.2 Design of the M3 anchor plate subjected to a bending moment according to SIS-CEN/TS 1992-4-1:2010

Design of the M3 anchor plate subjected to a bending moment according to SIS-CEN/TS 1992-4-1:2010

Note that no partial coefficients nor safety factors are used in these calculations



Section and material data

Length: $l := 0.24$ [m]

Width: $w := 0.24$ [m]

Spacing in x direction: $s_x := 0.1$ [m]

Spacing in z direction: $s_z := 0.14$ [m]

Effective embedment depth: $h_{ef} := 0.225$ [m]

Cross-sectional area of one anchor: $A_s := 0.020 \cdot 0.025 = 5 \times 10^{-4}$ [m²]

Concrete cylinder strength: $f_{ck} := 20 \cdot 10^6$ [Pa]

Concrete cube strength: $f_{ck.cube} := 25 \cdot 10^6$ [Pa]

Concrete elastic modulus: $E_c := 30 \cdot 10^9$ [Pa]

Steel yield strength: $f_{yk} := 270 \cdot 10^6$ [Pa]

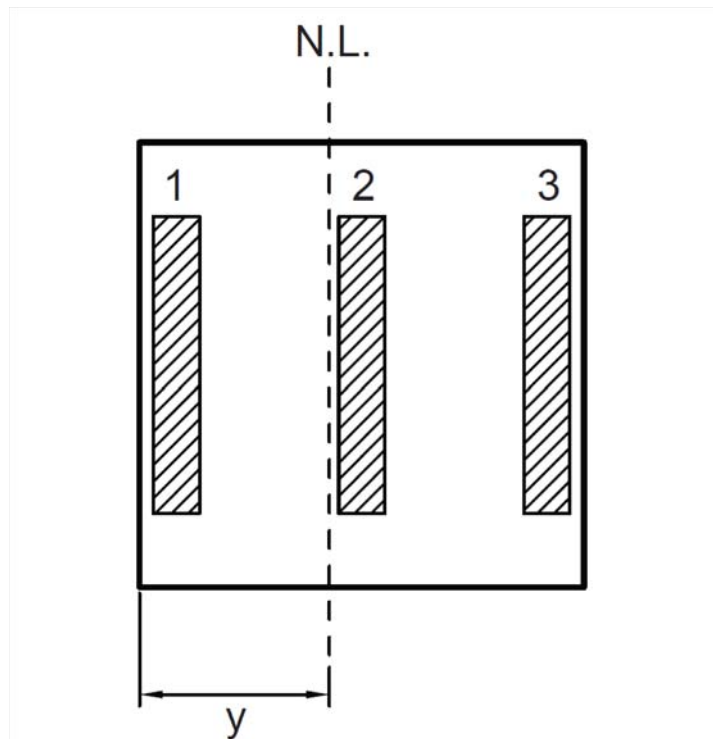
Steel ultimate strength: $f_{uk} := 430 \cdot 10^6$ [Pa]

Steel elastic modulus: $E_s := 200 \cdot 10^9$ [Pa]

Determination of the load condition

Since the anchor plate is subjected to a bending moment, all of the anchors will not be subjected to tensile loads. According to TS, the distribution of forces may be calculated by assuming a linear distribution of strains across the fixture and a linear relationship between stress and strain.

The distribution of forces will be calculated analogous to the elastic analysis of a reinforced concrete beam, where the anchors will be seen as reinforcement. An iterative method found in "Betonghandbok - Konstruktion" section 3.6:46 will be used.



The six anchors will be idealised into three reinforcement layers as seen above. The iteration process is based on assumptions on where the neutral layer is placed. The iteration process is finished when equilibrium is achieved. In this case, a force equilibrium is requested since a load case of pure bending moment is seeked. According to TS, the anchors in the compressive zone are not assumed to carry forces.

$$\text{The strain at which the steel yields is calculated as: } \epsilon_{sy} := \frac{f_y k}{E_s} = 1.35 \times 10^{-3}$$

The strain in the reinforcement layers is calculated as:

$$\epsilon_s(u, y) := 0.0035 \cdot \frac{u}{y} \quad \begin{aligned} u & \text{ is the distance from the reinforcement layer to the neutral layer} \\ y & \text{ is the position of the of the neutral layer} \\ 0.0035 & \text{ is the strain of the concrete at ultimate failure} \end{aligned}$$

A rectangular compressive zone is assumed, which gives a resultant compressive force:

$$F_c(y) := -0.8 \cdot w \cdot y \cdot f_{ck}$$

The resulting reinforcement forces may be calculated as:

$$F_s(\sigma_{s2}, \sigma_{s3}) := (\sigma_{s2} + \sigma_{s3}) \cdot A_s$$

Assumption 1

The neutral layer is placed at: $y := 0.11$ [m]

1: The layer lies within the compressive zone

$$2: u_2 := s_x + 0.020 - y = 0.01 \quad \epsilon_s(u_2, y) = 3.182 \times 10^{-4}$$

$$\sigma_{s2} := \left[\begin{array}{l} (\epsilon_s(u_2, y) \leq \epsilon_{sy}) \cdot (\epsilon_s(u_2, y) \cdot E_s) \\ + (\epsilon_s(u_2, y) > \epsilon_{sy}) \cdot f_{yk} \end{array} \dots \right] = 6.364 \times 10^7 \quad [\text{Pa}]$$

$$3: u_3 := 2 \cdot s_x + 0.02 - y = 0.11 \quad \epsilon_s(u_3, y) = 3.5 \times 10^{-3}$$

$$\sigma_{s3} := \left[\begin{array}{l} (\epsilon_s(u_3, y) \leq \epsilon_{sy}) \cdot (\epsilon_s(u_3, y) \cdot E_s) \\ + (\epsilon_s(u_3, y) > \epsilon_{sy}) \cdot f_{yk} \end{array} \dots \right] = 2.7 \times 10^8 \quad [\text{Pa}]$$

Equilibrium equation:

$$F_c(y) + F_s(\sigma_{s2}, \sigma_{s3}) = -8.876 \times 10^4$$

No equilibrium, due to the large force in the compressive zone. A smaller compressive zone should be assumed

Assumption 2

The neutral layer is placed at: $y := 0.10$ [m]

1: The layer lies within the compressive zone

$$2: u_2 := s_x + 0.020 - y = 0.02 \quad \epsilon_s(u_2, y) = 7 \times 10^{-4}$$

$$\sigma_{s2} := \left[\begin{array}{l} (\epsilon_s(u_2, y) \leq \epsilon_{sy}) \cdot (\epsilon_s(u_2, y) \cdot E_s) \\ + (\epsilon_s(u_2, y) > \epsilon_{sy}) \cdot f_{yk} \end{array} \dots \right] = 1.4 \times 10^8 \quad [\text{Pa}]$$

$$3: u_3 := 2 \cdot s_x + 0.02 - y = 0.12 \quad \epsilon_s(u_3, y) = 4.2 \times 10^{-3}$$

$$\sigma_{s3} := \left[\begin{array}{l} (\epsilon_s(u_3, y) \leq \epsilon_{sy}) \cdot (\epsilon_s(u_3, y) \cdot E_s) \\ + (\epsilon_s(u_3, y) > \epsilon_{sy}) \cdot f_{yk} \end{array} \dots \right] = 2.7 \times 10^8 \quad [\text{Pa}]$$

Equilibrium equation:

$$F_c(y) + F_s(\sigma_{s2}, \sigma_{s3}) = 2.6 \times 10^4$$

No equilibrium, due to the large force in the reinforcement. A larger compressive zone should be assumed.

Assumption 3

The neutral layer is placed at: $y := 0.1025$ [m]

1: The layer lies within the compressive zone

$$2: u_2 := s_x + 0.020 - y = 0.018 \quad \varepsilon_s(u_2, y) = 5.976 \times 10^{-4}$$

$$\sigma_{s2} := \left[\begin{array}{l} (\varepsilon_s(u_2, y) \leq \varepsilon_{sy}) \cdot (\varepsilon_s(u_2, y) \cdot E_s) \dots \\ + (\varepsilon_s(u_2, y) > \varepsilon_{sy}) \cdot f_{yk} \end{array} \right] = 1.195 \times 10^8 \quad [\text{Pa}]$$

$$3: u_3 := 2 \cdot s_x + 0.02 - y = 0.118 \quad \varepsilon_s(u_3, y) = 4.012 \times 10^{-3}$$

$$\sigma_{s3} := \left[\begin{array}{l} (\varepsilon_s(u_3, y) \leq \varepsilon_{sy}) \cdot (\varepsilon_s(u_3, y) \cdot E_s) \dots \\ + (\varepsilon_s(u_3, y) > \varepsilon_{sy}) \cdot f_{yk} \end{array} \right] = 2.7 \times 10^8 \quad [\text{Pa}]$$

Equilibrium equation:

$$F_c(y) + F_s(\sigma_{s2}, \sigma_{s3}) = -4.088 \times 10^3$$

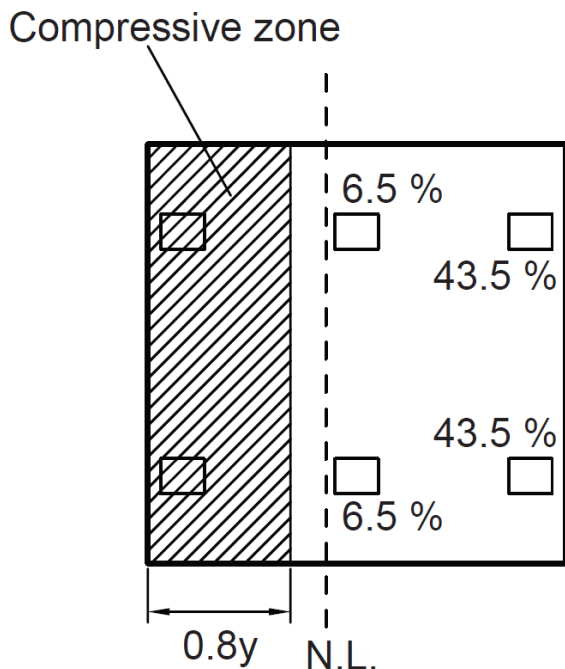
The result of the iteration is considered close enough. Compared to the total load of 325 kN for the pure tensile load case.

The distribution of forces is now calculated from the strains received in assumption 3.

$$\text{Layer 2: } N_2 := \frac{100 \varepsilon_s(u_2, y)}{\varepsilon_s(u_2, y) + \varepsilon_s(u_3, y)} = 13 \quad [\%] \quad \text{per anchor} \quad \frac{N_2}{2} = 6.5 \quad [\%]$$

$$\text{Layer 3: } N_3 := \frac{100 \varepsilon_s(u_3, y)}{\varepsilon_s(u_2, y) + \varepsilon_s(u_3, y)} = 87 \quad [\%] \quad \text{per anchor} \quad \frac{N_3}{2} = 43.5 \quad [\%]$$

The distribution of forces and the final neutral layer can be seen below.



Design according to SIS-CEN/TS 1992-4-1:2010

The four anchors subjected to tensile loads will now be treated as an anchor group, while the compressive zone is neglected for now. The following failure modes will be controlled: Concrete cone failure, pull-out failure and steel failure. The design methods used below are described in more detail in chapter 4 of the thesis.

Concrete cone failure

The concrete is considered to be uncracked, which gives the resistance of a single anchor:

$$N_{Rkc0} := 11.9 \sqrt{f_{ck,cube} \cdot 10^{-6}} \cdot (h_{ef} \cdot 1000)^{1.5} = 2.01 \times 10^5 \quad [N]$$

The reference projected area is equal to:

$$A_{cN0} := (3 \cdot h_{ef})^2 = 0.456 \quad [m^2]$$

The projected area of the anchor group is equal to (see Fig. 4.1):

$$A_{cN} := (3h_{ef} + s_x) \cdot (3h_{ef} + s_z) = 0.632 \quad [m^2]$$

Since the anchor plate is assumed to be positioned far from any edges $\psi_{sN} := 1$

$h_{ef} > 100$ mm which gives $\psi_{reN} := 1$

Due to the distribution of the tensile forces in the anchor group, an eccentricity from the center of gravity of the anchor group in the x direction is calculated as

$$e_N := \frac{s_x}{2} - \frac{N_2}{100}s_x = 0.037 \text{ [m]} \quad \text{which results in} \quad \psi_{ecN} := \frac{1}{1 + 2 \frac{e_N}{3 \cdot h_{ef}}} = 0.901$$

The failure load due to concrete cone failure may now be calculated as:

$$N_{Rkc} := N_{Rkc0} \cdot \frac{A_{cN}}{A_{cN0}} \cdot \psi_{sN} \cdot \psi_{reN} \cdot \psi_{ecN} = 2.509 \times 10^5 \text{ [N]}$$

Pull-out failure

The pull-out resistance of a single anchor is calculated as:

Since the concrete is assumed to be uncracked $\psi_{ucrN} := 1.4$

The load bearing area of a single anchor is $A_h := 0.05 \cdot 0.070 - A_s = 3 \times 10^{-3} \text{ [m}^2]$

This results in a failure load:

$$N_{Rkp} := 6 \cdot A_h \cdot f_{ck, cube} \cdot \psi_{ucrN} = 6.3 \times 10^5 \text{ [N]}$$

For the total anchor group this results in a load:

$$4 \cdot N_{Rkp} = 2.52 \times 10^6 \text{ [N]}$$

Steel failure

The capacity of the steel in a single anchor is calculated as

$$N_{Rks} := f_{uk} \cdot A_s = 2.15 \times 10^5 \text{ [N]}$$

For the total anchor group this results in a load:

$$4 \cdot N_{Rks} = 8.6 \times 10^5 \text{ [N]}$$

From this it can be seen that the concrete cone failure load is decisive since the failure load for the entire anchor group due to pull-out and steel failure exceeds the concrete cone failure load.

Concrete pressure under the compressive zone

The resultant force from the compressive stresses must equal the failure load of the idealised anchor group.

$$\sigma_c := \frac{N_{Rkc}}{0.8w \cdot y} = 1.275 \times 10^7 \text{ [Pa]} \quad \text{which is less than the compressive strength of the concrete}$$

Finding the maximum moment load

The lever arm between the resultant compressive force and the tensile force acting on the idealised anchor group is calculated as.

$$l_x := e_N + \frac{s_x}{2} + (s_x + 0.02) - 0.8 \cdot \frac{y}{2} = 0.166 \text{ [m]}$$

Which gives a maximum moment $M_z := N_{Rkc} \cdot l_x = 4.165 \times 10^4 \text{ [Nm]}$

Appendix B

Photos

B.1 Photos of anchor plates



Figure B.1: Cast-in-place anchor plate.



Figure B.2: Cast-in-place anchor plate (top) and post-installed anchor plate (bottom).



Figure B.3: Post-installed anchor plate.



Figure B.4: Post-installed anchor plate.



Figure B.5: Post-installed anchor plate.

@Seismicisolation